SYNTHESIS, CHARACTERIZATION AND CATALYTIC APPLICATION OF NOVEL CYCLOPALLADATED PYRIDINE FUNCTIONALIZED N-HETEROCYCLIC CARBENE COMPLEXES

CHIANG MINYI

SCHOOL OF PHYSICAL AND MATHEMATICAL SCIENCES

A thesis submitted to the Nanyang Technological University in fulfilment of the requirement for the degree of

Doctor of Philosophy in Chemistry

2011

ACKNOWLEDGEMENTS

I have to express my gratitude towards my PhD supervisor Professor Leung Pak Hing for initiating this meaningful experience for me. I have to thank him for his guidance and support throughout my PhD candidature.

I am very grateful to my past and present research group members. My seniors Dr Li Yongxin, Dr Sumod A. Pullarkat, Dr Chen Shuli, Dr Zhang Yi, Dr Ding Yi, Dr Liu Fengli, Dr Luo Ding and Dr Ma Mengtao for their invaluable advice and for sharing their technical expertise with me. I am especially grateful towards Dr Li and Dr Sumod, the completion of this thesis would be impossible without their generous advice and assistance. I would like to thank my laboratory mates Mingjun, Cheow, Deepa, Yinhua, Xu Chang, Chen Ke, Zhang Na, Jeanette, Selvi, Kim and Zhiyi for their help; Kim who has worked together with me on my projects during her undergraduate years.

To Jocelyn, Vivian, Jenefer, Anita, Jaslyn, Aihua and Yvonne, I would like to thank them for all their encouragements especially during the uphill battles. They have brightened up and enriched my life in NTU.

I am grateful to the staff Eeling, Wenwei and Shuqi for their assistance in NMR, elemental analysis and mass spectrometry and to Celine for her help with regards to graduate matters.

I am grateful to Nanyang Technological University for my research scholarship.

Most importantly, to my parents, I would like to express my heartfelt gratitude for their love and support during the pursuit for my PhD degree. Their absolute faith in me has motivated me during the challenging moments and made this thesis possible.

TABLE OF CONTENTS

Chapter 1 INTRODUCTION

SUMMARY

In this thesis, a series of novel chiral cyclopalladated pyridine functionalized NHC complexes were synthesized *via* a new methodology. The catalytic abilities and the selectivities of new NHC palladacycles were tested against the allylic alkylation reaction.

Chapter 1 provides a brief history and development of NHC. Emphasis has been placed on palladium complexes of NHC; their abilities to mediate different catalytic reactions were discussed.

Chapter 2 highlights the synthesis of a series of novel cyclopalladated pyridine functionalized NHC dichloride complexes. The common 2-(chloro(phenyl)methyl)pyridine can be synthesized in 2 simple steps. The different ligands were prepared by subsequent reactions of 2-(chloro(phenyl)methyl)pyridine with their respective imidazoles. Finally, transmetalation of the ligands with Ag_2O gave the desired palladacycles. The structures of the palladacycles were investigated through single crystal X-ray diffraction studies. From X-ray crystallography, the six membered rings in the palladacycles were all in the boat conformation with the bulky α phenyl group in the axial position. The ring conformations in solution were studied via 2D ^1H-^1H ROESY NMR. From the ROESY NMR spectra, the rigidities of the palladacycles were maintained in solution with the rings locked in the boat conformation.

In chapter 3, new methodology was developed to synthesize chiral NHC bidentate palladium complexes *via* optical resolution. The palladacycles that were synthesized in chapter 2 have a potential chiral centre within the NHC

chelate ring. Upon coordination with the sodium salt of chiral amino acid, the formation of a pair of diastereomers can be observed by ^{1}H NMR. The diastereomeric pair was then separated by fractional crystallization. Subsequent treatment with 1M HCl resulted in the cleavage of the chiral amino acid auxiliary to give the optically active dichloride complexes. The dichloride palladium complexes displayed limited solubility in a range of common organic solvents. Hence, 1 molar equivalent of triphenylphosphine was added to the complexes to improve their solubilities. The addition of triphenylphosphine to the complexes were highly regioselective, with the incoming triphenylphosphine ligand selectively replacing the chloride *trans* to $N_{pyridine}$. The hemilability of the chelate system can be observed in complex (±)-**58**. The $N_{pyridine}$-Pd cleaved upon introduction of the triphenylphosphine ligand. The hemilability of the $N_{pyridine}$-Pd in complex (±)-**58** was observed even when a weaker triphenylarsine ligand was added. The new methodology that was developed provides a general method to synthesize chiral NHC palladium complexes without the use of expensive chiral starting materials and a whole range of cheap commercially available chiral amino acids to choose from for the chiral auxiliary.

The catalytic abilities of the previously described NHC palladium complexes were investigated in chapter 4. The palladium complexes were used to mediate the allylic alkylation reaction to test their catalytic abilities. A model study was first conducted on complex (±)-**56** under different conditions. A variety of bases, solvents and temperatures were used in different combinations to identify the optimal conditions for catalysis. The triphenylphosphine

coordinated palladium complexes had the best activities with the reaction completing in 30 mins at 25°C. However, none of the chiral palladium complexes displayed any selectivity.

In conclusion, the simple and efficient methodology that was developed was successfully applied to the synthesis of a series of chiral novel pyridine functionalized NHC palladium complexes. The palladacycles exhibited remarkable activities in catalytic allylic alkylation reaction but exert insignificant stereo control over the reaction.

LIST OF NEW COMPOUNDS AND COMPLEXES

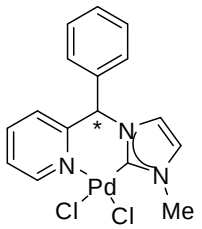

(±)-**56**

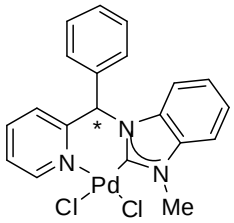

(±)-**57**

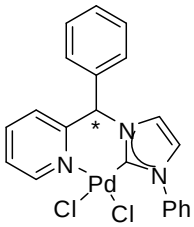

(±)-**58**

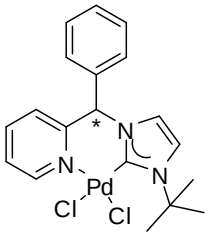

(±)-**59**

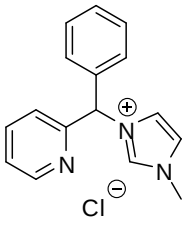

60

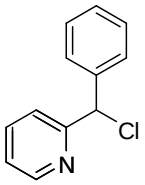

62

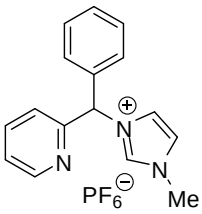

63

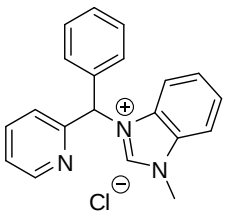

65

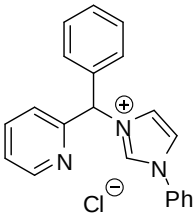

67

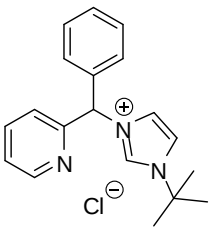

68

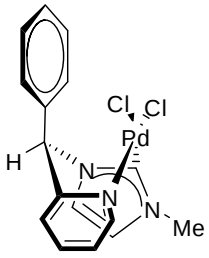

(*R*)-**56**

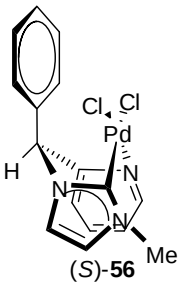

(*S*)-**56**

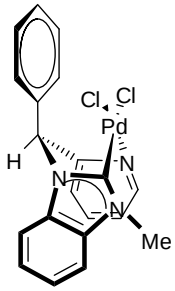

(*S*)-**57**

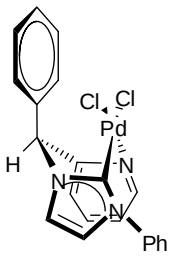

(*S*)-**58**

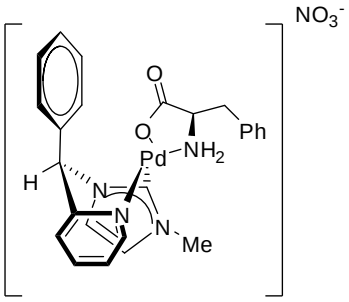

(R_C,S_C)-**78**

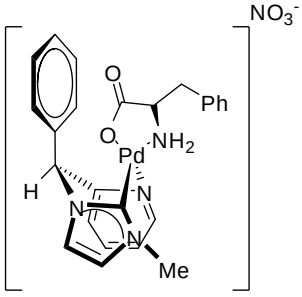

(S_C,S_C)-**78**

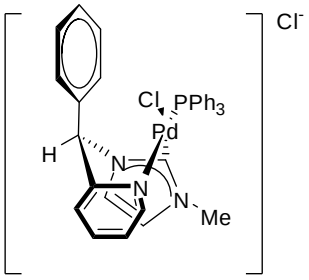

(*R*)-**79**

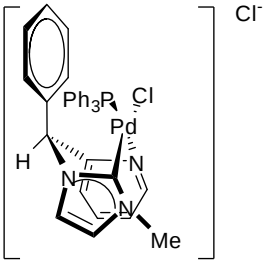

(*S*)-**79**

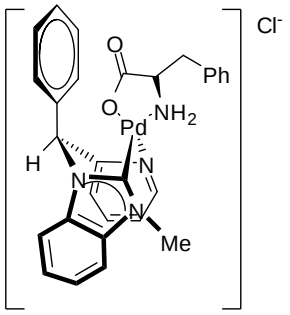

(S_C,S_C)-**80**

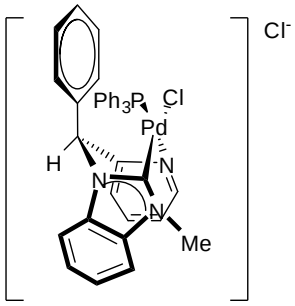

(*S*)-**81**

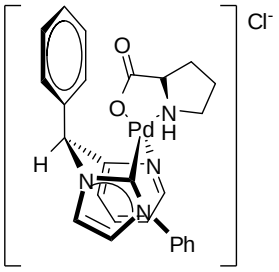

(S_C,S_C)-**82**

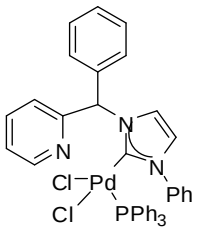

84

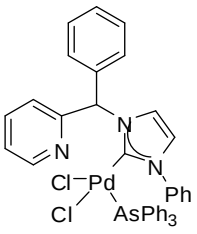

87a

LIST OF TABLES

LIST OF FIGURES

ABBREVIATION AND SYMBOLS

acac	acetylacetonate
Ar	aryl group
br	broad
c	sample concentration for O.R.D analysis
ca.	Circa
calcd	calculated
$CDCl_3$	chloroform-d_1
COSY	correlation spectroscopy
d	doublet (in NMR assignments)
dd	doublet of doublet (in NMR assignments)
de	diastereomeric excess
DMSO	dimethyl sulphoxide
ee	enantiomeric excess
g	grams
h	hour(s)
HMBC	Heteronuclear Multiple Bond Coherence
HCl	hydrochloric acid

HMQC	Heteronuclear Multiple Quantum Coherence
Hz	hertz
m	multiplets (in NMR assignments)
Me	methyl
mg	milligram(s)
min	minute(s)
mmol	millimole(s)
M.p	melting point
MS	mass spectroscopy
NMR	Nuclear Magnetic Resonance
Ph	Phenyl
^{31}P NMR	$^{31}P\{^{1}H\}$ NMR
ppm	parts per million
q	quartet (in NMR assignments)
R	rectus (Latin: right absolute configuration)
ROESY	2D rotating frame nuclear Overhauser enhancement
S	sinister (Latin: left absolute configuration)
s	singlet (in NMR assignment)

t	triplet (in NMR assignment)
δ	NMR chemical shift in ppm

Chapter 1

Introduction

1.1 Brief history of Metal Carbenes

Metal complexes of carbenes can be broadly classified into two categories, Fischer and Schrock carbenes; both with very distinctive characteristics. Fischer carbenes can be identified by the characteristic electrophilic nature of the carbene, which typically coordinates with low oxidation state metals. Whereas for Schrock carbenes, their carbene carbon is generally regarded as nucleophilic in nature and they preferentially coordinate with metals in higher oxidation state.

Fischer successfully reported the synthesis and proton NMR and IR characterisation of the first ever carbene metal complex **1** in 1964.[1] Its structure was confirmed crystallographically in 1965.[2] Fischer carbenes are well stabilized by their heteroatom substituents. For example in complex **1**, the carbene is stabilized by a methoxy group. Due to the presence of the additional stabilization, a significant energy gap exists between the singlet and triplet state, resulting in the Fischer carbene existing as a singlet carbene (Figure 1.1).

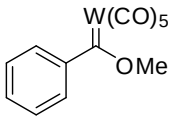

Complex **1**

Approximately 10 years after the first Fischer carbene metal complex was synthesized, Schrock reported the synthesis of a distinctly different class of metal carbene complexes from Fischer which are subsequently known as the

Schrock carbenes. For example, the first Schrock alkyl carbene complex, complex **2** that was synthesized in 1974 is significantly different compared to the Fischer carbenes.[3] This report by Schrock opened up a new concept in carbene chemistry. Prior to Schrock, all the earlier reported carbenes complexes display electrophilic character on the carbene moiety. However for Schrock, his carbene centre displays a nucleophilic character. Unlike Fischer carbenes that are stabilized by hetereoatoms, Schrock carbenes are weakly stabilized with an insignificant singlet and triplet state energy gap. Therefore, Schrock carbenes exist as neither exclusively (Figure 1.1).

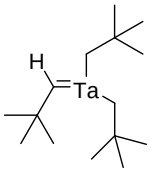

Complex **2**

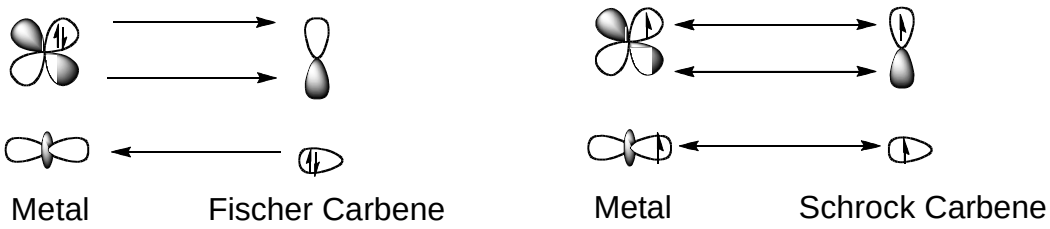

Figure 1.1 Fischer and Schrock Carbene

However, the major breakthrough in carbene chemistry occurred in 1991 when Arduengo *et al.* reported the first crystalline structure of a free carbene ligand, ligand **3**.[4] This is the first stable free carbene ligand that has ever been reported. Prior to Arduengo's report on the isolation of ligand **3**, all the Fischer and Schrock type carbenes have been isolated as metal complexes. Following the isolation of the stable carbene in crystalline form, the notion that

carbenes are transient intermediates no longer stands and the chemistry of *N*-*H*eterocyclic *C*arbenes (NHC) also known as Arduengo's carbene has experienced unprecedented development.

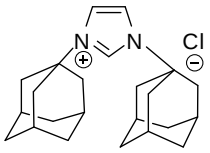

Ligand **3**

1.2 N-Heterocyclic Carbenes (NHC)

1.2.1 Synthesis of NHC

The popularity of NHC can be attributed to the fact that both their electronic and steric properties can be easily modified like phosphines ligands, which have been the ligand of choice in the field of organometallic catalysis. However, unlike phosphine ligands, NHC are much less sensitive to both air and moisture. Therefore, the general synthetic routes of NHC are usually more hassle free compared to the synthesis of phosphines. More often than not, the synthesis of NHCs can be achieved under ambient conditions without having to proceed under inert atmosphere and moisture free conditions like phosphine ligands.

As summarized by Herrmann in a recent review, NHC can easily be synthesized *via* a one pot method as described in Scheme 1.1.[5] NHC can be synthesized in a one pot fashion with readily available glyoxal, amines and formaldehyde. By varying the amine used, different R substituents on the wingtip N on the imidazolium ring can be introduced. In the presence of

phosphoric acid, unsymmetrical R groups can be introduced into the wingtip as seen in Scheme 1.1(b). Due to the simplicity in the synthetic methodology and the vast choice of different commercially available amines, the one pot method is by far one of the most popular methods to synthesize NHC.

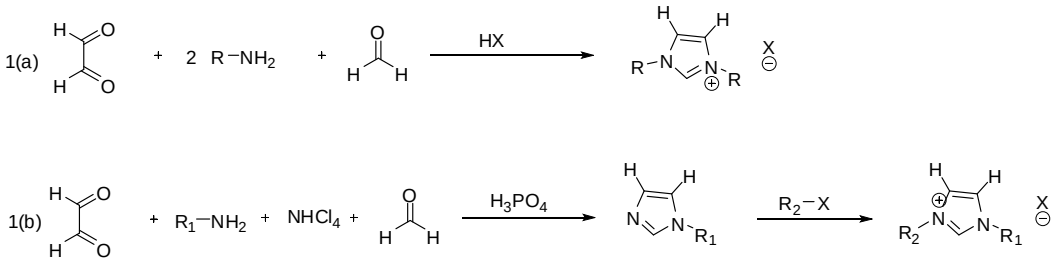

Scheme 1.1

Herrmann *et al.* demonstrated that chiral NHC ligands can also be synthesized directly from the above one pot method (Scheme 1.2).[6] Through the use of chiral amines, a C_2 symmetrical NHC can be generated as illustrated in Scheme 1.2.

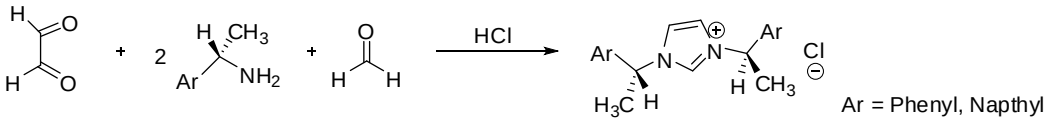

Scheme 1.2

Imidazoliniums and their chiral derivatives are readily accessible from chiral amines.[7] This method can also be employed in the synthesis of NHC with substitution at the C4 and C5 by starting with an α substituted amine. An optically active NHC can be generated by choosing bulky substituents on the

C4 and C5 that will restrict free rotation due to steric repulsion between the bulky groups as seen in Scheme 1.3.[8]

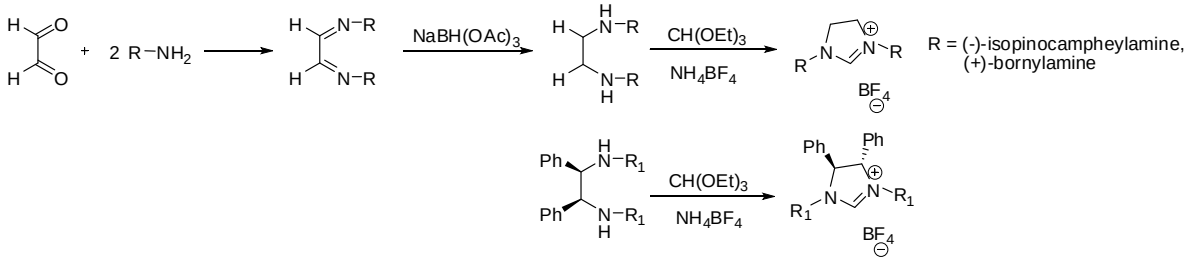

Scheme 1.3

Different R groups can also be introduced into the wingtip substituents *via* reaction of commercially available imidazole or benzimidazole with alkyl or aryl halides in the presence of catalysts like copper (I) complexes.[9] Therefore, imidazolium and benzimidazolium based chiral ligands can be readily synthesized from chiral alkyl or aryl halides (Scheme 1.4). Direct substitution on the wingtip N is also possible in the absence of any catalyst at elevated temperature as demonstrated in Scheme 1.5. Chiral groups like the oxazolines can be introduce into the imidazole in the absence of a catalyst.[10]

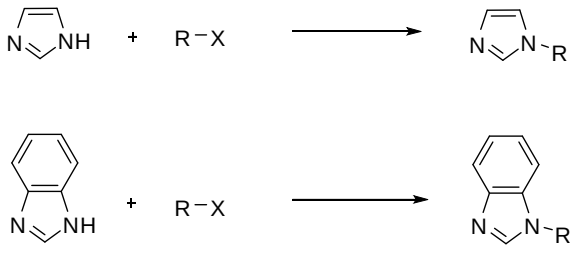

Scheme 1.4

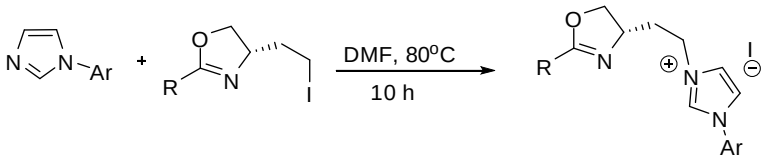

Scheme 1.5

As such, different functionalities can be easily introduced into the NHC. More importantly, as seen in Scheme 1.4 and Scheme 1.5, groups with different functionalities can be introduced into the same NHC, giving rise to chiral unsymmetrical NHC.

1.2.2 Steric and Electronic Properties of NHC

The steric bulkiness of phosphines is commonly described in terms of cone angle. However, in the case of NHC, measuring its steric bulkiness in terms of cone angle no longer provides an apt description of its steric bulkiness. Instead, the steric bulkiness of NHC can be described in terms of percent buried volume, $\%V_{bur}$.[11] This model describes the volume that a NHC ligand occupies in a sphere in terms of percentage volume it occupies around the coordination sphere of the metal centre (Figure 1.2). A web application is available for the calculation of $\%V_{bur}$ using crystallographic data.[12] In a recent review, Nolan *et al.* summarised based on monodentate NHC coordinated Au(I) chloride complexes that substituents have to be only 2 to 3 atoms away from the N to exert a pronounced effect on the $\%V_{bur}$. In addition, different variations in the NHC backbone has little effect on the $\%V_{bur}$ except in the case of NHCs with isopropyl groups. In the presence of isopropyl groups, methyl substituents on the NHC's backbone will push the isopropyl groups closer to the metal centre and hence increases the $\%V_{bur}$.[13]

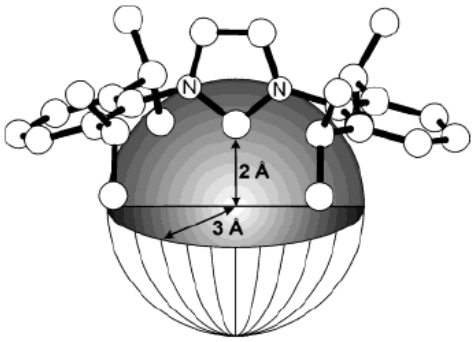

Figure 1.2 $\%V_{bur}$ for NHC

To date, the most sterically hindered monodentate carbene that has been documented is ligand **4**. Its AgBr complex has $\%V_{bur}$ = 47.8 %. This ligand which has a simple NHC backbone and bulky substituted cyclohexyl groups 1 atom away from the N epitomizes the general criteria observed by Nolan *et al.* for a NHC ligand to have high $\%V_{bur}$ as stated above.

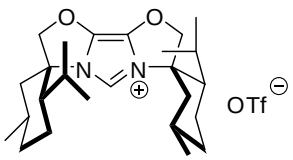

Ligand **4**

In addition, ligand **4** exhibits fluxionality that can be altered in accordance to the requirements of the catalytic system. The cyclohexyl rings can undergo chair flip dynamically to adapt to the different requirements of the systems as shown in Scheme 1.6 and can give enantioselectivity of up to 97% ee for asymmetric intramolecular α-arylation of amides which will be further elaborated in section 1.4.2.[14]

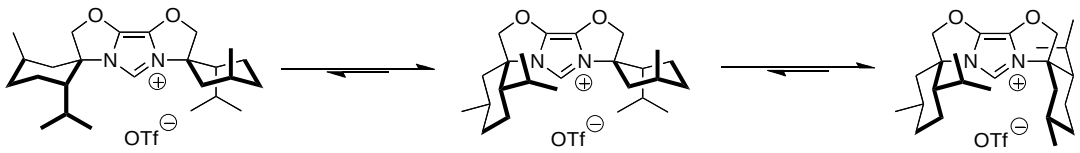

Scheme 1.6

Compared to phosphines, NHC are mainly strong σ donors and weak π accepting ligands.[15] Due to the strong metal-NHC bond, NHC based catalytic systems typically exhibit a high degree of stability against heat, moisture and air during the course of their synthetic applications. Several methods have been used to study the electronic properties of NHC. Amongst the methods, observation of the IR stretching frequencies of CO coordinated NHC metal complexes is quite popular.[16] Nevertheless, the observation of the electronic properties of NHC *via* the ^{13}C NMR chemical shifts of the carbene carbon which does not involve any further manipulations to coordinate the CO *trans* to the NHC system offers a more straight forward approach to the study of NHCs' electronic properties.[17] As seen in Figure 1.3, the donor strengths of various NHC ligands can be compared effectively based on their ^{13}C NMR chemical shift with a downfield shift indicating increasing donor strengths. Therefore, the ^{13}C NMR chemical shift of the carbene carbon is generally the fastest and most readily available method to offer insights into the donor strengths of NHC and its complexes.

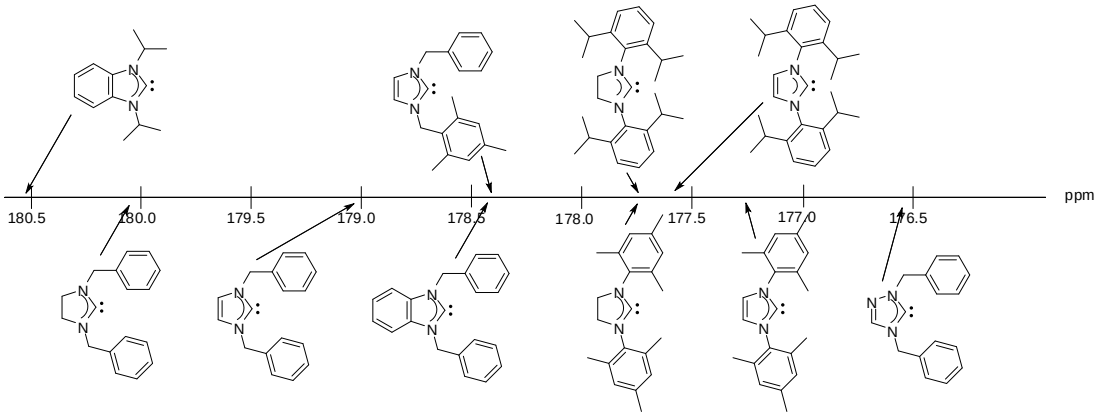

Figure 1.3 ^{13}C NMR chemical shift of the carbene carbon [17(c)]

1.3 NHC Palladium Complexes

1.3.1 Synthesis of NHC Pd (II) Complexes

NHC complexes of Pd (II) complexes can be readily synthesized *via* a Pd (II) source in the presence of an external base that deprotonates the carbene proton to facilitate the carbene coordination to the Pd (II) centre. External inorganic base like *tert*-butoxides (Scheme 1.7), [18] or organic bases like triethylamine (Scheme 1.8) [19] is commonly employed for the deprotonation of the carbene proton.

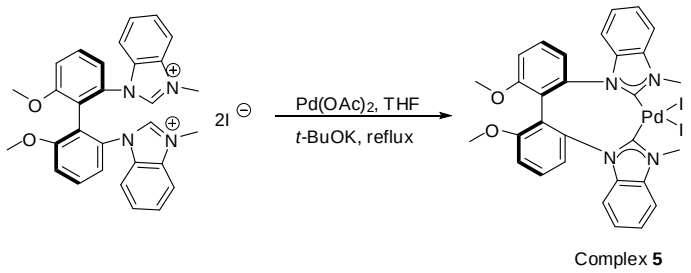

Scheme 1.7

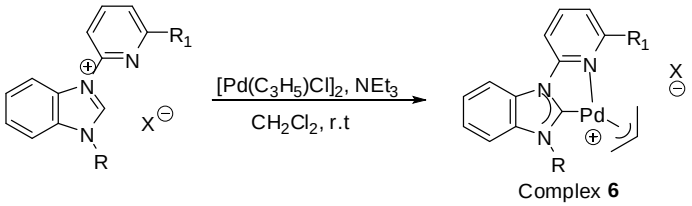

Scheme 1.8

NHC form significantly strong bonds with the Pd centre. Therefore, in the presence of relatively weak ligands like acetate, NHC can be coordinated to the Pd (II) centre through ligand replacement of one or both of the acetate ligands when Pd $(OAc)_2$ is used as the palladation source at elevated temperatures as seen in Scheme 1.9.[20]

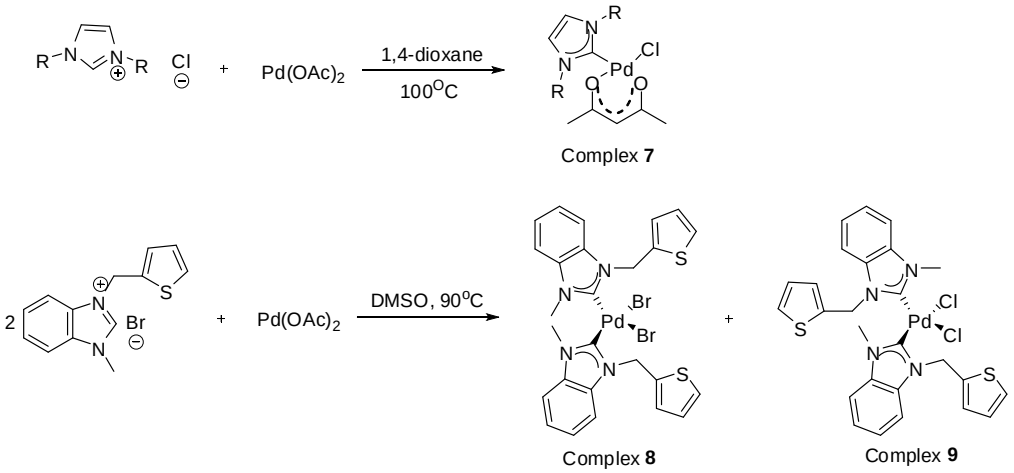

Scheme 1.9

Transmetalation *via* the transfer of NHC from a silver centre to a palladium centre is one of the most common methods employed in the synthesis NHC palladium complexes ever since it was developed by Lin *et al.* in 1998.[21] The NHC silver complex intermediate generated from Ag_2O in CH_2Cl_2 is relatively stable and easy to handle and can be isolated usually as a stable precipitate. This method is mild enough to tolerate a range of different

functionalities on the N substituents like amines, [22] pyridines and carbonyls,[23]imines[24] and sulphur (Scheme 1.10).[25]

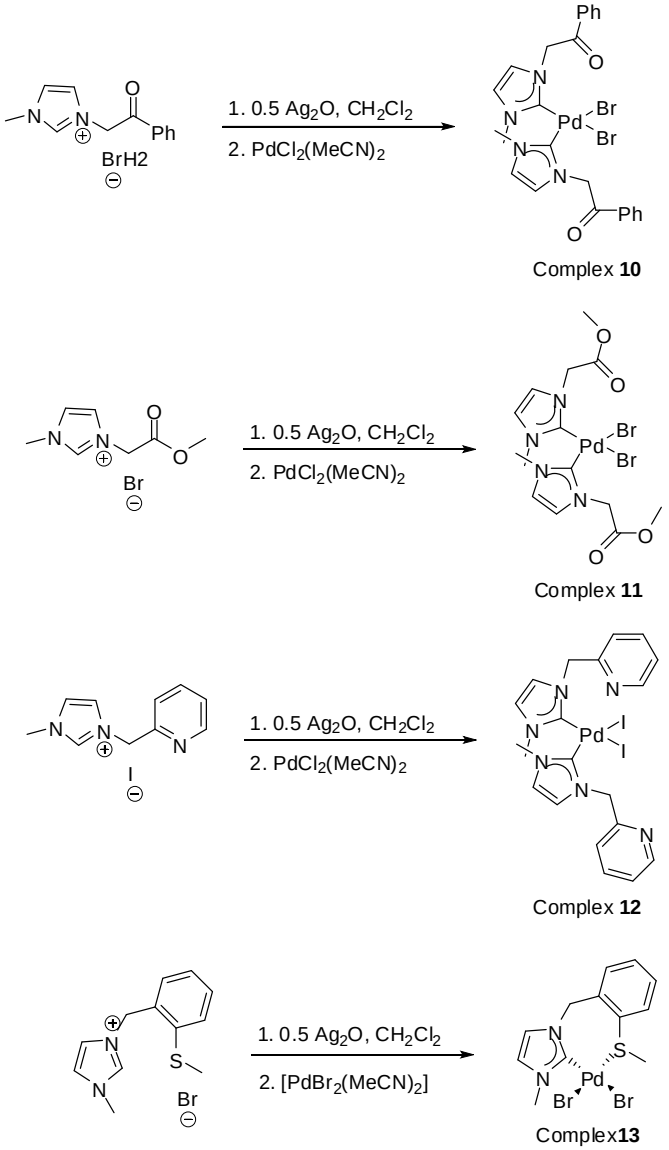

Scheme 1.10

In more recent years, it has been demonstrated that NHC can also be successfully transferred from a Au (I) centre to a Pd (II) centre (Scheme 1.11).[26]

Transmetallation *via* an Au (I) centre can be achieved for NHC containing pyridine and thio functionalities.

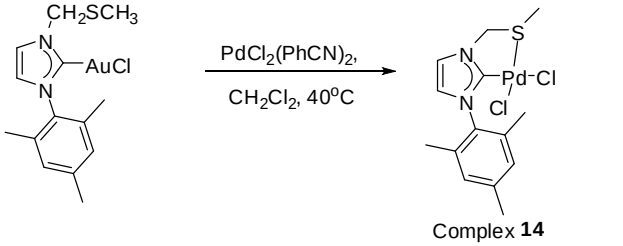

Complex **14**

C

Scheme 1.11

NHC palladium complexes can also be generated though the oxidative addition of biimidazolium ion into a Pd (0) centre as demonstrated in Scheme 1.12 in respectable yields.[27]

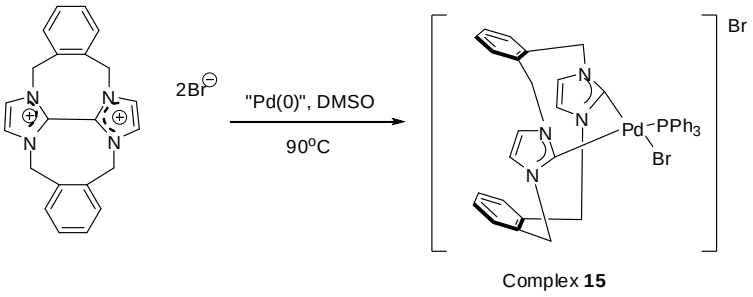

Complex **15**

Scheme 1.12

1.3.2 NHC Palladium Complexes Catalyzed Achiral Cross Coupling Reactions

As mentioned above, NHC forms strong and stable bonds with metal, hence they are choice candidates as chiral auxiliaries in catalytic system as they are robust under different catalytic conditions. One of the most famous and

widely used NHC metal complex to date is Grubbs second generation catalyst, complex **16** which Grubbs *et al.* developed in 1999 for the olefin metathesis.[28] Since then, NHC metal complexes have received much attention in the field of catalysis.

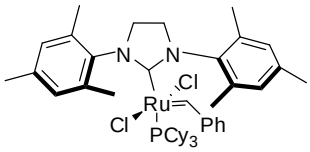

Complex **16**

NHC palladium complexes are another class of highly popular NHC metal complexes, due to the fact that they exhibit superior activity as compared to its phosphines analogues especially in the mediation of cross coupling reactions. Palladium NHC complexes are more stable at higher temperatures and can better stabilize the Pd centre during the course of the catalysis than their phosphine analogues. Therefore much effort has been placed in the synthesis of different NHC Pd complexes.

1.3.2.1 Heck Reaction

The ability of NHC palladium complexes to be able to mediate Heck reaction was first identified and described by Herrmann *et al.* in 1995.[29] In this article, Herrmann stated two reasons for his diversion from the more popular phosphine ligands at that time to NHC. Firstly, in a phosphine-palladium system, an excess amount of phosphine ligand, usually at about 100: 1 phosphine to palladium ratio is usually required for the catalysis to compensate ligand loss due to P–C bond cleavage. This excess amount of ligand required

decreases the cost efficiency of such systems. Secondly, phosphine palladium complexes usually require careful handling under dry

and inert atmosphere. By switching to NHC palladium system to catalyzed the Heck reaction, all the problems mentioned above can be circumnavigated. Herrmann showed that the complex **17** can effectively catalyze the Heck reaction (Scheme 1.13) with 2:1 NHC to palladium ratio with high turnover rates of >99%. More importantly, complex **17** exhibits high stability even after several days in O_2 and boiling THF. Hence complex **17** is stable enough to be handled conveniently under ambient conditions.

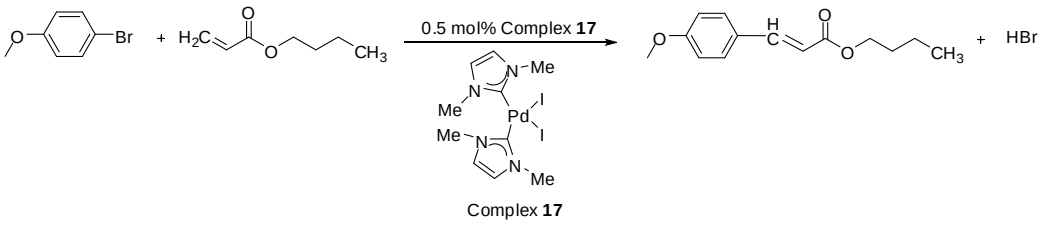

Scheme 1.13

1.3.2.2 Suzuki Reaction

Suzuki coupling reaction is another cross coupling reaction that can be mediated by NHC palladium complexes. As shown in Scheme 1.14, complex **18** is able to successfully catalyzed the reaction between aryl bromides and aryl boronic acid with yields of up to 99%.[30] The same system can be applied to less activated aryl chlorides such as chloroacetophenone with a lower yield of 60%.

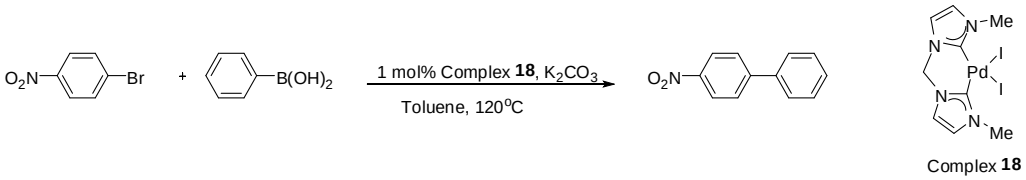

Complex **18**

Scheme 1.14

1.3.2.3 Sonogashira Reaction

Sonogashira reaction, another class of C–C bond formation between alkynes and organo halides can also be catalyzed by NHC palladium complexes. The typical conditions of Sonogashira reaction involves both a palladium catalyst and a copper (I) co catalyst. However, Herrmann *et al.* demonstrated that alkynes' coupling reaction is possible without a copper(I) co-catalyst in the presence of complex **18**, giving the product in 76 % yield (Scheme 1.15) .[30]

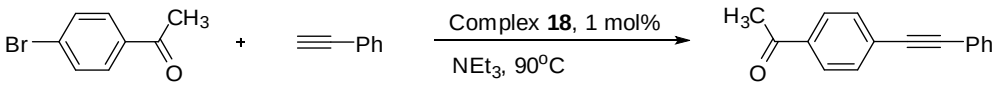

Scheme 1.15

As illustrated in Scheme 1.16, when the typical Sonogashira condition is applied, in the presence of CuI as the co catalyst, complex **19** can be achieved up to 85% in yield.[31]

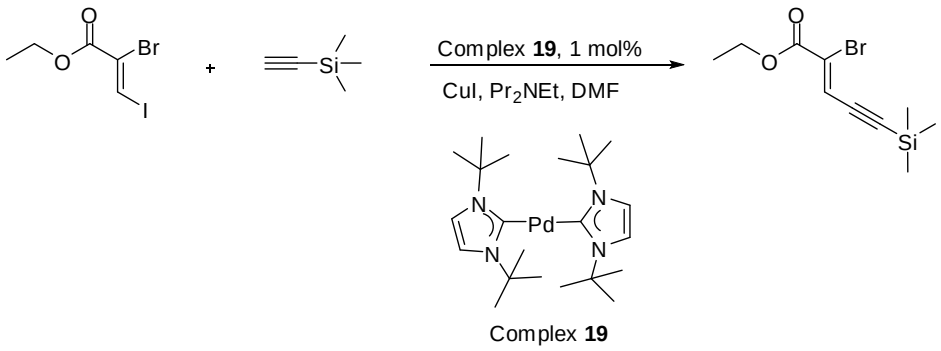

Scheme 1.16

1.3.2.4 Kumada Reaction

In 1999, Nolan *et al.* demonstrated that NHC palladium complexes can successfully mediate the typical Kumada reaction that involves C–C bond formation between aryl chlorides and Grignard reagents with yields of up to 99% (Scheme 1.17).[32]

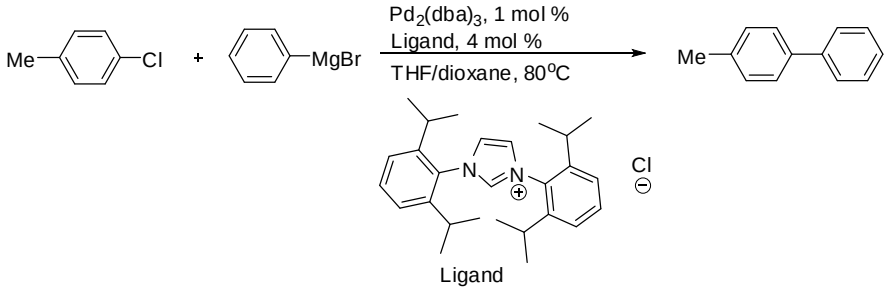

Scheme 1.17

Beller *et al.* made further contributions to this area. He expanded the substrate scope from aryl chlorides to alkyl chlorides. Through the utilization of preformed NHC palladium complex **20**, alkyl chlorides can successfully undergo catalytic C–C bond formation with Grignard reagents as seen in Scheme 1.18 to give the desired coupling product.[33]

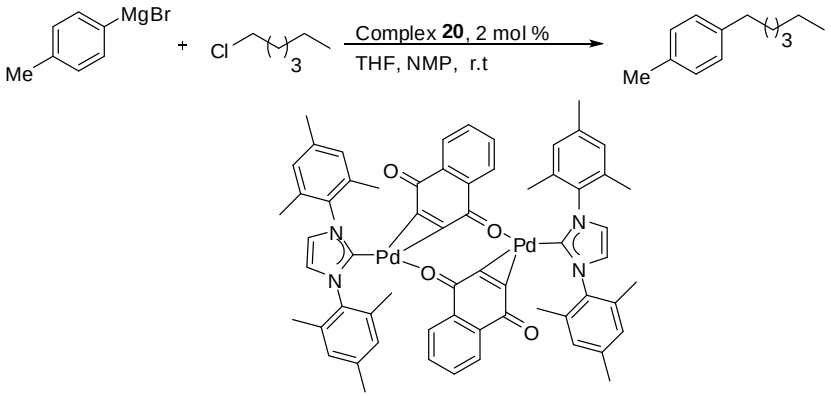

Complex **20**

Scheme 1.18

1.3.2.5 Negishi Reaction

Similar to the Kumada reaction, the Negishi reaction is also a C–C coupling between an organic halide and a metallated organic compound. But instead of the organo magnesium compound used in Kumada reaction, an organo zinc compound is used in the Negishi reaction. The first attempt to use a NHC palladium complex to catalyze the Negishi reaction was attempted by Fu *et al.* with 1,3-bis(mesityl)-4,5-dihydroimidazolium tetrafluoroborate as the ligand.[34] However, the yield obtained for this initial attempt was at a dismal 4%.

However, by switching the R groups on the wingtip nitrogen atoms of the imidazolium from mesityl to diisopropylphenyl, Organ *et al.* showed that moderate to 92% yield can be achieved by both linear[35] and branched[36] organo halides and organ zinc substrates (Scheme 1.19). In the presence of complex **21**, 100% yield is achievable as shown in Scheme 1.20.[37]

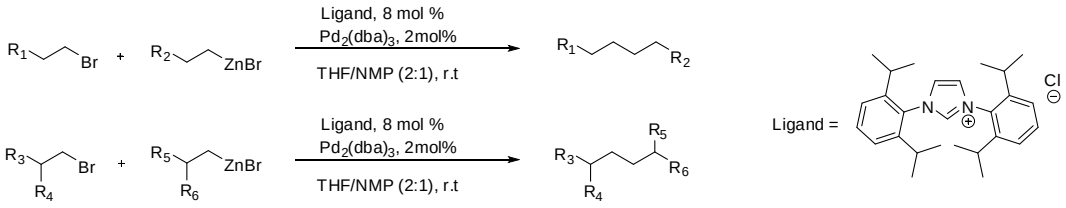

Scheme 1.19

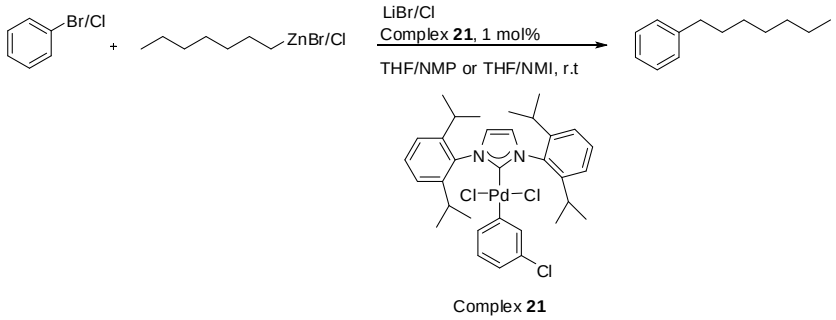

Scheme 1.20

1.3.2.6 Stille Reaction

Stille reaction is another popular reaction used in organic synthesis for the coupling reaction between organo halides and organo tin compounds. Herrmann *et al.* reported the first ever NHC palladium complex catalyzed Stille reaction with complex **22** (Scheme 1.21). [38] Nolan *et al.* subsequently expanded the substrate scope to vinyl stannanes (Scheme 1.22).[39]

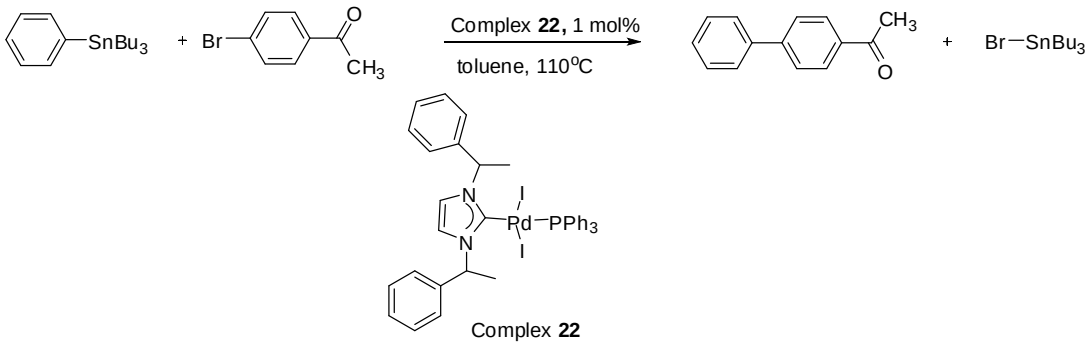

Scheme 1.21

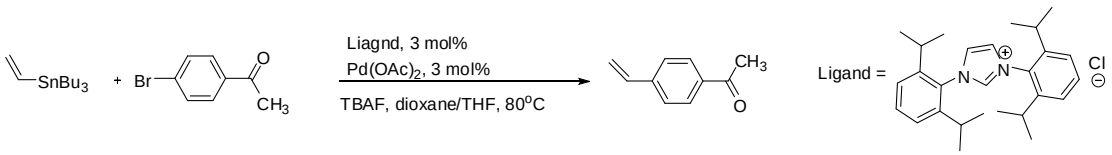

Scheme 1.22

1.3.2.7 Hartwig-Buchwald Amination Reaction

The Hartwig-Buchwald amination reaction is another class of cross coupling reaction that can be mediated by NHC-palladium complexes. Different from the Heck and Suzuki which are C–C coupling reactions, the Hartwig-Buchwald is essentially a C–N coupling reaction whereby an aryl halide is aminated in the presence of a palladium catalyst. Initially, Nolan *et al.* developed a system as shown in Scheme 1.23. Without the hassle of preforming the NHC palladium catalyst, in the presence of free ligand and a palladium source, this system gave the desired product in 98% yield in the presence of the isopropyl derivatized NHC ligand. [40]

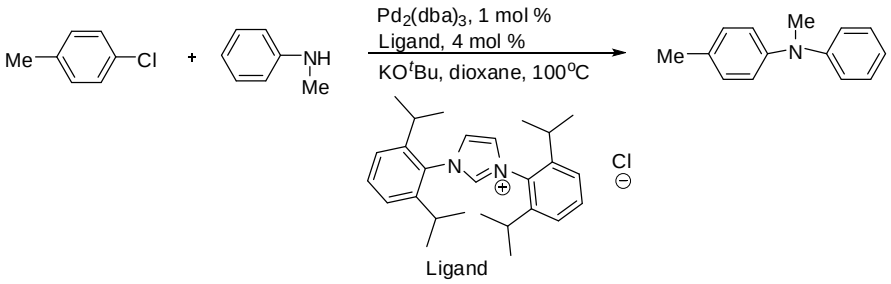

Scheme 1.23

Subsequently, well defined pre formed NHC palladium complexes bearing only 1 NHC ligand in the palladium complexes have also been shown to be able to successfully catalyze the Hartwig-Buchwald reaction.[41]

1.3.3 NHC Palladium Complexes Catalyzed Asymmetric Reactions

Due to the excellent reactivity displayed by the NHC palladium complexes in the cross coupling reactions mentioned above, the selectivity of NHC palladium complexes have also been tested against some asymmetric reactions and they exhibit moderate to excellent selectivity.

1.3.3.1 Asymmetric Intramolecular *α*-arylation of Amides

The ability of NHC palladium complexes to catalyze the asymmetric intramolecular α-arylation of amides was first explored by Hartwig *et al*. They demonstrated that in the presence of ligand **24**, an ee value of 67% is achievable (Scheme 1.24).[42]

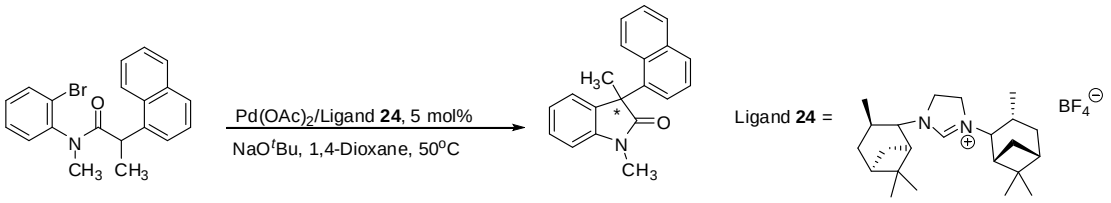

Scheme 1.24

The reaction was further optimized by Kündig *et al.*, who showed that in the presence of bulky ligand **25**, high enantioselectivity of up to 95% ee can be obtained as shown in Scheme 1.25.[43]

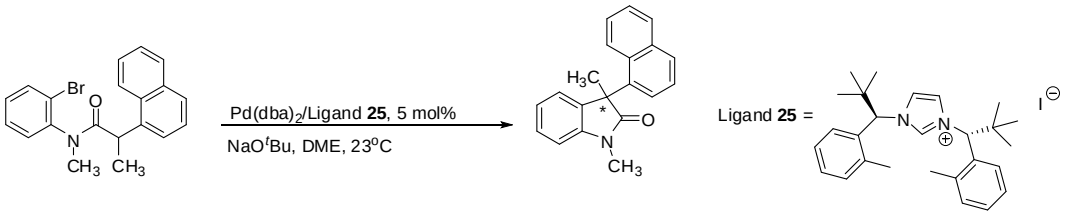

Scheme 1.25

As mentioned in section 1.2.2, ligand **4** can mediate the asymmetric intramolecular α-arylation of amides with ee values of 97%.

1.3.3.2 Asymmetric Addition of Arylboronic Acids to Cyclic Enones

Shi *et al.* was able to achieve ee values of up to 97% with complex **27**. In the course of his study, he indicated that the two halides coordinated to palladium centre had to be replaced by weakly coordinating ligands like

carboxylate groups for effective catalysis. In the absence of these weakly coordinating ligands, the yield of the reaction is at < 5 % (Scheme 1.26).[44]

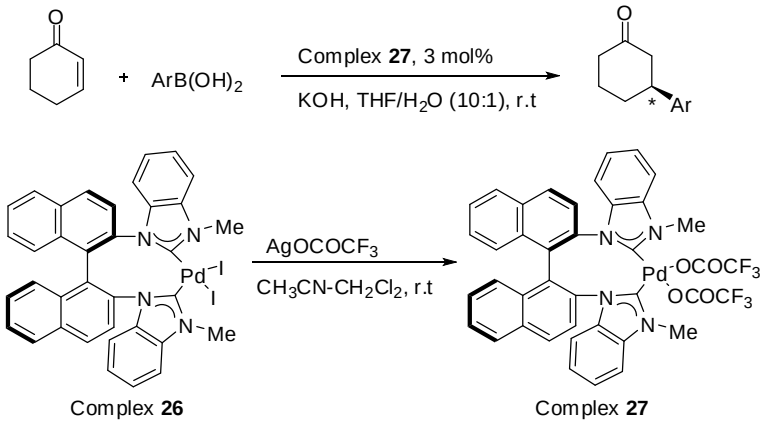

Scheme 1.26

The conditions stated above can also be applied to 2,3-dihydropyridones with achievable ee values of up to >99.5% (Scheme 1.27).[45]

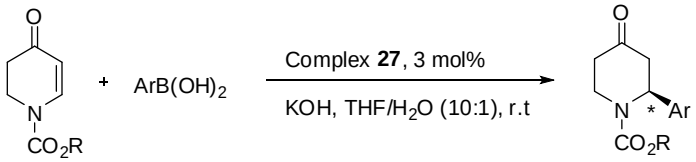

Scheme 1.27

1.3.3.3 Asymmetric Arylation of N–Tosylimines or N–Boc Imines with Arylboronic Acids

After the successful application of BINAP functionalized NHC palladium complexes in the asymmetric addition of arylboronic acids to cyclic enones, Shi *et al.* went on to test out its applications in different asymmetric catalytic reactions. As shown in Scheme 1.28, Shi *et al.* successfully catalyzed

the arylation reaction with up to 99% ee with complex **28a**.[46] When the N–Tosyl group is replaced by N–Boc, the ee values drops slightly to about 90% when complex **28b** was used as the catalyst (Scheme 1.29).[47]

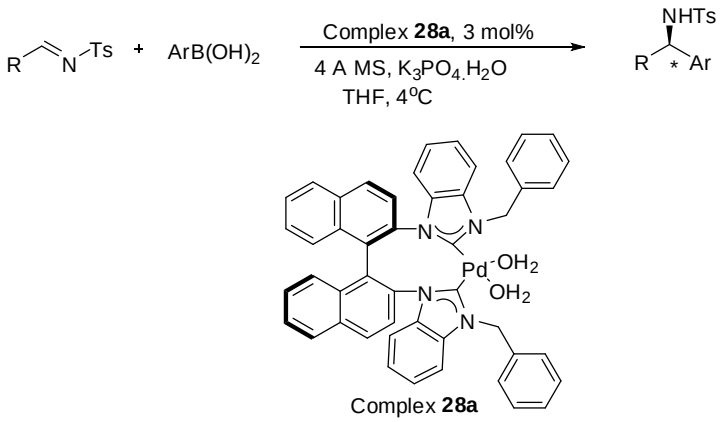

Scheme 1.28

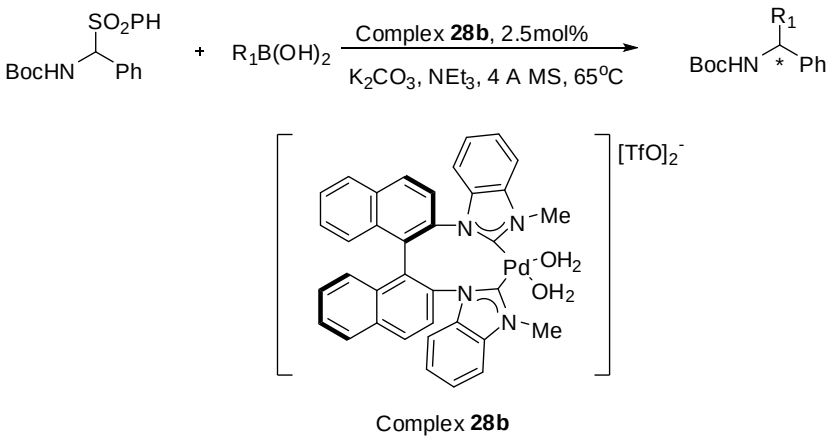

Scheme 1.29

1.3.3.4 Asymmetric Friedel-Crafts Reaction

Shi *et al.* further applied the BINAP functionalised NHC palladium complexes **29** to catalyze the Friedel-Crafts reaction as shown in Scheme 1.30 with moderate ee values of 74%.[48]

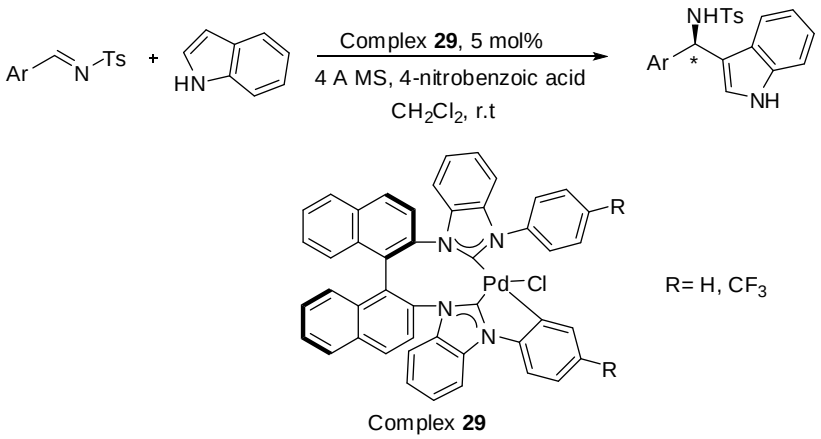

Scheme 1.30

1.3.3.5 Asymmetric Umpolung Allylation of Aldehydes

In the presence of Et_2Zn, NHC palladium complex **30** is able to catalyze the allylation of aldehydes, as shown in Scheme 1.31, with moderate ee values of up to 64%.[49]

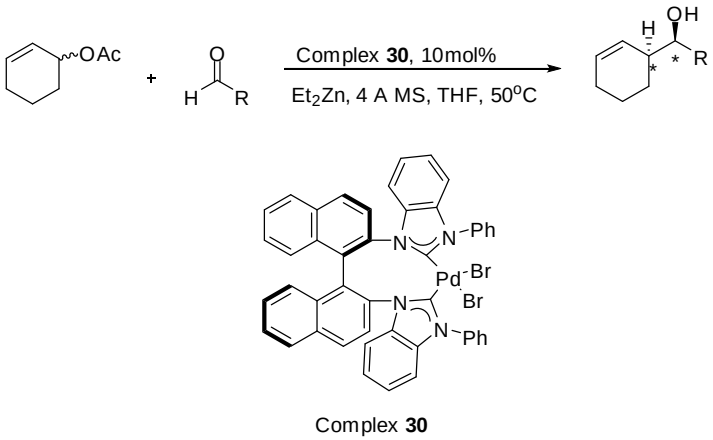

Scheme 1.31

1.3.3.6 Asymmetric Micheal Addition of Cyclic β-keto Esters

Shi *et al.*, as shown in Scheme 1.32, demonstrated that complex **29** can effectively provide ee values of up to 97% in the enantioselective addition of β-keto esters to N-Boc imines.[50]

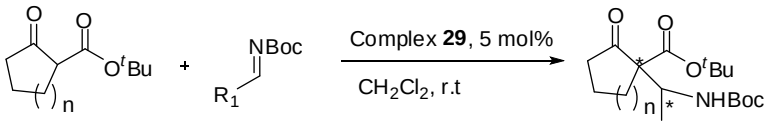

Scheme 1.32

1.3.3.7 Asymmetric Aza-Claisen Rearrangement

Slaugther *et al.* synthesized an acyclic NHC palladium complex **31** and demonstrated its ability to mediate the Aza-Claisen rearrangement reaction with moderate ee values of up to 59% (Scheme 1.33).[51]

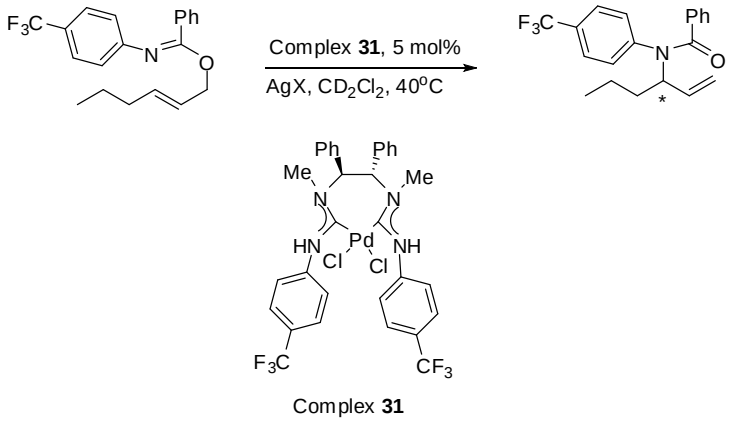

Scheme 1.33

1.3.3.8 Asymmetric Intermolecular Boron Heck-Type Reaction

The potential of NHC palladium complexes to mediate C–C coupling reaction has been previously explored by various groups. For example, the asymmetric Boron-Heck type reaction can be catalyze by tridentate NHC palladium complex **32** with ee values of up to 94% for aliphatic enones and a slightly lower 88% for cyclic enones (Scheme 1.34).[52]

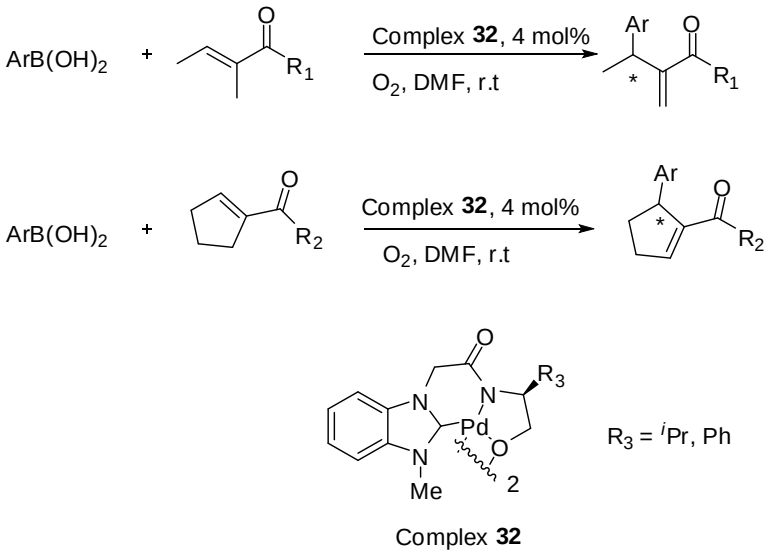

Scheme 1.34

1.3.4 Chiral NHC Palladium Complexes as Catalysts for the Resolution of Secondary Alcohols

NHC palladium complexes were first used by Sigman *et al.* as catalysts for the aerobic kinetic resolution of secondary alcohols.[53] In the presence of chiral amine (-)–sparteine, the usage of either non chiral NHC palladium complexes or chiral NHC complexes can both catalyze the resolution of secondary alcohols successfully with ee values of up to 96% (Scheme 1.35).

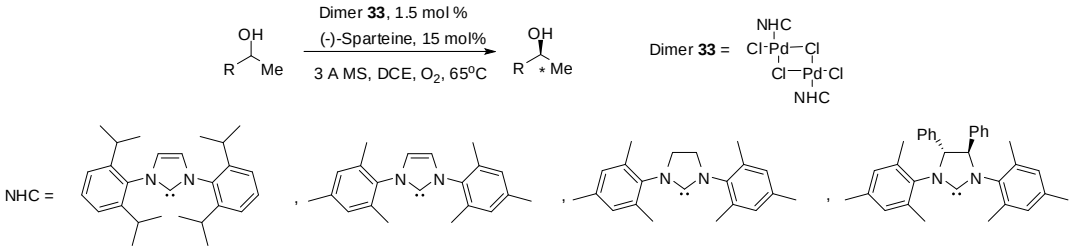

Scheme 1.35

Shi *et al.* who had successfully employed BINAP functionalized NHC palladium complexes in a range of asymmetric reactions, expanded the scope of this group of catalysts to include the resolution of secondary alcohols. Under the optimized conditions, the presence of chiral amine (-)–sparteine is no longer required and excellent ee values of 99% is achievable with either complex **26** or complex **34** (Scheme 1.36).[54]

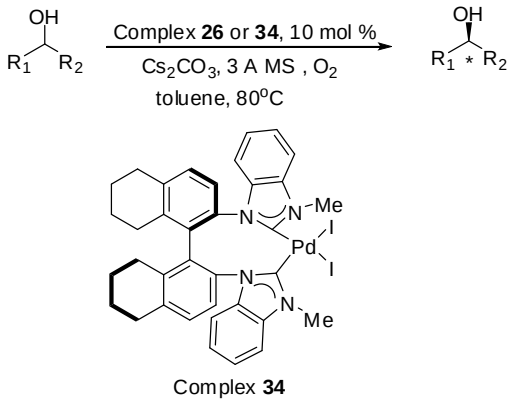

Scheme 1.36

1.3.5 Allylic Substitution Reactions

Allylic substitution is an important class of reactions and they usually serve as a benchmark reaction to test out the reactivity and selectivity of newly

synthesized NHC palladium complexes. The most popular class of allylic substitution reaction is the allylic alkylation reaction as shown in Scheme 1.37.

The versatility of allylic substitution reaction allows the introduction of different nucleophiles into the system to achieve different substituted product. For example, when the introduced nucleophile is an amine, a C–N bond formation can be achieved instead of the formation of a C–C bond. Details of the application of NHC palladium complexes in both achiral and asymmetric allylic substitution reaction will be further elaborated in Chapter 4.

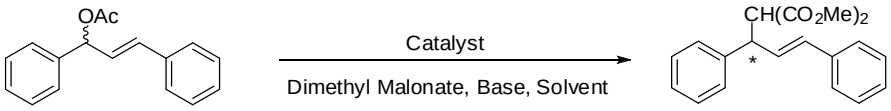

Scheme 1.37

1.4 Conclusion

From humble beginnings as just transient intermediates to possible substitutes to the highly popular and utilized phosphines, NHC have emerged as viable contenders to phosphines and at times even surpassing phosphines in terms of their catalytic capabilities. Numerous literature reports have been dedicated to the search for newer and more efficient methods to synthesize both chiral and achiral NHC, their different metal complexes and their applications. In the following chapters, our quest to contribute to the developing chemistry of NHC will be documented. The synthesis of several novel NHC palladated complexes will be illustrated. A simple methodology will be applied to generate chiral six membered NHC palladium complexes with the chiral centre within

the six membered ring. In the final chapter, the reactivity and the selectivity of the newly synthesized NHC palladium complexes will be tested against the allylic alkylation reaction.

Chapter 2

Cyclopalladated Pyridine-NHC Complexes

2.1 Introduction

As mentioned in the chapter 1, NHC metal complexes have become a popular class of catalysts. Recent efforts have been placed in the synthesis of chelating NHCs metallacycles with oxazolines, S and N donor functionalized NHC bidentate systems. Chelating systems are believed to be able to provide a more rigid environment in the course of catalysis, thereby providing more steric control to induce better selectivity in asymmetric scenario.[55]

2.1.1 Oxazolines Functionalized NHC Bidentate Systems

Oxazolines functionalized NHC bidentate systems are one of the most developed chelating systems. Its popularity can be credited to it being a ready source to introduce chirality into the chelating ring of the bidentate NHC system. Herrmann *et al.* synthesized the first rhodium oxazoline-NHC bidentate metallacycles (complexes **35a-d**) in 1998.[56]

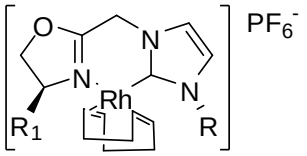

Complexes **35a-35d**

	R_1	R
a	Methyl	Benzyl
b	Methyl	Isopropyl
c	tert-Butyl	Benzyl
d	tert-Butyl	Isopropyl

Following Herrmann's report, Burgess published in 2001 the synthesis of Ir complexes **36a-36d** which can give ee values of up to 98% when they are used in the catalytic asymmetric hydrogenation.[57] Gade subsequently developed

the palladacycle **37** which showed excellent reactivity towards C–C coupling reaction.[58] Oxazoline functionalized NHC metallacycles have proven to be a competent class of complexes in the mediation of a range of asymmetric reactions.[59] In all the cases mentioned above, the oxazoline moiety generally forms metal chelates to the metal centre *via* the N atom preferentially instead of the O atom.

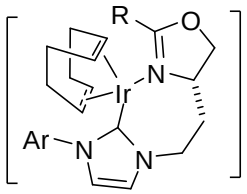

BARF-

Complexes **36a**-**36d**

	R
2a	Ph
2b	Benzyl
2c	*tert*-Butyl
2d	1-Ad

Ar = 2,6-(^{i}Pr)$_2$C$_6$H$_3$

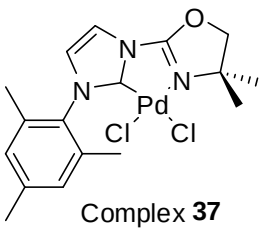

Complex **37**

2.1.2 Sulfur Functionalized NHC Bidentate Systems

Compared to the other classes of functionalized NHC bidentate systems, the sulfur functionalized ones are less common. Only a handful of reports with regards to the synthesis of sulfur functionalized NHC metallacycles have been published.[60]

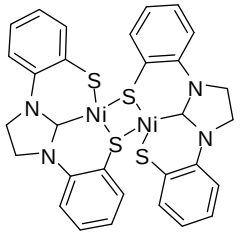

Complex **38**

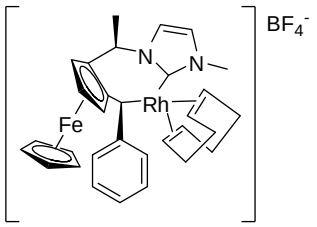

Complex **39**

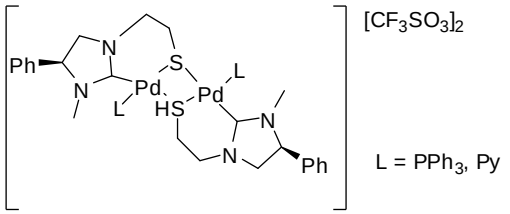

Complex **40**

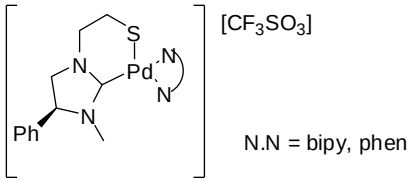

Complex **41**

In 2006, Huynh *et al.* demonstrated the hemilabile character of the sulfur functionalized NHC palladacycle (Scheme 2.1).[61] Upon the introduction of triphenylphosphine, the Pd–S bond will cleave and in turn PPh_3 will coordinate to the Pd metal centre. A hemilabile nature in the catalytic system is much sought after as it can provide another potential coordination site during the course of the catalytic cycle depending on the requirements of catalytic reaction.

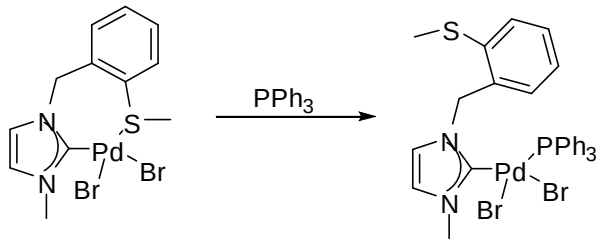

Complex **42** Complex **43**

Scheme 2.1

The excellent reactivity of this class of carbene complexes has also been demonstrated by several groups in different catalytic scenarios.[62] Following the synthesis of a series of sulfur functionalized chiral NHC palladacycles,[63] Fernández *et al.* proceeded to show that excellent enantioselectivity can be achieved by sulfur functionalized NHC palladacycles in his later work.[64] In that report, sulfur functionalized NHC complex **44** displayed remarkable ee values of up to 91 % in the allylic alkylation reaction.

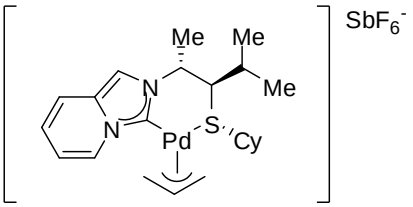

Complex **44**

2.1.3 Nitrogen Functionalized NHC Bidentate Systems

Nitrogen functionalized NHC chelating ligands can be regarded as one of the most popular class of hemilabile NHC ligands. Compared to its sulfur functionalized counterpart, there are many more reports on this class of complexes. Nitrogen functionalized NHC complexes can be broadly classified into 3 main groups; they are the amino, imino and the pyridine functionalized NHC metallacycles. The oxazolines which generally coordinates to the metal *via* its N atom have been previously discussed in section 2.1.1.

Amino functionalized NHC metallacycles are quite a popular class of nitrogen functionalized NHC complexes. Several groups have successfully demonstrated that this class of ligands can be effectively coordinated to

different metal centers and in the case of complex **47**, act as efficient catalysts in hydrosilylation reaction.[65]

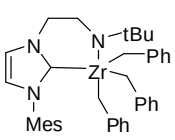

Complex **45**

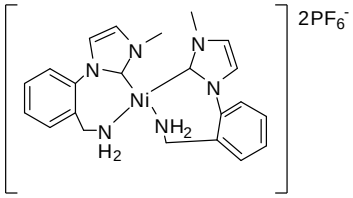

Complex **46**

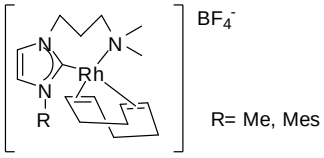

Complex **47**

Palladacycles of amino functionalized NHC chelating ligands have also been explored. [66] Worthy to note is that complex **48** showed remarkable reactivity in asymmetric allylic alkylation reaction giving ee values of up to 80%.

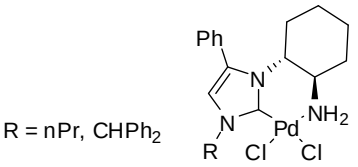

Complex **48**

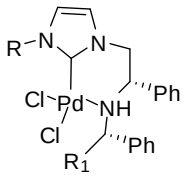

	R	R_1
14a	Mes	Me
14b	2,6-(^{i}Pr)$_2$C$_6$H$_3$	Et

Complex **49 a**-**b**

Palladacycle of the imino derivative of complex **49** have also been characterized and they can provide enantioselectivity of up to 92% in similar asymmetric allylic alkylation reaction.[67]

Pyridine functionalized NHC metallacycles can be further subcategorised into the bidentate and tridentate systems. The tridentate systems are commonly referred to as the pincer systems. Similar to the other N functionalized systems, the pyridine functionalized bidentate systems can coordinate to different metal centres and exhibited good reactivities in different

catalytic reactions. [68] For example, complex **50** is able to catalyze allylic alkylation as well as allylic amination reactions.

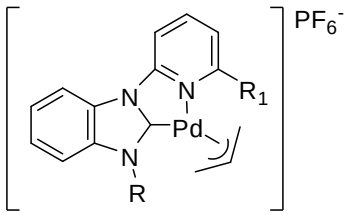

Complex **50a**-**50d**

	R	R_1
a	2,6-diisopropylphenyl	H
b	CH_3	2.6-diisopropylphenyl
c	2,6-diisopropylphenyl	2,4,6-triisoproplyphenyl
d	CH_3	H

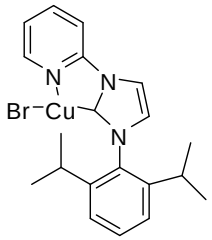

Complex **51**

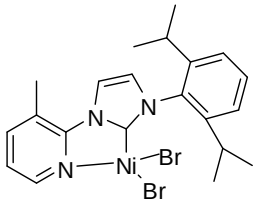

Complex **52**

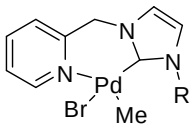

R = tert-Butyl, Mes

Complex **53**

The tridentate systems are commonly referred to as the pincer systems. There have been reports on Cr,[69] Fe[70], Rh[71] and Os[72] tridentate systems, to name a few. Crabtree *et al.* synthesized a series of palladium tridentate complexes **54** and successfully applied them to catalyze the Heck reaction.[73] Four years later, Hahn *et al.* synthesized the analogous benzimidazole complexes **55** which are also effective in catalyzing Heck type reaction.[74]

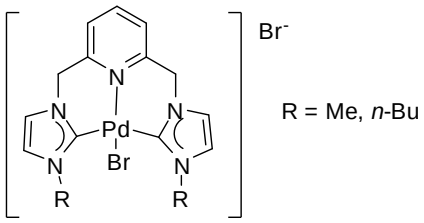

R = Me, *n*-Bu

Complex **54**

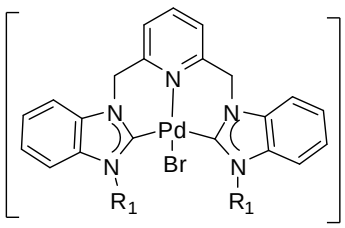

R_1 = Me, Et. *n*-Pr, *n*-Bu

Complex **55**

However, to the best of our knowledge, none of the above mentioned pyridine-NHC palladacycles exhibited any chirality in the carbon chelate backbone. We envisaged that a more rigid chiral chelating system would be more effective in controlling the stereochemistry in an asymmetric reaction scenario. Therefore we sought to synthesis pyridine functionalized NHC palladacycles (±)-**56** to (±)-**59** with a potential chiral centre on the *α* carbon that can be resolved to give chiral palladacycles for asymmetric catalysis mediation. The resolution of the palladacycles and their catalytic ability will be described in subsequent chapters. Palladacycle (±)-**56** and palladacycle (±)-**57** were synthesized in order to compare the electronic and steric effects between the 2 most popular commercially available imidazole and benzimidazole. With asymmetric catalysis in mind, palladacycle (±)-**58** and palladacycles (±)-**59** were synthesized to explore the electronic and more importantly the steric effects of a bulkier R group on the N of the imidazolium ring will have in a chiral environment.

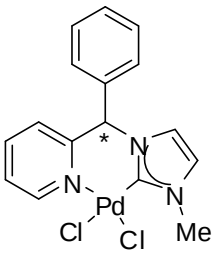

(±)-**56**

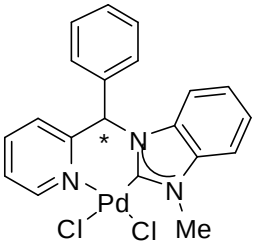

(±)-**57**

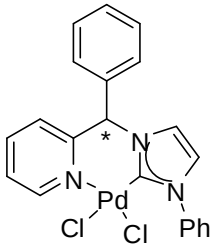

(±)-**58**

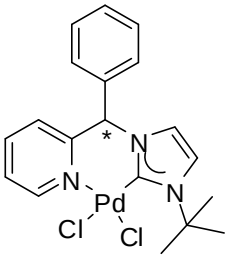

(±)-**59**

2.2 Results and Discussions

2.2.1 Synthesis and Characterisation of Ligand 60

The synthesis of the new pyridine functionalized imidazolium salt **60** was achieved by the initial reduction of the commercially available

2-benzoylpyridine followed by halogenation to give

2-(chloro(phenyl)methyl)pyridine. Subsequent reaction of

2-(chloro(phenyl)methyl)pyridine with 1-methylimidazole yielded the target imidazolium salt **60** as shown in Scheme 2.2. Target intermediate, compound **61** was prepared according to literature method.[75] Compound **61** is isolated as a colorless oil after extraction and solidified into a white solid upon standing. Compound **61** is relatively stable and it can be stored under ambient conditions for up to 3 months without any signs of decomposition. The purity and identity of compound **61** is determined by ^{1}H and ^{13}C NMR, in which both are in agreement with reported literature values.

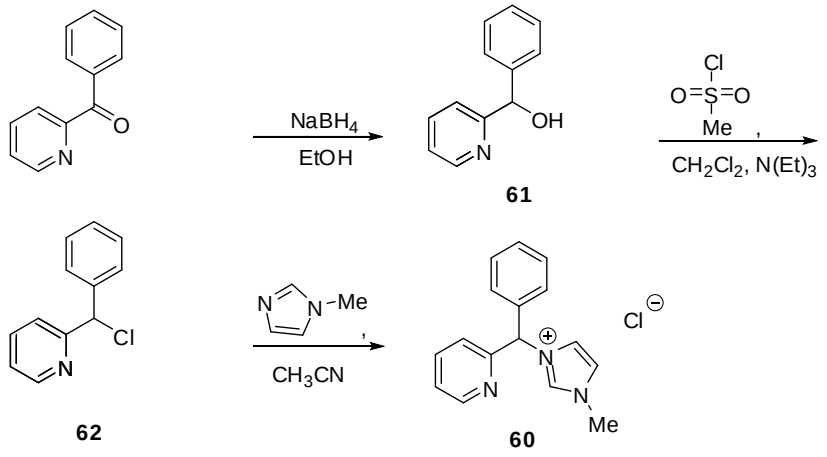

Scheme 2.2

As shown in Scheme 2.2, Phenyl(pyridin-2-yl)methanol **61** was reacted with Methane sulfonyl chloride in the presence of triethylamine in CH_2Cl_2 to give compound **62** in 80 % yield. Compound **62** was isolated in the form of a yellow oil after column chromatography. The identity of compound **62** was confirmed by the presence of its molecular ion peak $[M+H]^+$ at m/z 204.0585 by HRMS (calcd = 204.0580). The ^{1}H NMR chemical shifts of compound **61** and compound **62** were too similar to be distinguishable, therefore ^{13}C NMR spectra were used to determine the conversion of OH into Cl. This is observed in the characteristic upfield shift of the α carbon from δ = 75.15 ppm in compound **61** to δ = 64.58 ppm in compound **62**.

After a 48 hour reflux, compound **60** can be isolated in 70 % yield as a hygroscopic off white solid after 3 successive precipitation from CH_3Cl and diethyl ether. The molecular ion peak $[M-Cl]^+$ at m/z 250.1345 can be observed by HRMS (calad value = 250.1344). The characteristic imidazolium proton peak can be seen in ^{1}H NMR at δ = 10.15 ppm. The wingtip methyl group on the imidazole shows up as a singlet in the ^{1}H NMR at δ = 4.01ppm. The α

proton on the potential chiral centre of the ligand has downfield chemical shift that showed up in the aromatic proton region and was indistinguishable from the other aromatic protons.

2.2.1.1 Synthesis of 1-methyl-3-(phenyl(pyridin-2-yl)methyl)-1H-imidazol-3-ium hexafluorophosphate, Ligand 63

Attempts to obtain the X-ray grade crystals for ligand **60** were unsuccessful. Therefore, the chloride counter anion was changed to hexafluorophosphate to facilitate the crystallization process. The switch in counter anion can be readily achieved from the reaction of ligand **60** which was dissolved in CH_2Cl_2 with a saturated aqueous solution of NH_4PF_6 shown in Scheme 2.3. Ligand **63** can be isolated in the form of an off white filtrate in quantitative yield.

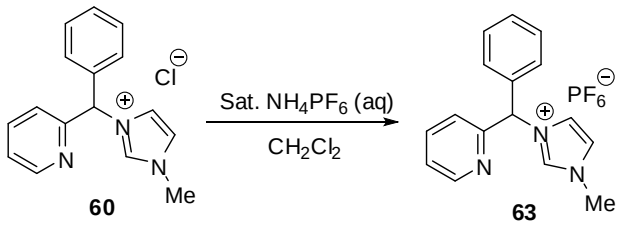

Scheme 2.3

2.2.1.2 Molecular Structure of 1-methyl-3-(phenyl(pyridin-2-yl)methyl)-1H-imidazol-3-ium hexafluorophosphate, Ligand 63

Colourless single crystals of ligand **63** were obtained *via* the slow addition of hexane into a CH_2Cl_2 solution of ligand **63.** The structure of ligand **63** was confirmed crystallographically. However, similar to ligand **60**, ligand **63** is also hygroscopic. The molecular structure and selected bond lengths and angles are presented in Figure 2.1 and Table 2.1, respectively. From the bond lengths of N(1)–C(4), N(2)–C(4) and C(3)–C(2) which are all approximately 1.33 Å, it is evident that the positive charge delocalized over the entire five membered imidazole ring which arise from the resonance structures as illustrated in Scheme 2.4. Therefore, offering the cationic ligand additional stability.

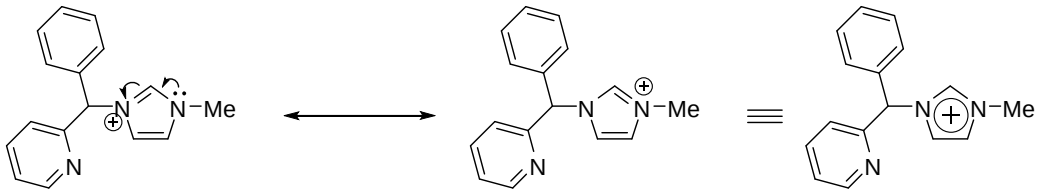

Scheme 2.4

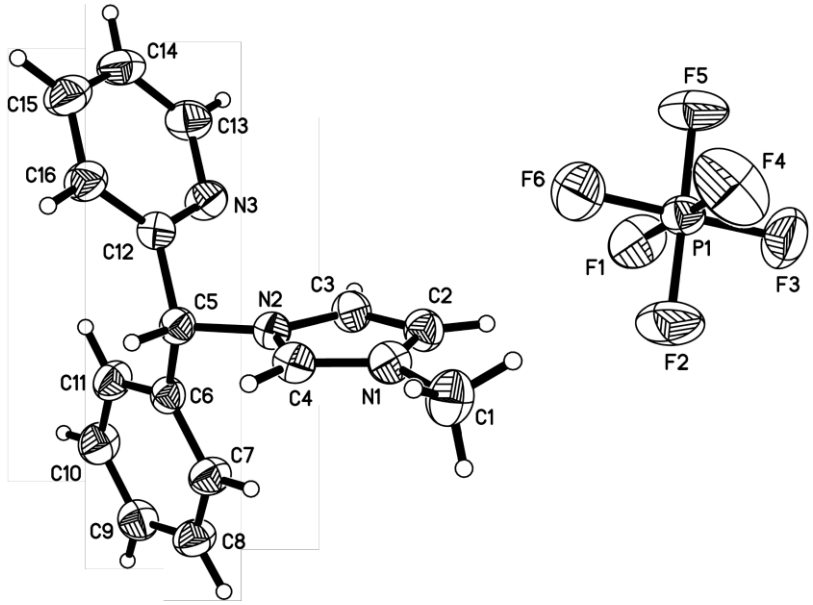

Figure 2.1 Molecular structure of ligand **63** with thermal ellipsoids at 50% probability

Table 2.1 Selected bond lengths (Å) and angles (°) for racemic ligand **63**

N(2)–C(4)	1.334(2)	N(2)–C(3)	1.384(2)
N(2)–C(5)	1.484(2)	N(1)–C(1)	1.470(3)
N(1)–C(4)	1.331(3)	N(1)–C(2)	1.380(3)
C(3)–C(2)	1.331(3)	N(3)–C(13)	1.349(3)
N(3)–C(12)	1.341(2)	N(2)–C(5)–C(12)	110.1(15)
N(3)–C(12)–C(5)	116.7(17)	C(12)–N(3)–C(13)	116.9(18)

2.2.2 Synthesis and Characterisation of Racemic Cyclopalladated Complex (±)-56

2.2.2.1 Synthesis of Racemic Cyclopalladated Complex (±)-56

The imidazolium salt **60** was then subjected to the transmetalation method developed by Lin *et al.* to give the racemic palladacyclic complex (±)-**56** as presented in Scheme 2.5.[76] The silver complex **64** was generated *in situ* and its formation was confirmed by the disappearance of the characteristic imidazolium proton peak at δ 10.15 in ^{1}H NMR. The crude silver complex was filtered through a short plug of celite and was immediately subjected to the proceeding step to yield complex (±)-**56** as yellow solid in 61% yield after precipitation from a concentration reaction mixture in diethyl ether.

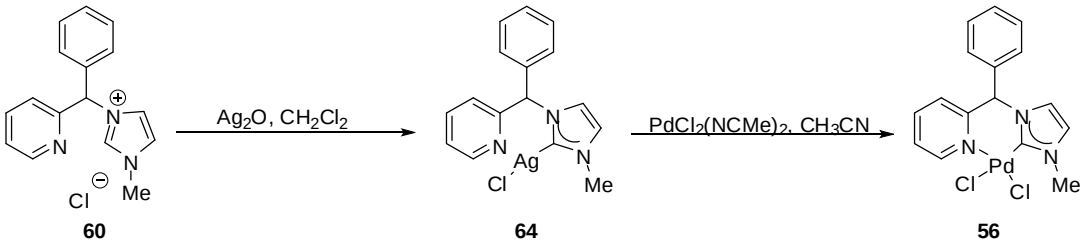

Scheme 2.5

2.2.2.2 Molecular Structure of Racemic Cyclopalladated Complex (±)-56

The solubility of the palladium complex (±)-**56** posed the main challenge in the course of the synthesis. Complex (±)-**56** was found to be insoluble in an array of organic solvents like CH_2Cl_2 and $CHCl_3$; sparingly

soluble in more polar solvents like tetrahydrofuran (THF), acetonitrile (CH_3CN) and methnol (MeOH); and was only completely soluble in dimethyl sulfoxide (DMSO). Due to the poor solubility of complex (±)-**56**, it is necessary to add a few drops of DMSO to the MeOH solution to enable complex (±)-**56** to be completely soluble in the solvent. X-ray crystallography grade single crystals of complex (±)-**56** can then be obtained *via* slow diffusion of diethyl ether into a solution of complex (±)-**56** in MeOH and DMSO. An X-ray diffraction study of complex (±)-**56** was performed (Figure 2.2) and the selected bond lengths and angles are provided in Table 2.2. The X-ray diffraction study of complex (±)-**56** showed that the six-membered ring is in the boat conformation, with the Ph ring in the axial position. The boat conformation of complex (±)-**56** is more evident in the rotated view as seen in Figure 2.3. The Palladium centre adopts a square planar geometry with the tetrahedral distortion angle θ = 5.76 ° between the {N(3)–Pd(1)–C(1)} and {Cl(1)–Pd(1)–Cl(2)} planes (Figure 2.4). The Pd(1)–Cl(1) bond is 0.064 Å longer than the Pd(1)–Cl(2) bond. This can be attributed to the *trans* effect as Cl(1) is *trans* to a strong *trans* directing ligand NHC as compared the Cl(2). There is no significant difference observed in the bond lengths between free ligand **63** and the palladated complex (±)-**56**. The electron density of the double bond is evenly shared between the 2 nitrogen atoms in the imidazole ring as evident from the similar bond lengths of N(2)–C(1) and N(1)–C(1), which are both approximately equal to 1.34 Å. Several interesting features can be observed in the structure of complex (±)-**56**.

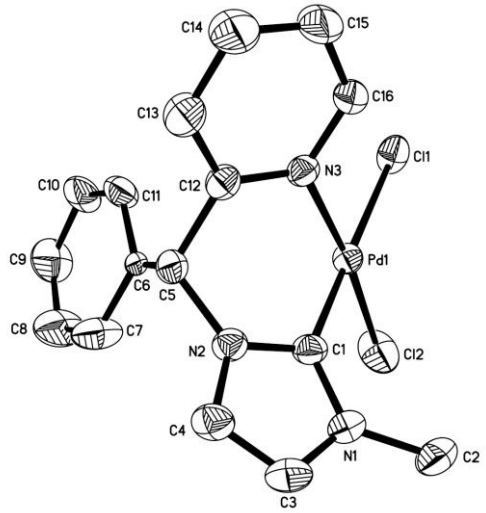

Figure 2.2 Molecular structure of complex (±)-**56** with thermal ellipsoids at 50% probability. Hydrogens are omitted for clarity.

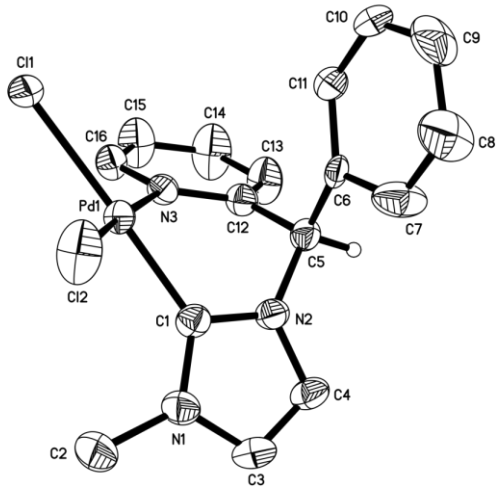

Figure 2.3 Rotated view of complex (±)-**56**

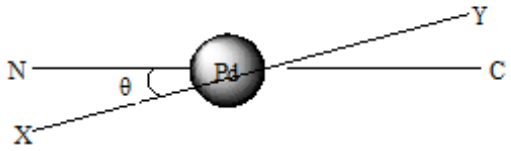

Figure 2.4 Tetrahedral distortion at the palladium centres for the six-membered palladacycles

Firstly, a boat conformation instead of the more stable chair conformation is observed in the six membered ring. This can be attributed to the presence of the numerous sp^2 hybridised atoms in the six membered ring and the planar pyridine and imidazole ring; the angles in the pyridine and imidazole ring will be highly strained in order for complex (±)-**56** to adopt the chair conformation. Therefore, the boat conformation is the preferred and more stable conformation for complex (±)-**56**.

Secondly, the bulkier phenyl ring is in the axial instead of equatorial position. In normal cases, the bulkier group will tend to be in the equatorial position to avoid the unfavourable flagpole steric intereaction between to the 2 axial position in the boat conformation. However in complex (±)-**56**, even if the bulky Ph is in the axial postion, no unfavourable flagpole interaction will be experience by the Ph group since the palladium centre is in a square planar geometry, the chlorides will be pointing away from the Ph group and hence avoiding the steric intereaction as illustrated in Figure 2.5.

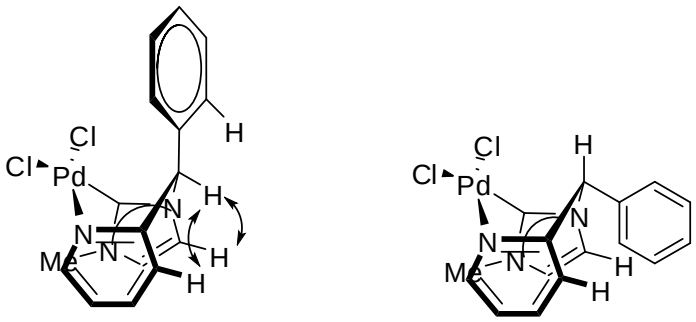

Figure 2.5 Two possible positions of the *α* phenyl group for complex (±)-**56**

Moreover, as seen in Figure 2.5, the Ph group will experience more severe steric interaction with both the pyridine and the imidazole ring if it was to be in the equatorial position. Hence to avoid the unfavourable steric interaction with the pyridine and the imidazole ring, the Ph group in complex (±)-**56** is in the axial instead of the equatorial position where it experiences minimal steric interactions.

Table 2.2 Selected bond lengths (Å) and angles (°) for racemic complex (±)-**56**

Pd(1)–C(1)	1.951(3)	Pd(1)–N(3)	2.055(2)
Pd(1)–Cl(2)	2.310(7)	Pd(1)–Cl(1)	2.374(7)
N(2)–C(1)	1.348(3)	N(2)–C(4)	1.385(3)
N(2)–C(5)	1.472(3)	N(1)–C(1)	1.347(3)
N(1)–C(3)	1.390(4)	N(1)–C(2)	1.470(3)
C(1)–Pd(1)–N(3)	86.2(9)	C(1)–Pd(1)–Cl(2)	90.8(7)
N(3)–Pd(1)–Cl(2)	173.7(6)	C(1)–Pd(1)–Cl(1)	176.6(7)
N(3)–Pd(1)–Cl(1)	91.3(6)	Cl(2)–Pd(1)–Cl(1)	91.8(3)
N(1)–C(1)–Pd(1)	133.8(2)	N(2)–C(1)–Pd(1)	120.8(2)
C(16)–N(3)–Pd(1)	119.7(16)	C(12)–N(3)–Pd(1)	121.1(2)

2.2.2.3 Ring Conformation of Racemic Cyclopalladated Complex (±)-56 in Solution

The conformation of complex (±)-**56** in solution was determined by 2D ^{1}H-^{1}H ROESY NMR (Figure 2.6). The assignment of proton signals was made by a combination of COSY and HMQC. From the key correlations (A) and (B) observed in 2D ^{1}H-^{1}H ROESY NMR, namely between H5–H4 and H5–H13 (protons were numbered in accordance to the carbon numbers that they are directly attached to in Figure 2.2), it can be established that the six membered ring remained locked in the boat conformation with no rotational conformers present in room temperature. A weak correlation (C) can be observed between the phenyl ring and the H4 proton which 3.092 Å away. As illustrated in Figure 2.5, if the Ph group is in the equatorial position, the Ph group will interact with both the pyridine and imidazole ring. These correlations were absent from the 2D ^{1}H-^{1}H ROESY NMR which further confirmed the absence of other rotational conformers and complex (±)-**56** remained locked in the boat conformation with the Ph group in the axial position in solution state.

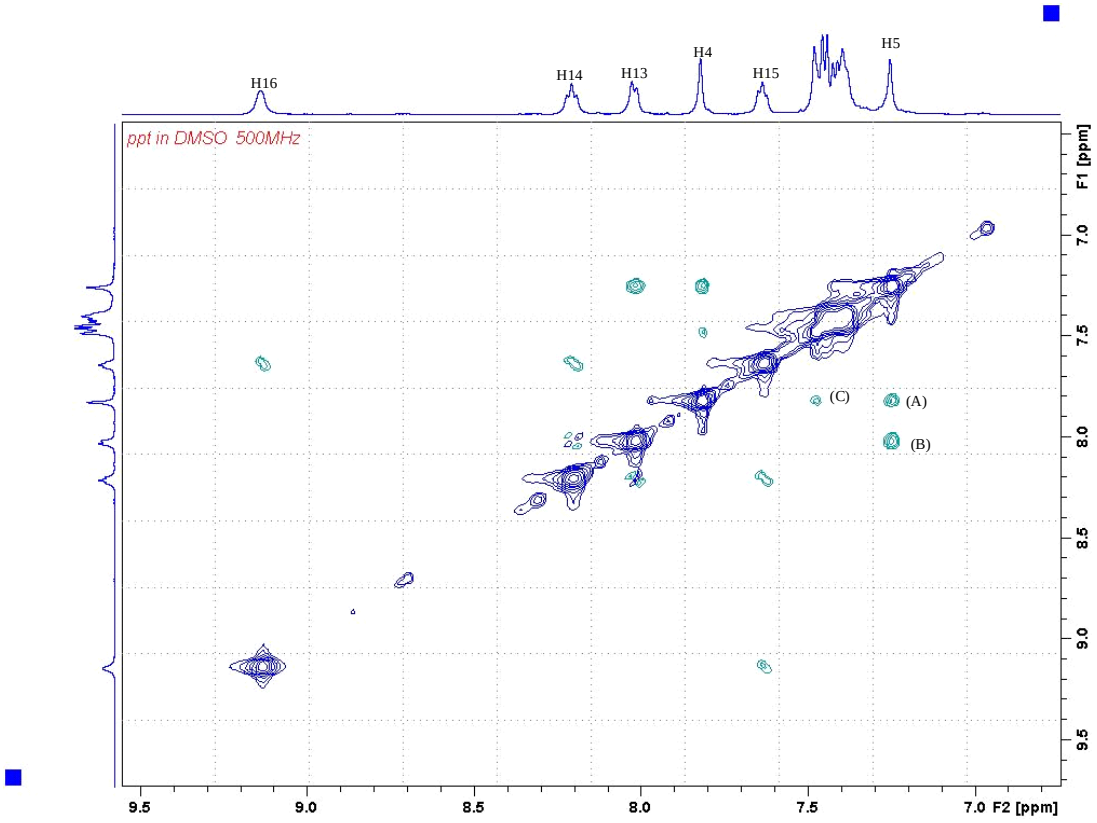

Figure 2.6 2D ^{1}H-^{1}H ROESY NMR of complex (±)-**56**

2.2.3 Synthesis and Characterization of Cyclopalladated Complex (±)-57

2.2.3.1 Synthesis of 1-methyl-3-(phenyl(pyridin-2-yl)methyl)-1H-benzo[d]imidazol-3-ium Chloride, Ligand 65

The synthesis of the common 2-(chloro(phenyl)methyl)pyridine, **62** backbone has been illustrated in Scheme 2.2. Subsequent reaction of compound **62** with commercially available benzimidazole resulted in the formation of our target ligand **65**. Target ligand **65** was isolated in the form of a red oil in 68% yield after 48 hours under refluxing condition as shown in Scheme 2.6. The characteristic benzimidazolium proton peak was observed as a singlet at δ =

11.33 ppm in ^{1}H NMR. The wingtip methyl group on the benzimidazole presents itself as a singlet at δ = 4.31 ppm in ^{1}H NMR. The molecular ion peak $[M\text{-}Cl]^{+}$ at m/z 300.1503 can be observed by HRMS (calcd = 300.1501).

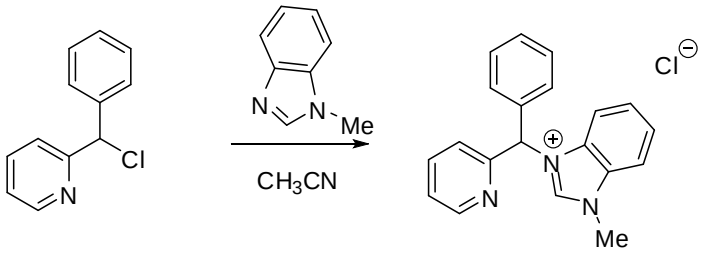

62 **65**

Scheme 2.6

2.2.3.2 Synthesis of Racemic Cyclopalladated Complex (±)-57

Cyclopalladated complex (±)-**57** was synthesized *via* the same method employed in the synthesis of cyclopalladated complex (±)-**56**. Complex (±)-**57** can be isolated in 65% yield in the form of a yellow powder as shown in Scheme 2.7. Similar to the synthesis of complex (±)-**56**, silver complex **66** was generated *in situ*.

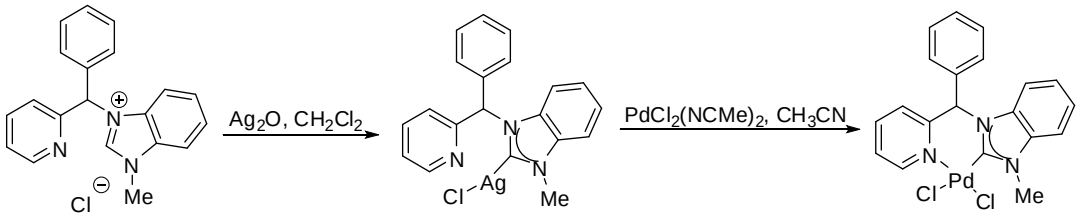

65 **66** **57**

Scheme 2.7

2.2.3.3 Molecular Structure of Racemic Cyclopalladated Complex (±)-57

Complex (±)-**57** proved to be as insoluble as complex (±)-**56**. X-ray grade single crystals of complex (±)-**57** are achieved *via* slow diffusion of diethyl ether into a MeOH/DMSO solution of complex (±)-**57.** Similar to complex (±)-**56**, the X-ray diffraction study of complex (±)-**57** as shown in Figure 2.7 and Figure 2.8 revealed that the six-membered ring of complex (±)-**57** is in the boat confirmation, with the phenyl group occupying the axial position. The selected bond lengths and angles are provided in Table 2.3. Complex (±)-**57** does not exhibit any marked differences in terms of bond lengths and bond angles as compared to its imidazolium analogue complex (±)-**56**. The X-ray crystallography studies revealed that Cl(2) being *trans* to the NHC will experience a stronger *trans* effect as compared to Cl(1) which is *trans* to a N atom. The *trans* effect is evident in the elongation of 0.062 Å in the Pd(1)–Cl(2) bond compared to the Pd(1)–Cl(1) bond. The palladium centre is in a square planar geometry with a small tetrahedral distortion angle θ of 2.55° between the {N(3)–Pd(1)–C(2)} and {Cl(1)–Pd(1)–Cl(2)} planes. The NMe group in the carbene moiety and the six membered CN-chelate are projecting in the opposite side of the square plane.

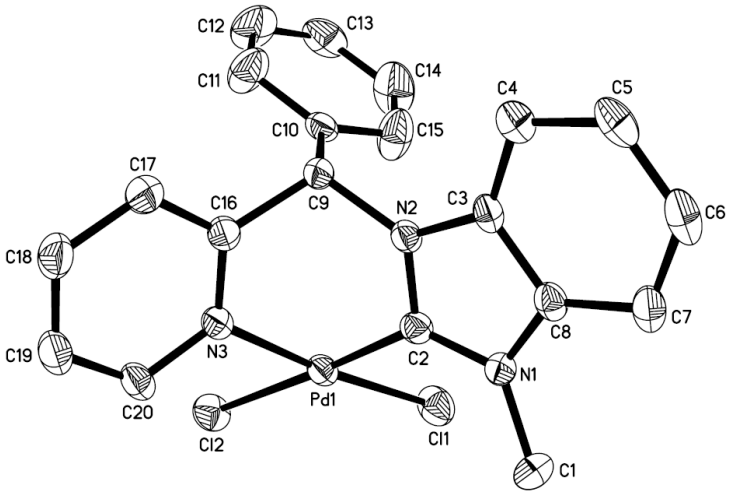

Figure 2.7 Molecular structure of complex (±)-**57** with thermal ellipsoids at 50% probability. Hydrogens are omitted for clarity

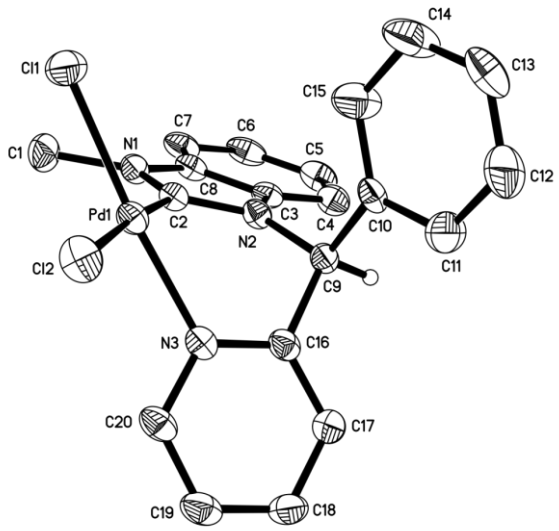

Figure 2.8 Rotated view of the molecular structure of complex (±)-**57**

Table 2.3 Selected bond lengths (Å) and angles (°) for racemic complex (±)-**57**

Pd(1)–C(2)	1.952(3)	Pd(1)–N(3)	2.051(2)
Pd(1)–Cl(1)	2.307(8)	Pd(1)–Cl(2)	2.369(7)
C(2)–N(1)	1.343(3)	C(2)–N(2)	1.351(3)
C(8)–N(1)	1.394(3)	C(3)–N(2)	1.394(3)
C(1)–N(1)	1.463(4)	C(9)–N(2)	1.471(3)
C(2)–Pd(1)–N(3)	85.53(10)	C(2)–Pd(1)–Cl(1)	91.01(8)
N(3)–Pd(1)–Cl(1)	174.71(6)	C(2)–Pd(1)–Cl(2)	175.88(8)
N(3)–Pd(1)–Cl(2)	90.36(6)	Cl(2)–Pd(1)–Cl(1)	93.07(3)
N(1)–C(2)–Pd(1)	133.7(2)	N(2)–C(2)–Pd(1)	119.14(19)
C(16)–N(3)–Pd(1)	121.09(18)	C(20)–N(3)–Pd(1)	118.84(19)

2.2.3.4 Ring Conformation of Racemic Cyclopalladated Complex (±)-57 in Solution

The conformation of complex (±)-**57** in solution was determined by 2D ^{1}H-^{1}H ROESY NMR (Figure 2.9). The assignment of proton signals was made by a combination of COSY, HMQC and HMBC. Figure 2.7 shows the numbering scheme of the protons, with the protons numbered in accordance to their respective carbons. From the key correlation (A) seen in the ROESY NMR, there is a strong interaction between H9–H17 and H9–H4. Therefore, the presence of the complex (±)-**57** in the boat conformation in solution with the phenyl ring in the axial position can be established. In additional, as illustrated in Figure 2.10, if the other isomer with the Ph group in the equatorial position is present in the solution, correlations between the H11-H15 protons with both

the H17 and H4 protons should be observable in the 2D ^{1}H-^{1}H ROESY NMR. However, these correlations were absent in the 2D ^{1}H-^{1}H ROESY NMR. Therefore, it can be concluded that in solution, no rotational conformers were present, complex (±)-**57** remained locked as it was in solid state in the boat conformation with its Ph group in the axial position.

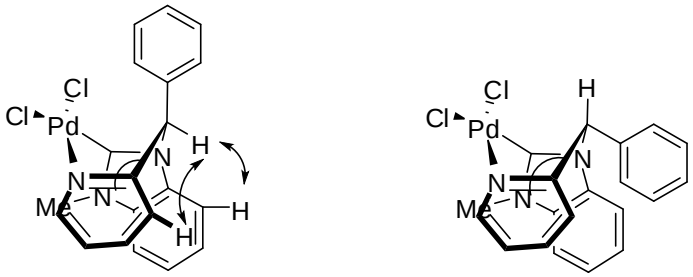

Figure 2.10 Two possible positions of the *α* phenyl group for complex (±)-**57**

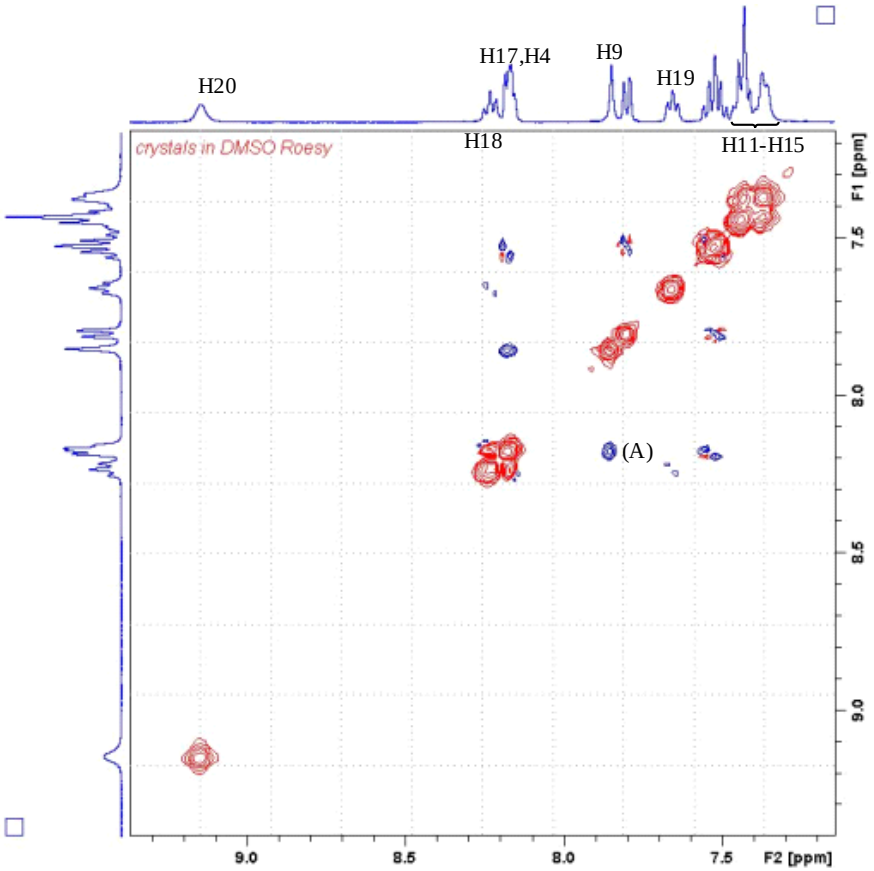

Figure 2.9 2D ^{1}H-^{1}H ROESY NMR of complex (±)-**57**

2.2.4 Synthesis and Characterization of Cyclopalladated Complex (±)-58

2.2.4.1 Synthesis of 1-phenyl-3-(phenyl(pyridin-2-yl)methyl)-1H-imidazol-3-ium Chloride, Ligand 67

Similarly, ligand **67** can be obtained from the reaction of compound **62** with 1-phenylimidazole which was synthesized *via* literature methods.[77] The target ligand **67** in 64% yield can be isolated after 48 hours under refluxing condition in the form of a brown oil as shown in Scheme 2.8. The characteristic benzimidazolium proton peak was observed as a singlet at δ = 11.18 ppm in ^{1}H

NMR. The molecular ion peak $[M–Cl]^+$ at m/z 312.1501 can be observed by HRMS (calcd = 312.1501).

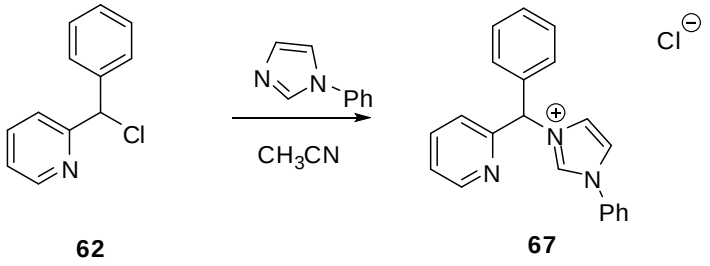

62 **67**

Scheme 2.8

2.2.4.2 Synthesis of Racemic Cyclopalladated Complex (±)-58

Cyclopalladated complex (±)-**58** was synthesized *via* the same method employed in the synthesis of cyclopalladated complex (±)-**56**. Complex (±)-**58** can be isolated in 65% yield in the form of a yellow powder as shown in Scheme 2.9. Upon palladation, a general downfield shift is observed in the ^{1}H proton NMR of complex (±)-**58** as compared to ligand **67**. The chemical shift of the α proton experienced a downfield coordination shift of 0.71 ppm from δ = 6.65 ppm to δ = 7.36 ppm.

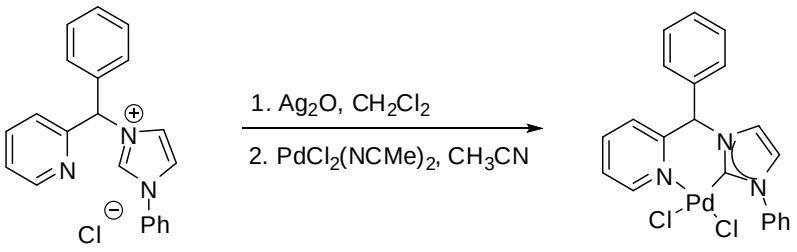

67 **58**

Scheme 2.9

2.2.4.3 Molecular Structure of Racemic Cyclopalladated Complex (±)-58

Complex (±)-**58** is as insoluble as the previously described complex (±)-**56** and complex (±)-**57.** X-ray grade single crystals of complex (±)-**58** are achieved *via* slow diffusion of diethyl ether into a MeOH/DMSO solution of complex (±)-**58.** As illustrated in Figure 2.11 and Figure 2.12, the X-ray diffraction study of complex (±)-**58** revealed that the six-membered ring of complex (±)-**58** is in the boat confirmation, with the phenyl group occupying the axial position. The selected bond lengths and angles are provided in Table 2.4. Complex (±)-**58** does not exhibit any marked differences in terms of bond lengths and bond angles as compared to its imidazolium analogue complex (±)-**56**. Cl(2) being *trans* to the NHC will experience a stronger *trans* effect as compared to Cl(1) which is *trans* to a the $N_{pyridine}$ atom. The *trans* effect is evident in the elongation of 0.068Å in the Pd(1)–Cl(2) bond compared to the Pd(1)–Cl(1) bond. The palladium centre is in a square planar geometry with minimal tetrahedral distortion angle θ of 0.16° between the {N(3)–Pd(1)–C(7)} and {Cl(1)–Pd(1)–Cl(2)} planes. Similar to complex (±)-**57**, the NPh group in the carbene moiety and the CN chelate in complex (±)-**58** is also projecting in the opposite side of the square planar palladium centre. Due to the bulkiness of the Ph group in complex (±)-**58** the NPh group is tilted at 42.8° away from the plane of the imidazole ring to avoid any unfavourable steric interaction with the Cl(1).

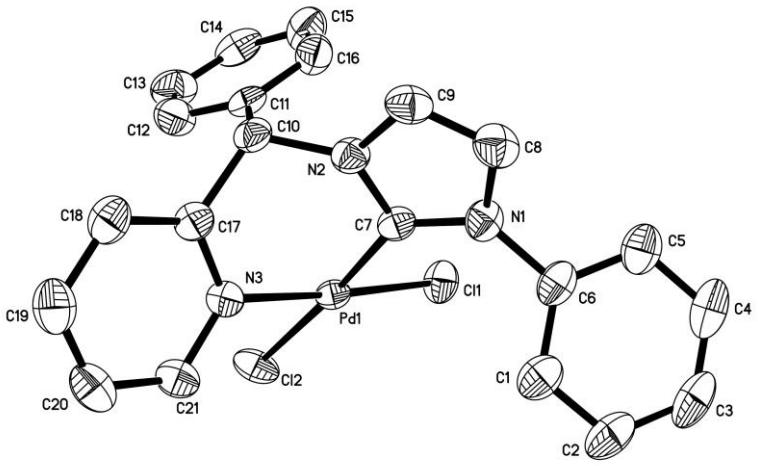

Figure 2.11 Molecular structure of complex (±)-**58** with thermal ellipsoids at 50% probability. Hydrogens are omitted for clarity.

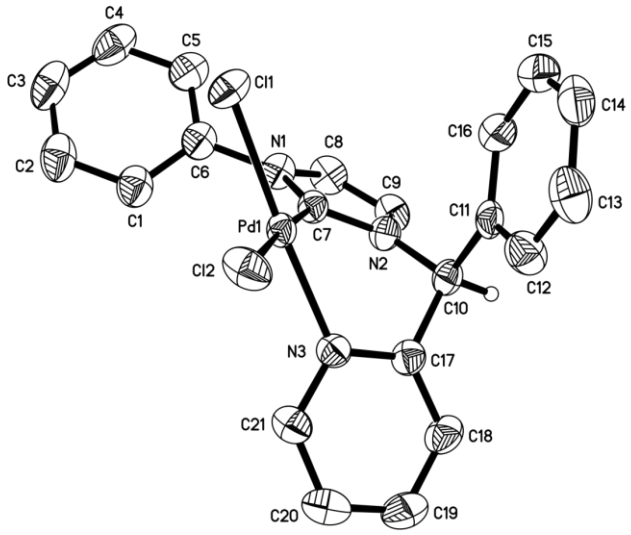

Figure 2.12 Rotated view of the molecular structure of complex (±)-**58**

Table 2.4 Selected bond lengths (Å) and angles (°) for racemic complex (±)-**58**

Pd(1)–C(7)	1.963(3)	Pd(1)–N(3)	2.052(2)
Pd(1)–Cl(1)	2.287(8)	Pd(1)–Cl(2)	2.355(8)
C(7)–N(2)	1.350(3)	C(7)–N(1)	1.347(4)
C(9)–N(2)	1.371(4)	C(8)–N(1)	1.396(4)
C(10)–N(2)	1.471(4)	C(6)–N(1)	1.438(4)
C(7)–Pd(1)–N(3)	86.06(10)	C(7)–Pd(1)–Cl(1)	91.81(8)
N(3)–Pd(1)–Cl(1)	176.64(7)	C(7)–Pd(1)–Cl(2)	176.05(9)
N(3)–Pd(1)–Cl(2)	90.78(7)	Cl(2)–Pd(1)–Cl(1)	91.24(3)
N(1)–C(7)–Pd(1)	136.1(2)	N(2)–C(7)–Pd(1)	119.0(2)
C(17)–N(3)–Pd(1)	121.12(19)	C(21)–N(3)–Pd(1)	120.3(2)

2.2.4.4 Ring Conformation of Racemic Cyclopalladated Complex (±)-58 in Solution

The conformation of complex (±)-**58** in solution was determined by 2D ^{1}H-^{1}H ROESY NMR (Figure 2.13). The assignment of proton signals was made by a combination of COSY, HMQC and HMBC. Figure 2.11 shows the numbering scheme of the protons, with the protons numbered in accordance to their respective carbons. The key correlation (A) shows that a strong interaction is present between the H10 and H18 and H10 and H9 protons. This indicated that complex (±)-**58** that is in a boat conformation with the phenyl group in the axial position is present in solution state.

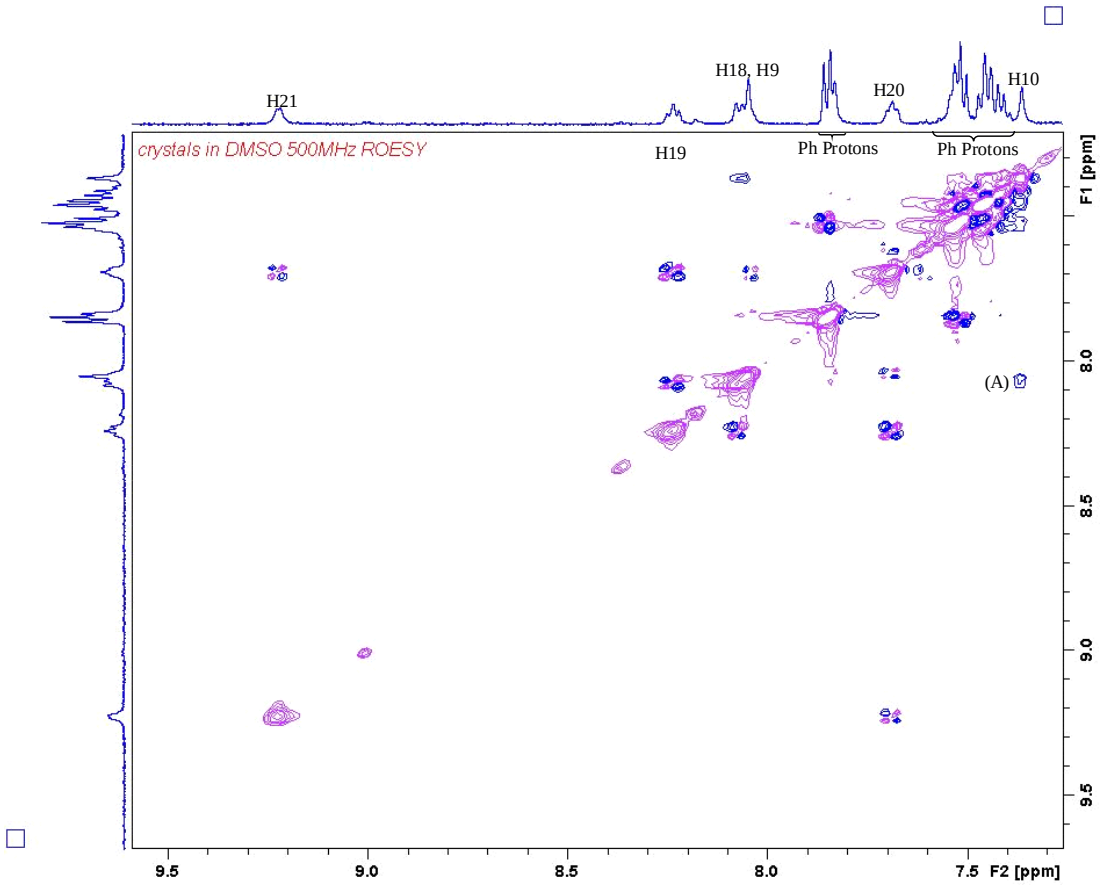

Figure 2.13 2D ^{1}H-^{1}H ROESY NMR of complex (±)-**58**

As shown in Figure 2.14, if the complex (±)-**58** is able to undergo ring flipping, the presence of the other rotational conformer with the *α* phenyl group in the equatorial position should be detected in the 2D ^{1}H-^{1}H ROESY NMR. Although the NMR signals of H12-H16 cannot be assigned conclusively due to overlapping with the H1-H5 protons, however, from the absence of any correlations between the Ph protons with both H18 and H9 in the 2D ^{1}H-^{1}H ROESY NMR, conclusion can be drawn that the other conformation does not exist in solution. Therefore, no rotational conformers are present in solution for complex (±)-**58**.

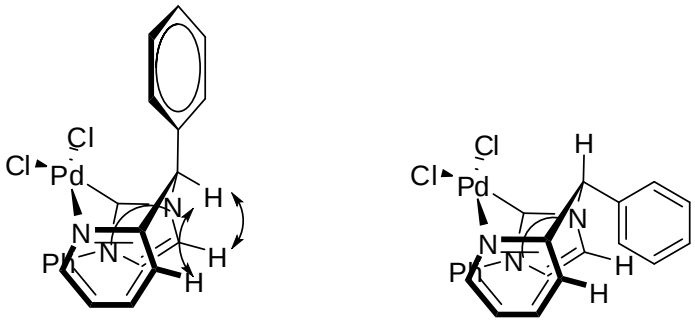

Figure 2.14 Two possible positions of the *α* phenyl group for complex (±)-**58**

2.2.5 Synthesis and Characterization of Cyclopalladated Complex (±)-59

2.2.5.1 Synthesis of Synthesis of Compound 1-tert-butyl-3-(phenyl(pyridin-2-yl)methyl)-1H-imidazol-3-ium Chloride, Ligand 68

Ligand **68** was obtained from the reaction of compound **62** with 1-*tert*butylimidazole which was synthesized *via* literature methods.[78] After 48 hours under refluxing condition, target ligand **68** can be achieved in the form of a brown oil in 60 % yield as shown in Scheme 2.10. The characteristic imidazolium proton peak was observed as a singlet at δ = 11.38 ppm in ^{1}H NMR. The molecular ion peak $[M–Cl]^{+}$ at m/z 292.1811 can be observed by HRMS (calcd = 292.1811I).

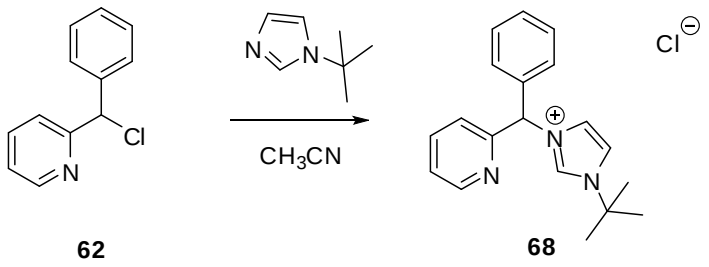

62 **68**

Scheme 2.10

2.2.5.2 Synthesis of Racemic Cyclopalladated Complex (±)-59

Cyclopalladated complex (±)-**59** was synthesized *via* the same method employed in the synthesis of cyclopalladated complex (±)-**56**. Complex (±)-**59** can be isolated in 70% yield in the form of a yellow powder as shown in Scheme 2.11. Upon coordination, a slight downfield coordination shift is observed in the *α* proton.

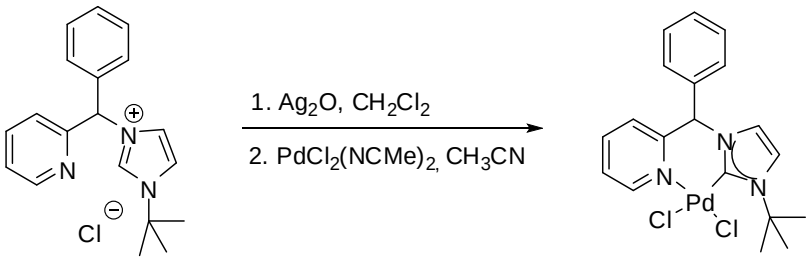

68 **59**

Scheme 2.11

2.2.5.3 Molecular Structure of Racemic Cyclopalladated Complex (±)-59

Complex (±)-**59** exhibited a slightly better solubility in MeOH as compared to all the previously described palladium complexes (±)-**56,** (±)-**57** and (±)-**58** which exhibited limited solubilities in MeOH. However, palladacycle (±)-**59** was still unable to dissolve completely in MeOH and CH_3CN. X-ray grade single crystals of complex (±)-**59** are achieved *via* slow diffusion of diethyl ether into a saturated MeOH solution of complex (±)-**59.** Similar to complex (±)-**56**, the X-ray diffraction study of complex (±)-**59** (Figure 2.15 and 2.16) revealed that the six-membered ring of complex (±)-**59** is in the boat confirmation, with the phenyl group occupying the axial position. The selected bond lengths and angles are provided in Table 2.5. Complex (±)-**59** does not exhibit any marked differences in terms of bond lengths and bond angles as compared to its imidazolium analogue complex (±)-**56**. Similar to all the previously described complexes, Cl(1) being *trans* to the NHC will experience a stronger *trans* effect as compared to Cl(2) which is *trans* to a N atom. The *trans* effect in complex (±)-**59** is the most evident amongst all the palladacycles with the elongation of 0.081 Å in the Pd(1)–Cl(1) bond compared to the Pd(1)–Cl(2) bond. A square planar geometry is adopted by the palladium centre with a tetrahedral distortion angle θ of 3.99° between the {N(1)–Pd(1)–C(13)} and {Cl(1)–Pd(1)–Cl(2)} planes. Similar to the other previously discussed complex (±)-**56**, complex (±)-**57** and complex (±)-**58**, the double bond is delocalized between the 2 nitrogen atoms in the imidazole ring and the

N-*tert*-Bu group and the CN chelate is projecting in the opposite sides of the square plane of the palladium.

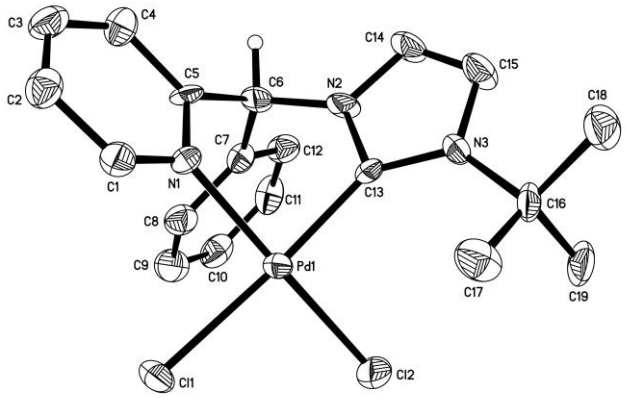

Figure 2.15 Molecular structure of complex (±)-**59** with thermal ellipsoids at 50% probability. Hydrogens except for the H(C6) are omitted for clarity.

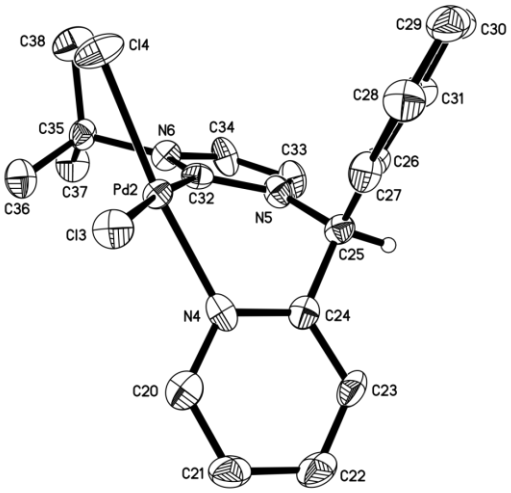

Figure 2.16 Rotated view of complex (±)-**59**

Table 2.5 Selected bond lengths (Å) and angles (°) for racemic complex (±)-**59**

Pd(1)–C(13)	1.963(7)	Pd(1)–N(1)	2.057(6)
Pd(1)–Cl(1)	2.375(19)	Pd(1)–Cl(2)	2.294(2)
C(13)–N(2)	1.374(8)	C(13)–N(3)	1.355(9)
C(14)–N(2)	1.373(8)	C(15)–N(3)	1.394(8)
C(6)–N(2)	1.458(9)	C(16)–N(3)	1.522(8)
C(13)–Pd(1)–N(1)	86.1(3)	C(13)–Pd(1)–Cl(1)	176.2(2)
N(1)–Pd(1)–Cl(1)	90.6(2)	C(13)–Pd(1)–Cl(2)	91.8(2)
N(1)–Pd(1)–Cl(2)	172.1(2)	Cl(2)–Pd(1)–Cl(1)	91.17(8)
N(3)–C(13)–Pd(1)	139.3(5)	N(2)–C(13)–Pd(1)	116.0(5)
C(5)–N(1)–Pd(1)	117.9(5)	C(1)–N(1)–Pd(1)	122.3(5)

2.2.5.4 Ring Conformation of Racemic Cyclopalladated Complex (±)-59 in solution

The conformation of complex (±)-**59** in solution was determined by 2D ^{1}H-^{1}H ROESY NMR (Figure 2.17). The assignment of proton signals were made by a combination of COSY, HMQC and HMBC. Figure 2.15 shows the numbering scheme of the protons, with the protons numbered in accordance to their respective carbons. From the key correlations (A) and (B) from ROESY NMR, this indicated a strong interaction between H6 and H4; H6 and H14 protons. These interactions confirm the existence of boat conformation of complex (±)-**59** with the α Ph in the axial in solution.

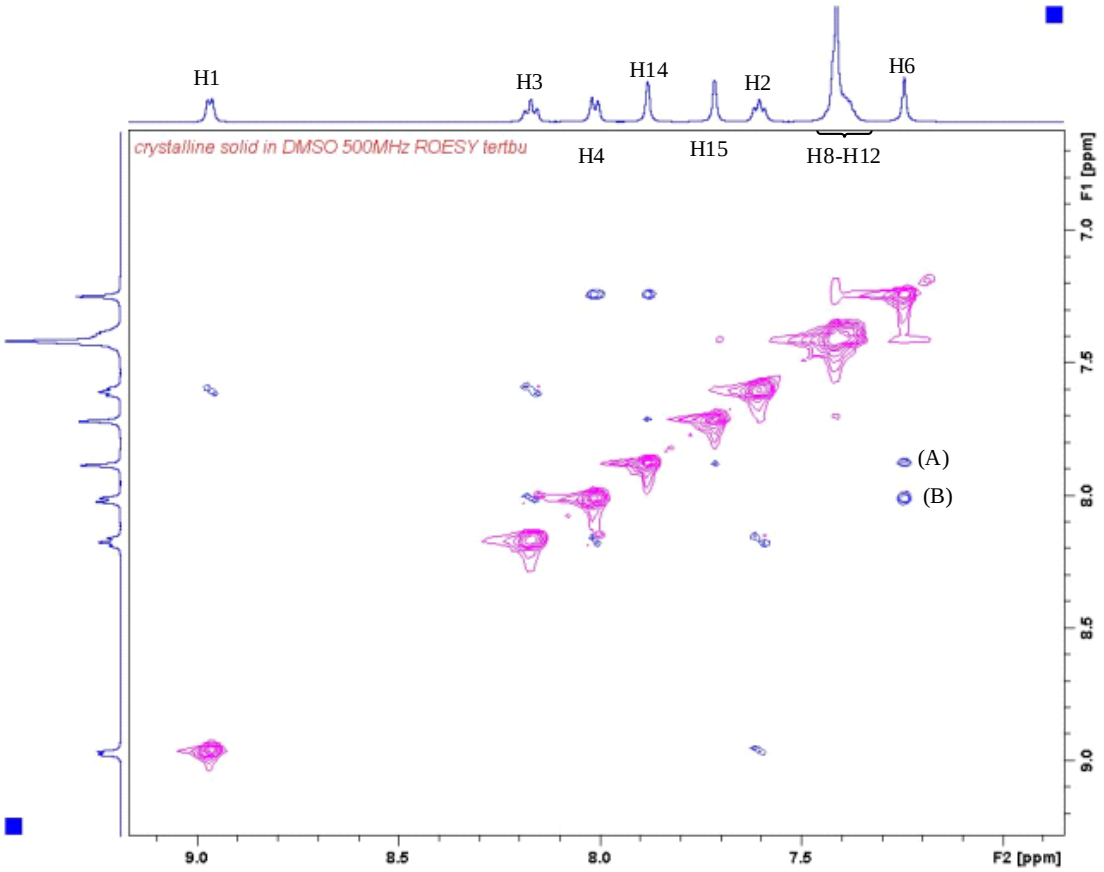

Figure 2.17 2D ^{1}H-^{1}H ROESY NMR of complex (±)-**59**

Furthermore, the absence of the other rotational conformer with the α Ph group in the equatorial position can be confirmed. As depicted in Figure 2.18, the expected correlations between an equatorial *α* Ph with H4 and H14 if the conformer was to exist was not observed in the 2D ^{1}H-^{1}H ROESY NMR. Therefore, the existence of the six membered CN chelate in the boat conformation with the *α* Ph in the axial position as the sole isomer in solution can be established.

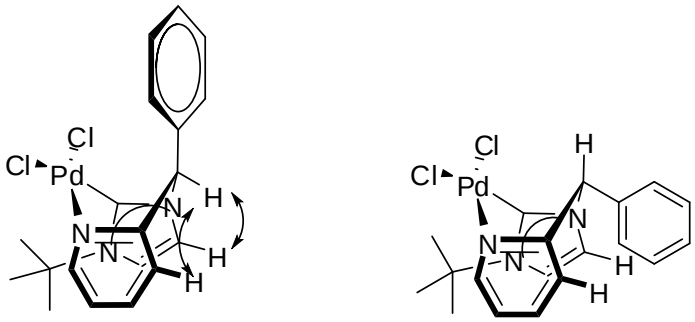

Figure 2.18 Two possible positions of the *α* phenyl group for complex (±)-**59**

2.2.6 Comparison between the Palladacycles based on X-ray crystallography data

In the solid state, the complexes (±)-**56** to (±)-**59** adopt the boat conformation, with the phenyl group on the *α* carbon in the axial position. This can be attributed the presence of the sp^2 hybridized C and N atoms within the six membered ring. From X-ray crystallographic examination of the palladacycles, the following can be observed.

Firstly, upon changing the carbene from imidazolium to benzimidazolium (palladacycle (±)-**56** and palladacycle (±)-**57** respectively), no significant differences can be observed in the bond lengths between the carbene carbon and the palladium centre. The $C_{carbene}$–Pd bond lengths of palladacycles (±)-**56** to (±)-**59** were all within reported literature values.[79] The degree of elongation of the Pd–Cl bond *trans* to the NHC is also comparable between them.

Secondly, upon the introduction of bulkier R groups like phenyl and *tert*-butyl in the case of complex (±)-**58** and complex (±)-**59**, there is a slight

increase of about 0.01 Å in the bond lengths between the carbene carbon and the palladium centers compared to the less bulky Me R groups in palladacycle (±)-**56** and palladacycle (±)-**57**. There is also a very minor increase in the elongation of the Pd–Cl bond length that is *trans* to the NHC in the case of palladacycle (±)-**58** of 0.004 Å compared to palladacycle (±)-**56**. However, in the case of palladacycle (±)-**59**, there is an increase of about 0017 Å compared to its Me analogue palladacycle (±)-**56**. Therefore, from X-ray crystallography, palladacycle (±)-**59** exerts the most significant *trans* effect compared to the rest of the palladacycles.

Thirdly, an increase in the carbene carbon-Pd–Cl (Cl *trans* to the $N_{pyridine}$) bond angle is observed with the increase in the bulkiness of the R group. This can be attributed to the need for the angle enlargement to accommodate the bulkier R groups. All of the above observations had been summarized in Table 2.6.

Table 2.6 Selected bond lengths (Å) and angles (°) for racemic complex (±)-**56** to complex (±)-**59**

Complex	(±)-**56**	(±)-**57**	(±)-**58**	(±)-**59**
Carbene C–Pd / Å	1.951(3)	1.952(3)	1.963(3)	1.963(7)
Pd–Cl bond elongation / Å	0.064	0.062	0.068	0.081
carbene carbon-Pd–Cl / °	90.8(7)	91.01(8)	91.81(8)	91.8(2)

The palladacycles were synthesized for asymmetric catalysis, therefore their ability to maintain their rigid structures in solution is of upmost

importance. Hence, their solution structures were examined *via* 2D ROESY NMR. The 2D ROESY NMR spectrums revealed that all the palladacycles were able to maintain their boat conformation at room temperature with no observable rotational conformers present at room temperature.

2.3 Conclusion

In this chapter, 4 novel achiral palladacycles (±)-**56**, (±)-**57**, (±)-**58** and (±)-**59** were successfully synthesized. The structures and their conformations in solid state had been investigated through single X-ray crystallography and 2D ROESY NMR for their solution state. In both solid and solution states, the palladacycles existed in a boat conformation with the phenyl group in the axial position. All the palladacycles were able to maintain their conformations in solution state. Therefore in a catalytic scenario, the palladacycles will be better able control the environment with will translate to better steric control for the catalysis reactions.

2.4 Experimental

Reactions involving air-sensitive compounds were performed under a positive pressure of purified argon using standard Schlenk techniques. All the commercially available chemicals and solvents were used without prior drying or purification. Phenyl(pyridin-2-yl)methanol **1**, $PdCl_2(NCMe)_2$, 1-phenylimidazole and 1-*tert*-butylimidazole were prepared according to literature methods. Proton nuclear magnetic resonance (^{1}H NMR) and carbon

nuclear magnetic resonance (^{13}C NMR) spectroscopy were performed on a Bruker Avance 300, 400 and 500 NMR spectrometers. The number of protons (n) for a given resonance is indicated by nH. Coupling constants are reported as a J value in Hz. Proton nuclear magnetic resonance spectra ^{1}H NMR are reported as δ in units of parts per million (ppm) downfield from $SiMe_4$ (δ 0.0). Carbon nuclear magnetic resonance spectra ^{13}C NMR are reported as δ in units of parts per million (ppm) relative to the signal of chloroform-*d* (δ 77.20, triplet). All chemical shifts reported are referenced to the chemical shifts of their respective residual solvent resonances. Unless stated otherwise, all NMR experiments are carried out at 300K. Mass spectra were recorded on a Thermo Finnigan MAT 95 XP Mass Spectrometer with EI mode and Waters Q-Tof Premimer Mass Spectrometer with ESI mode. Melting points were determined on SRS-Optimelt MPA-100 apparatus and were uncorrected. Optical rotations were measured on the specified solution in 0.1-dm cell at 25 °C with a Perkin-Elmer model 341 polarimeter. The Elemental Analysis Laboratory of the Division of Chemistry and Biological Chemistry at the Nanyang Technological University of Singapore performed elemental analyses.

2.4.1 Synthesis of Compound 2-(chloro(phenyl)methyl)pyridine, 62

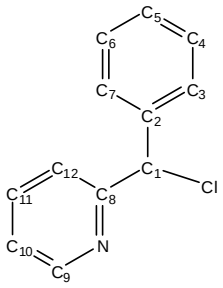

Phenyl(pyridin-2-yl)methanol **61** (1.85 g, 10.5 mmol) and triethylamine (3.4 mL, 24.4 mmol) in 32 mL of CH_2Cl_2 was stirred in an ice bath. Methane sulfonyl chloride (1.2 mL, 15.8 mmol) was added dropwise to the stirring solution. The reaction mixture was allowed to warm up slowly to room temperature. The reaction mixture was left to stir overnight and was then poured into a saturated aqueous $NaHCO_3$ solution. The aqueous layer was extracted with chloroform. The combined organic layers were washed with H_2O, dried over anhydrous $MgSO_4$ and evaporated *in vacuo* to give a red liquid. The resultant red liquid was subjected to a flash column (ethyl acetate/hexanes=1/4, V/V) to give a yellow oil 1.7g, 80 %. ^{1}H NMR (500 MHz, $CDCl_3$): δ = 6.17 (s, 1H, H1), 7.19–7.22 (m, 1 H, aromatic), 7.26–7.36 (m, 3 H, aromatic), 7.47–7.56 (m, 3 H, aromatic), 7.69–7.72 (m, 1 H, aromatic), 8.57–8.58 (d, 1 H, $J_{H,H}$ = 4.0 Hz, H9) ppm. ^{13}C NMR (100 MHz, $CDCl_3$): δ = 64.58(C1), 122.11 and 122.85 (Ph), 127.81 (C10), 128.31 (C12), 128.67 and 137.0 (Ph), 139.96 (C12), 149.21 (C8), 159.71(C9) ppm. HRMS (ESI) *m/*z: $[M+H]^+$ calcd for $C_{12}H_{10}ClN$ 204.0580, found 204.0585.

2.4.2 Synthesis of 1-methyl-3-(phenyl(pyridin-2-yl)methyl)-1H-imidazol-3-ium Chloride, Ligand 60

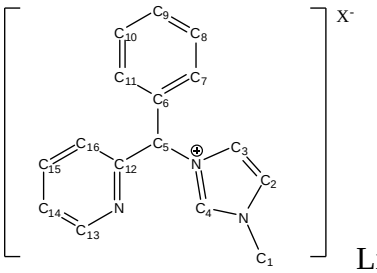

Liquid 1-methylimidazole (1.8 mL, 22.6 mmol) was added to a stirring solution of compound **62** (4.35g, 21.3 mmol) in 50 mL of CH_3CN. The reaction mixture was heated at refluxing temperature for 48 h. The reaction mixture was reduced *in vacuo* and the resulting oil was stirred in diethyl ether. The diethyl ether layer was decanted away to give an off white solid, 4.3g, 70 %. ^{1}H NMR (400 MHz, $CDCl_3$): δ = 4.01 (s, 3 H, H1), 7.25–7.34 (m, 4 H, aromatic), 7.41–7.43 (m, 2 H, aromatic), 7.52 (s, 1 H, aromatic), 7.61–7.64 (m, 2 H, aromatic), 7.68–7.72 (m, 2 H, aromatic), 8.57 (d, 1 H, $J_{H,H}$ = 4.5 Hz, H13), 10.15 (s, 1 H, H4) ppm. ^{13}C NMR (100 MHz, $CDCl_3$): δ = 36.74(C1), 66.06(C5), 121.90 (C2), 122.87(C3), 123.95(C14), 124.71(C16), 129.07, 129.42, 129.56, 136.54, and 137.82 (Ph), 138.63 (C15), 149.60, 155.18 (C13) ppm. HRMS (ESI) *m/z*: $[M\text{-}Cl]^+$ calcd for $C_{16}H_{16}N_3$ 250.1344, found 250.1345.

2.4.3 Synthesis of 1-methyl-3-(phenyl(pyridin-2-yl)methyl)-1H-benzo[d]imidazol-3-ium Chloride, Ligand 65

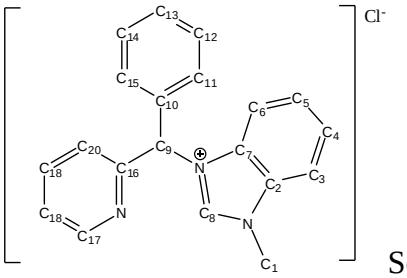

Solid 1-methylbenzimidazole (3.24 g, 24.5 mmol) was added to a stirring solution of compound **62** (5.00g, 24.5 mmol) in 50 mL of CH_3CN. The reaction mixture was heated at refluxing temperature for 48 h. The reaction mixture was reduced *in vacuo* and the resulting oil was stirred in diethyl ether. The diethyl ether layer was decanted away to give an off white solid, 5.3g, 64 %. ^{1}H NMR (400 MHz, $CDCl_3$): δ = 4.30 (s, 3 H, H1), 7.31–7.34 (m, 1 H, H18), 7.39–7.44 (m, 5 H, aromatic), 7.46–7.48 (m, 1 H, aromatic), 7.56–7.61 (m, 2 H, aromatic), 7.65–7.67 (m, 2 H, aromatic), 7.76–7.78 (m, 1 H, aromatic), 7.84 (t, 1H, $J_{H,H}$ = 3.9 Hz, aromatic), 8.56 (d, 1H, $J_{H,H}$ = 4.2 Hz, H17), 11.33 (s, 1 H, H8) ppm. ^{13}C NMR (100 MHz, $CDCl_3$): δ = 33.99(C1), 67.23(C9), 112.56, 116.16, 124.27, 124.77, 126.95, 127.07, 128.98, 129.61, 129.72, 131.57, 132.51, 134.87, 138.15, 144.27, 149.97 and 154.73 (aromatic), 155.93 (C17) ppm. HRMS (ESI) *m/*z: $[M\text{-}Cl]^+$ calcd for $C_{16}H_{16}N_3$ 300.1501, found 300.1503.

2.4.4 Synthesis of 1-phenyl-3-(phenyl(pyridin-2-yl)methyl)-1H-imidazol-3-ium Chloride, Ligand 67

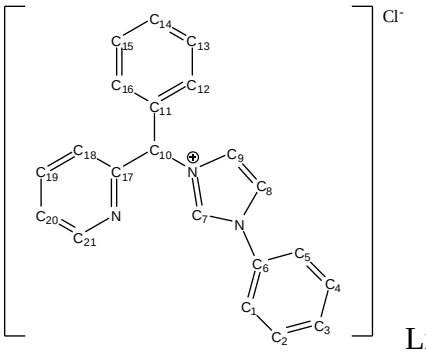

Liquid 1-phenylimidazole (3.24 g, 24.5 mmol) was added to a stirring solution of compound **62** (5.00g, 24.5 mmol) in 50 mL of CH_3CN. The reaction mixture was heated at refluxing temperature for 48 h. The reaction mixture was reduced *in vacuo* and the resulting oil was stirred in diethyl ether. The diethyl ether layer was decanted away to give an off white solid, 5.3g, 64 %. ^{1}H NMR (400 MHz, $CDCl_3$): δ = 6.65 (s, 1 H, aromatic), 7.35–7.37 (m, 3 H, aromatic), 7.42–7.52 (m, 3 H, aromatic), 7.56–7.58 (m, 2 H, aromatic), 7.68–7.76 (m, 5 H, aromatic), 7.92 (s, 1 H, aromatic), 8.17 (s, 1 H, H10), 8.59 (d, 1 H, $J_{H,H}$ = 4.7 Hz, H21), 11.18 (s, 1 H, H7) ppm. ^{13}C NMR (100 MHz, $CDCl_3$): δ = 65.97 (C10), 116.26 (C9), 119.64 (C8), 121.78 (C20), 123.52 (C18), 123.90, 124.87, 129.20, 129.35, 129.51, 130.26, 130.64, 134.58, 136.19, 136.46 and 137.80 (Ph), 149.47 (C19) and 150.10 (Ph), 155.06 (C21) ppm. HRMS (ESI) *m/*z: $[M\text{-}Cl]^+$ calcd for $C_{21}H_{18}N_3$ 312.1501, found 312.1501.

2.4.5 Synthesis of 1-*tert*-butyl-3-(phenyl(pyridin-2-yl)methyl)-1H-imidazol-3-ium Chloride, Ligand 68

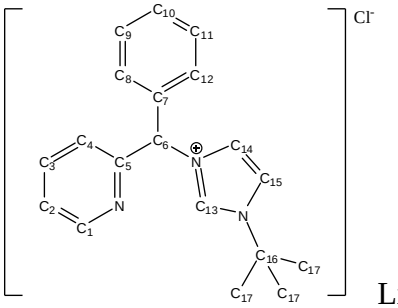

Liquid 1-*tert*-butylimidazole (5.00 g, 40.3 mmol) was added to a stirring solution of compound **62** (8.21g, 40.3 mmol) in 100 mL of CH_3CN. The reaction mixture was heated at refluxing temperature for 48 h. The reaction mixture was reduced *in vacuo* and the resulting oil was stirred in diethyl ether. The diethyl ether layer was decanted away to give a brown solid, 7.9 g, 60 %. ^{1}H NMR (400 MHz, $CDCl_3$): δ = 1.72 (s, 9 H, H17), 7.18 (s, 1 H, aromatic), 7.28–7.55 (m, 1 H, aromatic), 7.33–7.38 (m, 3 H, aromatic), 7.52–7.55 (m, 2 H, aromatic), 7.74 (td, 1 H, $J_{H,H}$ = 7.7 Hz, $J_{H,H}$ = 1.6 Hz, aromatic), 7.81–7.83 (m, 2 H, aromatic), 8.19 (s, 1 H, aromatic), 8.59 (d, 1 H, $J_{H,H}$ = 4.5 Hz, H1), 11.38 (s, 1 H, H13) ppm. ^{13}C NMR (100 MHz, $CDCl_3$): δ = 29.90 (C17), 60.01 (C16), 65.15(C6), 118.81 (C15), 122.41 (C14), 123.48 (C2), 124.42 (C4), 128.68, 128.92, 135.76 and 136.82 (Ph), 137.30 (C3), 149.30, 155.26 (C1) ppm. HRMS (ESI) *m/*z: $[M\text{-}Cl]^+$ calcd for $C_{19}H_{22}N_3$ 292.1814, found 292.1811.

2.4.6 Synthesis of Racemic Palladacycle (±)-56

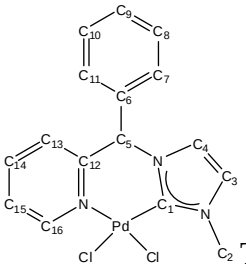

To a solution of compound **60** (3.57g, 12.5 mmol) in 30 mL of CH_2Cl_2, Ag_2O (1.59g, 6.9 mmol) was added in the dark. The reaction mixture was allowed to stir at room temperature for 12 hours and was filtered through celite. A $PdCl_2(NCMe)_2$ suspension (3.24g, 12.5 mmol in 100 mL of CH_3CN) was added to the filtrate in the dark. The reaction mixture was then allowed to stir overnight at room temperature and was filtered through a short plug of celite the next day. The filtrate was reduced *in vacuo* to approximately 50 mL and diethyl ether (200 mL) was added which resulted in the precipitation of an orange-yellow solid 3.3g, 61 %. M.p. = 249.2 – 249.8°C (dec.). ^{1}H NMR (400 MHz, DMSO-d_6): δ = 3.97 (s, 3 H, H2), 7.26 (s, 1 H, H5), 7.33–7.47 (m, 6 H, Ph), 7.62 (t, 1 H, H15), 7.84 (s, 1 H, H4), 8.02 (d, 1 H, $J_{H,H}$ = 7.6 Hz, H13), 8.20 (t, 1 H, H14), 9.12 (d, 1 H, $J_{H,H}$ = 5.6 Hz, H16) ppm. ^{13}C NMR (100 MHz, DMSO-d_6): δ = 37.86 (C2), 66.46 (C5), 122.41 (C3), 124.11 (C4), 125.10 (C15), 126.34 (C13), 126.98, 128.29, 128.78, 138.19 and 140.45 (Ph), 150.37 (C14), 154.60, 155.10 (C16) ppm. HRMS (ESI) *m/z*: $[M\text{-}CH_3]^+$ calcd for $C_{15}H_{12}Cl_2N_3Pd$ 409.9419, found 409.9417. Anal Calcd for $C_{16}H_{16}Cl_2N_3Pd\text{-}C_4H_{10}O$ (501.77): C, 47.87; H, 5.22; N, 8.37. Found: C, 48.06; H, 5.69; N, 8.38.

2.4.7 Synthesis of Racemic Palladacycle (±)-57

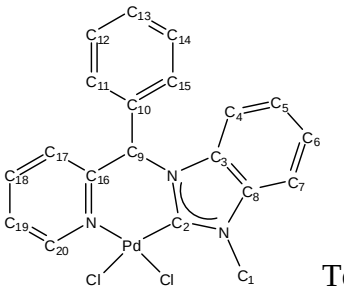

To a solution of compound **64** (4.50g, 13.4 mmol) in 30 mL of CH_2Cl_2, Ag_2O (1.70g, 7.3 mmol) was added in the dark. The reaction mixture was allowed to stir at room temperature for 12 hours and was filtered through celite. A $PdCl_2(NCMe)_2$ suspension (3.48g, 13.4 mmol in 100 mL of CH_3CN) was added to the filtrate in the dark. The reaction mixture was then allowed to stir overnight at room temperature and was filtered through a short plug of celite the next day. The filtrate was reduced *in vacuo* to approximately 50 mL and diethyl ether (200 mL) was added which resulted in the precipitation of an orange-yellow solid 4.01g, 63 %. M.p. = 330.0 – 330.5°C (dec.). ^{1}H NMR (400 MHz, DMSO-d_6): δ = 4.20 (s, 3 H, H1), 7.36–7.39 (m, 2 H, Ph), 7.41–7.46 (m, 3 H, Ph), 7.52 (quintet, 2 H, $J_{H,H}$ = 7.0 Hz, aromatic), 7.65 (t, 1 H, $J_{H,H}$ = 6.3 Hz, H19), 7.80 (d, 1 H, $J_{H,H}$ = 7.3 Hz, aromatic), 7.85 (s, 1 H, H9), 8.15–8.18 (m, 2 H, H17 and H4), 8.23 (t, 1 H, $J_{H,H}$ = 7.5 Hz, H18), 9.14 (s, 1 H, H20) ppm. ^{13}C NMR (100 MHz, DMSO-d_6): δ = 35.26 (C1), 63.36 (C9), 110.83, 111.98, 124.51, 125.31, 126.41, 126.98, 128.44, 128.94, 132.90, 134.18 and 138.06 (aromatic), 140.62 (C18), 154.40 and 155.19 (aromatic), 163.76 (C20) ppm. HRMS (ESI) *m/z*: $[M-H]^+$ calcd for $C_{20}H_{16}Cl_2N_3Pd$ 475.9727, found 475.9745. Anal Calcd for $C_{20}H_{17}Cl_2N_3Pd$ (476.70): C, 50.39; H, 3.59; N, 8.81. Found: C, 49.79; H, 3.65; N, 8.95.

2.4.8 Synthesis of Racemic Palladacycle (±)-58

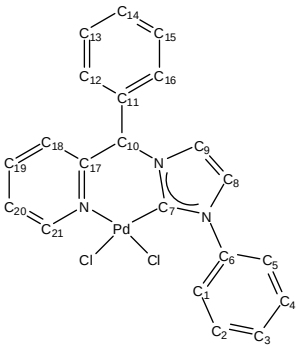

To a solution of compound **65** (4.50g, 13.4 mmol) in 30 mL of CH_2Cl_2, Ag_2O (1.70g, 7.3 mmol) was added in the dark. The reaction mixture was allowed to stir at room temperature for 12 hours and was filtered through celite. A $PdCl_2(NCMe)_2$ suspension (3.48g, 13.4 mmol in 100 mL of CH_3CN) was added to the filtrate in the dark. The reaction mixture was then allowed to stir overnight at room temperature and was filtered through a short plug of celite the next day. The filtrate was reduced *in vacuo* to approximately 50 mL and diethyl ether (200 mL) was added which resulted in the precipitation of an orange-yellow solid 4.01g, 63 %. M.p. = 294.8 – 296.5°C (dec.). ^{1}H NMR (400 MHz, DMSO-d_6): δ = 7.36 (s, 1 H, H10), 7.39–7.45 (m, 4 H, aromatic), 7.47–7.58 (m, 4 H, aromatic), 7.69 (t, 1 H, $J_{H,H}$ = 6.7 Hz, H20), 7.83–7.86 (m, 3 H, aromatic), 8.05–8.08 (m, 2 H, H18 and H9), 8.24 (t, 1 H, $J_{H,H}$ = 7.9 Hz, H19), 9.23 (s, 1 H, H21) ppm. ^{13}C NMR (100 MHz, DMSO-d_6): δ = 67.16 (C10), 123.15(C9), 123.87 (C8), 124.91 (C20), 125.21(C18), 127.15, 128.07, 128.45, 128.65, 128.84, 137.81 and 139.18 (Ph), 140.47 (C19), 154.17 (Ph), 155.16 (C21) ppm. HRMS (ESI) *m/z*: $[M\text{-}H]^+$ calcd for $C_{21}H_{16}Cl_2N_3Pd$ 487.9727, found 487.9719. Anal Calcd for $C_{21}H_{17}Cl_2N_3Pd$ (488.71): C, 51.61; H, 3.51; N, 8.60. Found: C, 52.01; H, 3.46; N, 8.13.

2.4.9 Synthesis of Racemic Palladacycle (±)-59

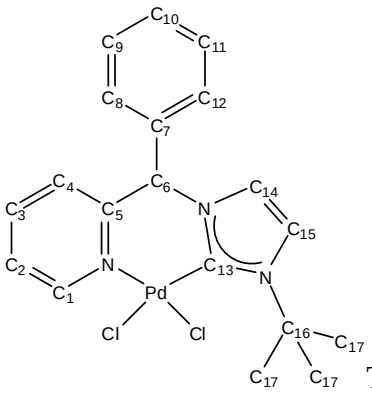

To a solution of compound **66** (4.50g, 13.4 mmol) in 30 mL of CH_2Cl_2, Ag_2O (1.70g, 7.3 mmol) was added in the dark. The reaction mixture was allowed to stir at room temperature for 12 hours and was filtered through celite. A $PdCl_2(NCMe)_2$ suspension (3.48g, 13.4 mmol in 100 mL of CH_3CN) was added to the filtrate in the dark. The reaction mixture was then allowed to stir overnight at room temperature and was filtered through a short plug of celite the next day. The filtrate was reduced *in vacuo* to approximately 50 mL and diethyl ether (200 mL) was added which resulted in the precipitation of an orange-yellow solid 4.01g, 63 %. M.p. = 311.3 – 312.0 °C (dec.). ^{1}H NMR (400 MHz, DMSO-d_6): δ = 1.88 (s, 9 H, H17), 7.24 (s, 1 H, H6), 7.37–7.41 (m, 5 H, Ph), 7.60 (t, 1 H, $J_{H,H}$ = 6.5 Hz, H2), 7.71 (s, 1 H, H15), 7.88 (s, 1 H, H14), 8.01 (d, 1 H, $J_{H,H}$ = 7.6 Hz, H4), 8.17 (t, 1 H, $J_{H,H}$ = 7.6 Hz, H3), 8.87 (d, 1H, $J_{H,H}$ = 5.2 Hz, H1) ppm. ^{13}C NMR (100 MHz, DMSO-d_6): δ = 31.11 (C17), 59.08 (C16), 67.72 (C6), 121.41(C15), 122.74 (C14), 125.13(C2), 126.12 (C4), 127.34, 128.10, 128.56, 137.79 and 140.20 (Ph), 150.73 (C3), 155.01(Ph), 155.08(C1) ppm. HRMS (ESI) *m/z*: $[MH\text{-}Cl]^+$ calcd for $C_{19}H_{22}N_3ClPd$ 434.0463, found 434.0527. Anal Calcd for $C_{19}H_{21}Cl_2N_3Pd$ (468.72): C, 48.69; H, 4.53; N, 8.96. Found: C, 46.06; H, 5.02;

N, 7.72. The deviation seen in the elemental analysis result is most likely due to the presence of DMSO solvent molecule in the crystal structure.

Chapter 3

Optical Resolution of Racemic Cyclopalladated Pyridine-NHC Complexes

3.1 Introduction

Optical resolution of racemic palladacycles upon coordination with chiral auxiliaries have been well documented. Various research groups including our group have employed this method to successfully achieve chiral palladacycles.[80] However, to the best of our knowledge, this method has yet to receive any attention in the synthesis of chiral donor functionalized NHCs based palladacycle. It needs to be noted that all the chiral metallacycles mentioned in the previous chapters were achieved in their enantiomerically pure forms *via* manipulation of chiral amines or other chiral starting material such as BINAP or by the incorporation of chiral oxazoline units.

3.1.1 Synthesis of Chiral NHC Palladacycles *via* functionalization of chiral amines

The synthesis of chiral palladium complex **67** can be readily completed with chiral diamine, *trans*-1,2-diaminocyclohexane in a few simple steps.[81] As shown in Scheme 3.1, the synthesis of the chiral ligand can be achieved in 3-4 steps. Subsequent transmetalation from its silver salt to palladium resulted in the formation of the desired chiral palladacycles. As illustrated in Scheme 3.1, structural variation can be achieved in the chiral ligand through the introduction of different R groups in the synthetic route. This method provides a flexible and straightforward way to the synthesis of a series of amino and imino

functionalized NHC based chiral palladacycles catalysts which can give ee values of up to 92% when they were used in the asymmetric allylic alkylation reaction as highlighted in Scheme 3.2.

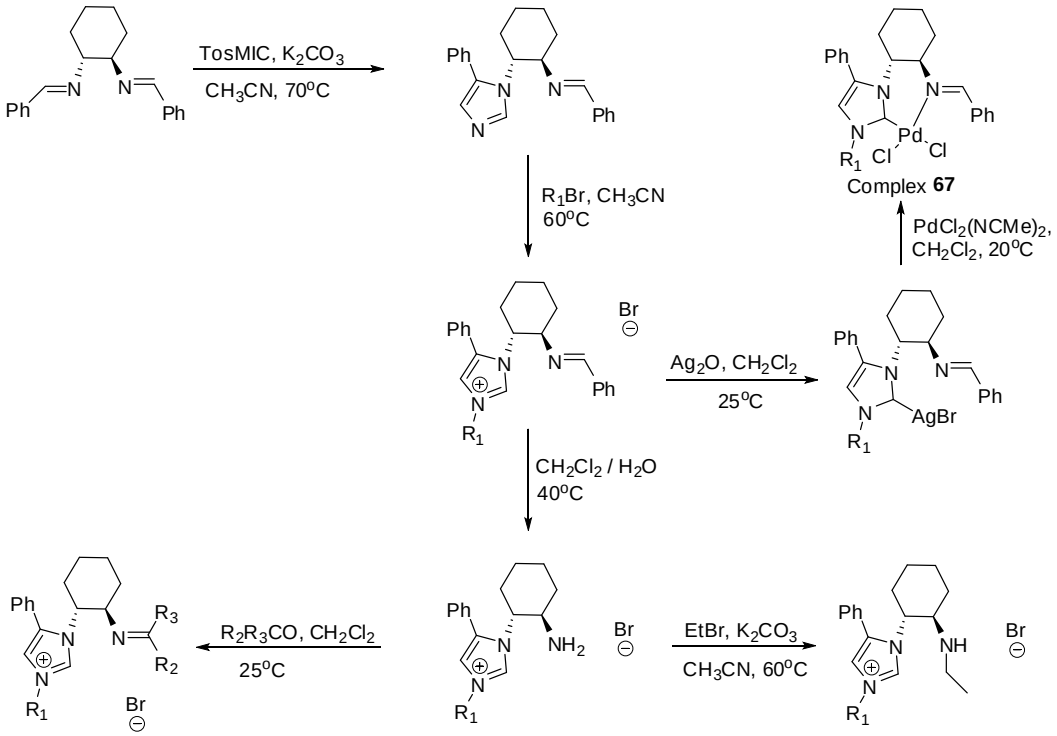

Scheme 3.1

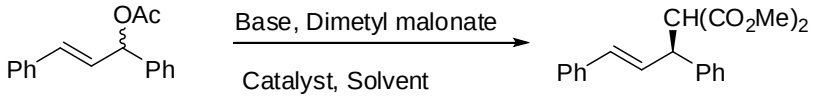

Scheme 3.2

Chiral NHC functionalized bidentate ligands can also be synthesized *via* chiral amino acids as shown by Williams *et al* (Scheme 3.3).[82] Through the use of the readily available chiral pool of amino acids, a small library of chiral imine functionalized NHC bidentate ligands were synthesized. However compared to chiral ligands in Scheme 3.1, the amino acids functionalized

ligands were not as efficient in the mediation of the similar asymmetric allylic alkylation reaction seen in Scheme 3.2; with the 53 % as the highest ee value obtained.

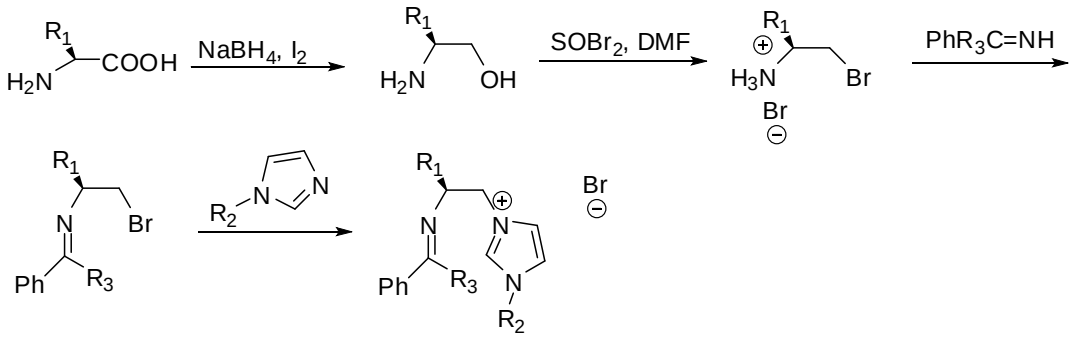

Scheme 3.3

Similarly, chiral amino functionalized NHC bidentate ligands can also be synthesized *via* the introduction of chiral amines as seen in Scheme 3.4 with achievable ee values of 80% for the identical asymmetric allylic alkylation reaction.[83]

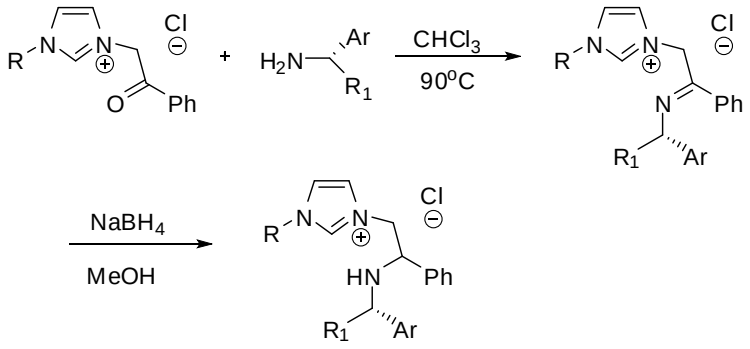

Scheme 3.4

3.1.2 Chiral NHC Palladacycles *via* BINAP functionalization

The first BINAP functionalized chiral palladacycle was synthesized by Rajanbabu *et al.* in 2000 as shown in Scheme 3.5.[84] However, it was Shi *et al.* who explored the different variations at the N substituents of this particular group of chiral palladium complexes and showed that they can mediate a range of asymmetric reactions with moderate to excellent ee as previously discussed in chapter 1.[85]

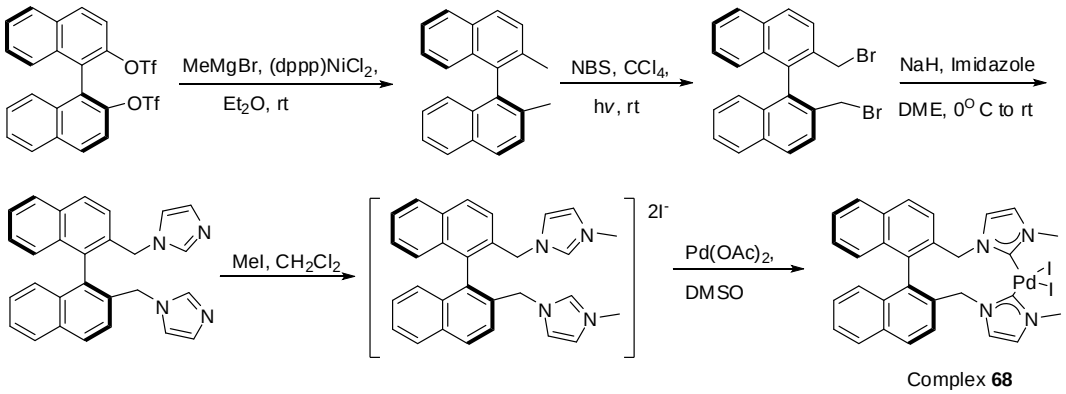

Complex **68**

Scheme 3.5

In addition to the bis NHC systems, Shi *et al*. also developed the BINAP chelating system with only one NHC in the palladated complexes that displayed catalytic ability in Suzuki and Heck type reactions.[86]

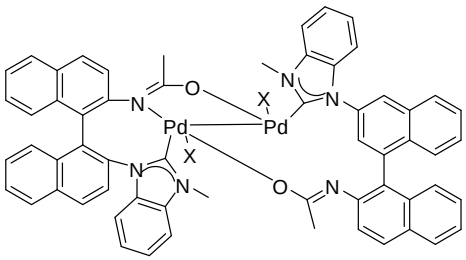

Complex **69**

X = I, OAc

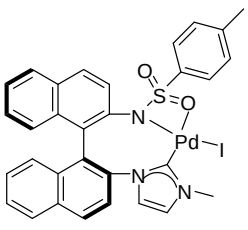

Complex **70**

3.1.3 Chiral NHC Palladacycles *via* Optical Resolution

As mentioned earlier, chiral palladacycles can be afforded *via* the optical resolution of its amino adducts. Our research group had previously successfully synthesized several palladacycles based on this method (Scheme 3.6). [79(h)]

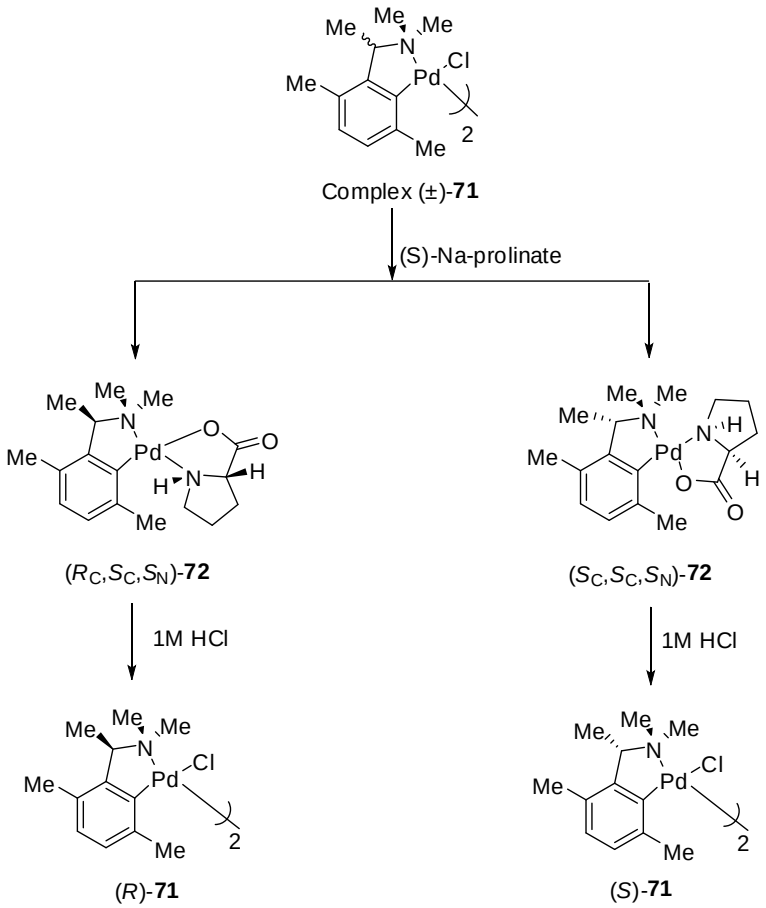

Scheme 3.6

The closest variation to this method employed to synthesize chiral NHC palladacycles was demonstrated by Chauvin *et al*, (Scheme 3.7) whereby the formation of diastereomers is achieved via the use of a chiral palladium source.[87]

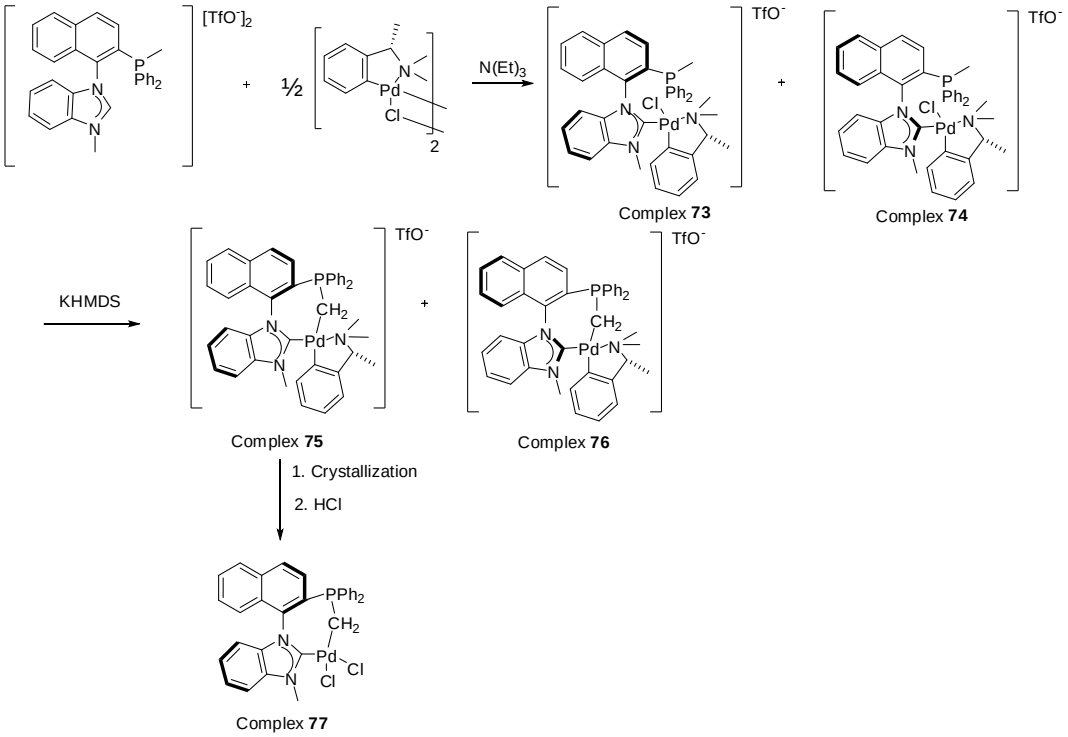

Scheme 3.7

Therefore, following the successful synthesis of the racemic palladacycles (±)-**56** to (±)-**69**, all with a potential chiral centre, the racemic palladacycles will be resolved *via* the formation of their respective amino acid adducts.

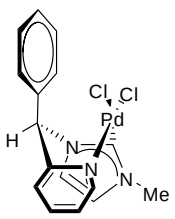

(*R*)-**56**

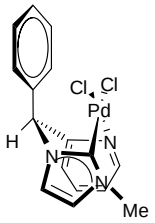

(*S*)-**56**

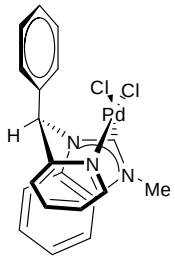

(*R*)-**57**

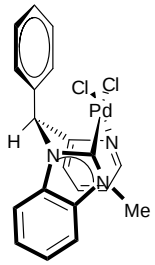

(*S*)-**57**

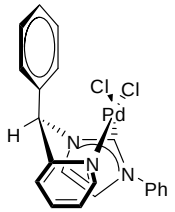

(*R*)-**58**

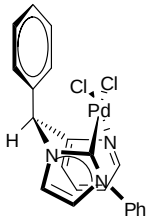

(*S*)-**58**

3.2 Results and Discussions

3.2.1 Optical Resolution of Racemic Cyclopalladated Complex (±)-56

3.2.1.1 Synthesis of Complex 78

After screening through a range of amino acid salts in different solvent systems, only sodium (S_C)-phenylalanate was found to be an effective resolving agent for the resolution of complex (±)-**56**. After the addition of 1 molar equivalent of sodium

(S_C)-phenylalanate in methanol, the progress of the diastereomeric salt formation was monitored by ^{1}H NMR. The two resulting diastereomers could not be separated and kept crystallizing out together in several failed attempts at fractional crystallization in different solvent system. The problem was eventually circumnavigated by changing the counter anion present in the diastereomeric complexes. After switching the counter anion from chloride to nitrate, successful optical resolution of racemic complex (±)-**56** was achieved using sodium (S_C)-phenylalanate as the auxiliary ligand.(Scheme 3.8) Sequential treatment of complex (±)-**56** with two molar equivalents of silver nitrate and one molar equivalent of sodium (S_C)-phenylalanate resulted in the formation of the expected 1:1 mixture of diastereomeric adducts (R_C,S_C)-**78** and (S_C,S_C)-**78** as evident from the presence of two distinct sets of proton resonances for each of the diastereomers.

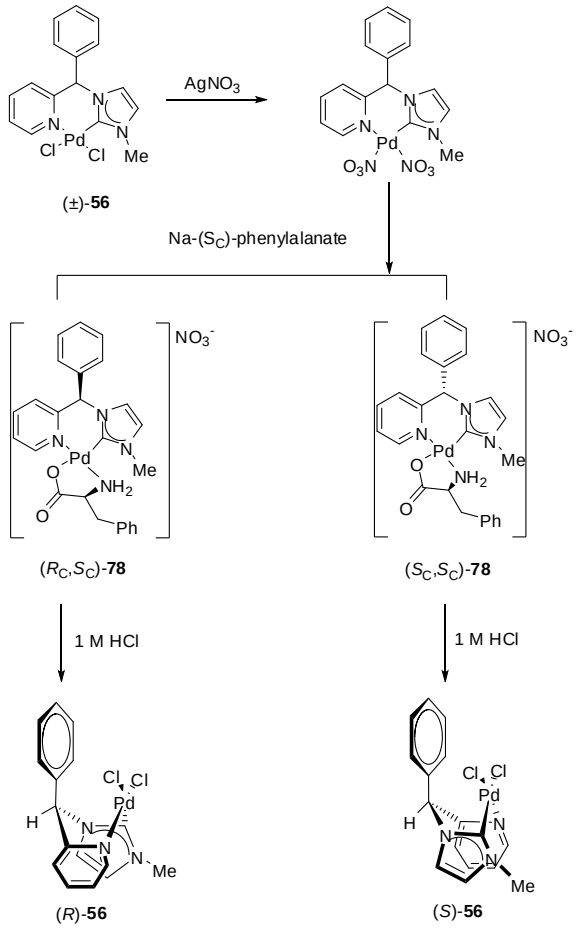

Scheme 3.8

Fractional crystallization from MeOH-diethyl ether afforded the less soluble diastereomer (R_C,S_C)-**78** in the form of an off-white crystalline solid in 70 % yield and > 99% *de* (according to the ^{1}H NMR spectrum) with $[\alpha]_{436}$ = +83.3 (*c* 0.5, DMSO). The ^{1}H NMR spectrum of complex (R_C,S_C)-**78** at room temperature presents itself as a sole isomer in solution, which was indicated by the presence of a solitary set of resonance observed for each chemically nonequivalent proton.

Slow diffusion of diethyl ether into a MeOH solution of the resulting diastereomer (S_C,S_C)-**78** enriched mother liquid allowed all of the remaining diastereomer (R_C,S_C)-**78** to crystallize out. The resulting mother liquor

comprised almost entirely of the more soluble diastereomer (S_C,S_C)-**78** > 99% *de* (according to the ^{1}H NMR spectrum) with $[\alpha]_{436}$ = +42.1 (*c* 0.5, MeOH). Diastereomer (S_C,S_C)-**78** was subsequently isolated as a light yellow colored solid in 67% yield.

The absolute configuration of diastereomer (R_C,S_C)-**78** was confirmed by an X-ray single crystal diffraction study. Compared to complex (R_C,S_C)-**78**, complex (S_C,S_C)-**78** displayed far superior solubility in an array of solvents. Therefore, efforts to obtain X-ray grade crystals of complex (S_C,S_C)-**78** were unsuccessful. However, the absolute configuration of (S_C,S_C)-**78** can be determined by subsequent cleavage of the chiral auxiliary phenylalanate ligand, thereby leading to the formation of the single crystals of the chiral complex (*S*)-**56**.

3.2.1.2 Molecular Structure of Diastereomer (R_C,S_C)-78

Off white crystals of diastereomer (R_C,S_C)-**78** suitable for X-ray crystallography were obtained by slow diffusion of diethyl ether into a methanol-DMSO solution of complex (R_C,S_C)-**78**. The molecular structure of diastereomer (R_C,S_C)-**78** is presented in Figure 3.1, selected bond lengths and bond angles are provided in Table 3.1. The X-ray crystallographic study revealed the *R* absolute configuration of the *α*-carbon stereocenter which was confirmed independently using (S_C)-phenylalanate as a reference point, as well as based on the anomalous X-ray scattering method with the Flack parameter of 0.003(18). The complex adopts a *trans*-(*N*,*N*) arrangement, with the *α*-phenyl

group (C7–C12) occupying the axial position. The tetrahedral distortion of the palladium coordination environment is minimal, with an angle of 5.5° between the {Pd(1)–C(16)–N(1)} and {Pd(1)–N(4)–O(1)} planes.

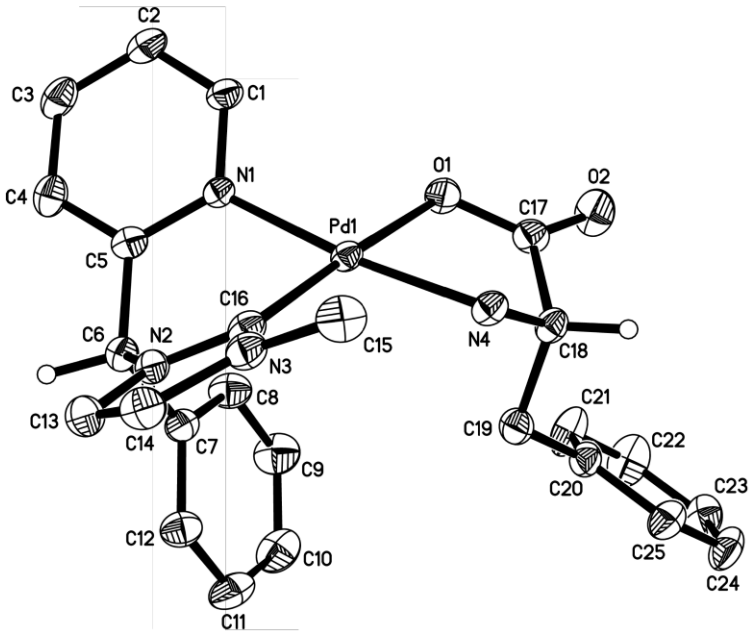

Figure 3.1 Molecular structure of diastereomer (R_C,S_C)**-78** with thermal ellipsoids at 50% probability. Hydrogens except H(C6) are omitted for clarity.

Table 3.1 Selected bond lengths (Å) and angles (°) for Complex (R_C,S_C)**-78**

Pd(1)–C(16)	1.960(4)	Pd(1)–N(1)	2.027(3)
Pd(1)–N(4)	2.028(3)	Pd(1)–O(1)	2.057(3)
C(16)–Pd(1)–N(1)	86.44(9)	C(16)–Pd(1)–N(4)	99.01(17)
N(1)–Pd(1)–N(4)	173.5(1)	C(16)–Pd(1)–O(1)	176.3(2)
N(1)–Pd(1)–O(1)	94.3(1)	N(4)–Pd(1) –O(1)	80.5(6)
N(2)–C(16)–Pd(1)	120.8(3)	N(3)–C(16)–Pd(1)	133.3(3)
C(1)–N(1)–Pd(1)	118.0(2)	C(5)–N(1)–Pd(1)	123.9(2)

3.2.1.3 Synthesis of Optically Active Complexes (*R*)-56 and (*S*)-56

As illustrated in Scheme 3.8, optically active dichloro palladacycle (*R*)-**56** can be obtained by stirring a MeOH solution of complex (R_C,S_C)-**78** with 1 M HCl. Optically active dichloro complex (*R*)-**56** can be isolated as a yellow powder in 51% yield with $[\alpha]_{436}$ = -12.5 (*c* 0.5, DMSO). The enantiomerically pure palladacycle (*S*)-**56** was prepared from complex (S_C,S_C)-**78** in a similar manner: $[\alpha]_{436}$ = +12.4 (*c* 0.5, DMSO). The absolute configurations of palladacycles (*R*)-**56** and (*S*)-**56** were confirmed by X-ray single crystal diffraction studies.

3.2.1.4 Molecular Structure of Optically Active Complex (*R*)-56

Yellow single crystals suitable for X-ray crystallography were obtained from a solution of complex (*R*)-**56** in MeOH, DMSO and diethyl ether and its molecular structure is depicted in Figure 3.2. The selected bond lengths and angles are listed in Table 3.2. The X-ray crystallographic study confirmed the expected *R* absolute configuration of the *α*-phenyl stereocenter of the palladacycle by the anomalous X-ray scattering method with the Flack parameter of -0.01(2). The coordination sphere of the palladium center is in a distorted square-planar geometry, with tetrahedral distortions of 1.5°. Similar to its racemic analogue, the phenyl group on the α carbon adopts the axial position.

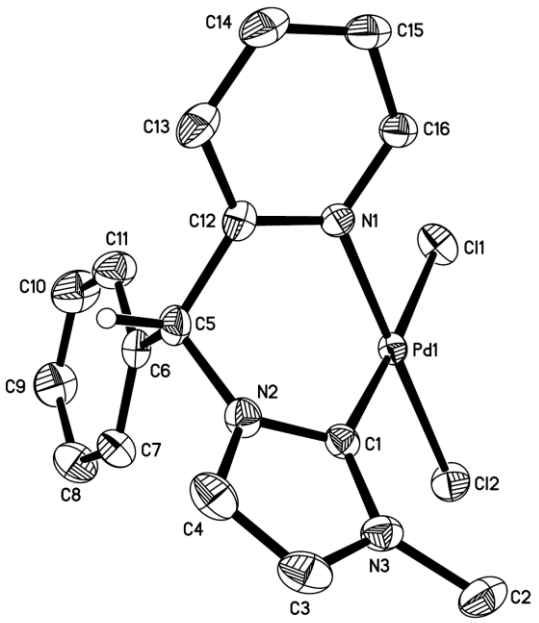

Figure 3.2 Molecular structure of complex (*R*)-**56** with thermal ellipsoids at 50% probability. Hydrogens except for the H(C5) are omitted for clarity.

Table 3.2 Selected bond lengths (Å) and angles (°) for complex (*R*)-**56**

Pd(1)–C(1)	1.980(2)	Pd(1)–N(1)	2.045(2)
Pd(1)–Cl(2)	2.292(5)	Pd(1)–Cl(1)	2.356(5)
C(1)–N(2)	1.353(3)	C(1)–N(3)	1.346(3)
C(4)–N(2)	1.385(3)	C(3)–N(3)	1.384(3)
C(2)–N(3)	1.455(3)	C(5)–N(2)	1.471(3)
C(1)–Pd(1)–N(1)	87.0(7)	C(1)–Pd(1)–Cl(2)	92.7(6)
N(1)–Pd(1)–Cl(2)	179.5(5)	C(1)–Pd(1)–Cl(1)	176.4(6)
N(1)–Pd(1)–Cl(1)	89.9(5)	Cl(2)–Pd(1)–Cl(1)	90.5(2)
N(3)–C(1)–Pd(1)	136.1(2)	N(2)–C(1)–Pd(1)	118.9(1)
C(16)–N(1)–Pd(1)	118.7(1)	C(12)–N(1)–Pd(1)	121.7(1)

3.2.1.5 Molecular Structure of Optically Active Complex (*S*)-56

Yellow colored single crystals were obtained from a MeOH, DMSO and diethyl ether solution of complex (*S*)-**56**. The solid state structure of the complex (*S*)-**56** was determined by X-ray crystallography (refer to Figure 3.3). Selected bond lengths and angles are listed in Table 3.3. The X-ray crystallographic study confirmed the *S* absolute configuration of the *α*-phenyl stereocenter of the palladacycle and was supported by the anomalous X-ray scattering method with the Flack parameter of –0.008(19). The Pd center experienced a slight tetrahedral distortion and the dihedral angle between the {N(1)–Pd(1)–C(1)} and {Cl(1)–Pd(1)–Cl(2)} planes was 1.9°.

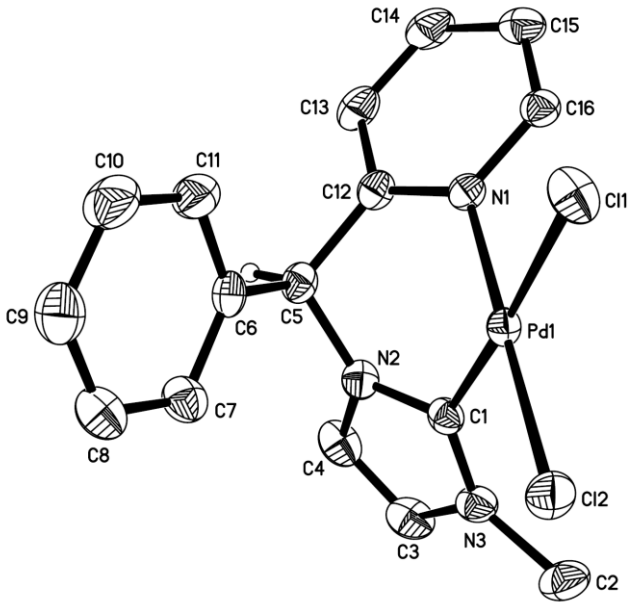

Figure 3.3 Molecular structure of complex (*S*)-**56** with thermal ellipsoids at 50% probability. Hydrogens except for the H(C5) are omitted for clarity.

Table 3.3 Selected bond lengths (Å) and angles (°) for complex (*S*)-**56**

Pd(1)–C(1)	1.984(2)	Pd(1)–N(1)	2.045(2)
Pd(1)–Cl(2)	2.292(5)	Pd(1)–Cl(1)	2.357(5)
N(2)–C(1)	1.347(3)	N(2)–C(4)	1.389(3)
N(3)–C(3)	1.385(3)	N(3)–C(2)	1.456(3)
N(3)–C(1)	1.345(3)	N2(1)–C(5)	1.470(3)
C(1)–Pd(1)–N(1)	86.9(8)	C(1)–Pd(1)–Cl(2)	92.8(6)
N(1)–Pd(1)–Cl(2)	179.6(5)	C(1)–Pd(1)–Cl(1)	176.2(6)
N(1)–Pd(1)–Cl(1)	89.9(5)	Cl(2)–Pd(1)–Cl(1)	90.5(2)
N(3)–C(1)–Pd(1)	135.9(2)	N(2)–C(1)–Pd(1)	118.9(1)
C(12)–N(1)–Pd(1)	121.7(1)	C(16)–N(1)–Pd(1)	118.9(1)

3.2.1.6 Synthesis and Characterisation of Optically Active Complexes (*R*)-79 and (*S*)-79

3.2.1.6.1 Synthesis of Optically Active Complexes (*R*)-79 and (*S*)-79

One of the chloride ligand of the complex (*S*)-**56** and complex (*R*)-**56** can be easily removed in the presence of triphenylphosphine. Therefore, in order to improve the solubility of the complex in organic solvents, one of the chloro ligand on the palladium centre had been changed to a triphenylphosphine as shown in Scheme 3.9. The introduction of bulky triphenylphosphine into the complex is postulated to be able to disrupt the π π stacking in the lattice, and therefore leading to the increase in solubility of the complexes. Enantiomerically pure complexes (*R*)-**56** and (*S*)-**56** are stirred with 1 molar

equivalent of triphenylphosphine in CH_2Cl_2 for 1 h at room temperature to give complex (*R*)-**79** and complex (*S*)-**79** respectively in quantitative yield. The progress of the reaction is monitored by ^{31}P NMR with the presence of a single new phosphorus peak at δ = 28.31 ppm. This indicated that the presence of a sole regio isomer, with the triphenylphosphine replacing one of the chloro ligands specifically. After coordination with triphenylphosphine, the solubility of complex (*R*)-**79** and complex (*S*)-**79** did improve remarkably in CH_2Cl_2.

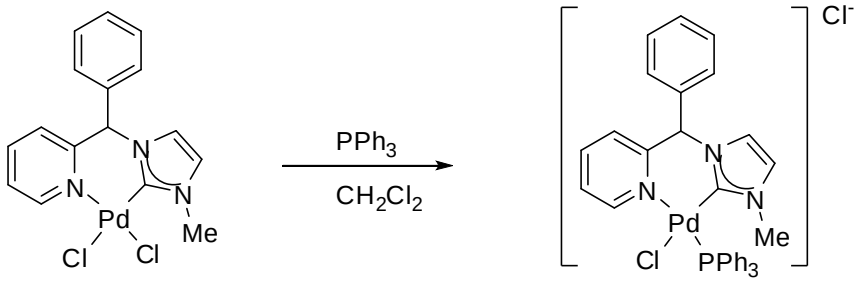

(±)-**56** (±)-**79**

Scheme 3.9

3.2.1.6.2 Molecular Structure of Optically Active Complex (*R*)-79

Pale yellow crystals of complex (*R*)-**79** suitable for X-ray diffraction studies can be achieved *via* the slow diffusion of diethyl ether into a MeOH solution of complex (*R*)-**79**. The molecular structure and selected bond lengths and bond angles of complex (*R*)-**79** is displayed in Figure 3.4 and Table 3.4 respectively. From the X-ray study, the absolute stereochemistry of complex (*R*)-**79** at the α carbon is revealed to be *R* as confirmed by the Flack parameter value of 0.007(13), with the phenyl group adopting the axial position. The boat configuration of the six membered ring is retained upon coordination with

triphenylphosphine. The triphenylphosphine is coordinated selectively *trans* to the N. The regioselectivity observed here can be explained by the reluctance of the triphenylphosphine to coordinate to the Pd centre *trans* to the NHC as triphenylphosphine and NHC are both strong σ donors. Upon coordination with the Pd centre, NHC a strong σ donor will use up majority of the d orbital of the Pd centre for bonding leaving less for the ligand trans to it. Therefore triphenylphosphine being a strong σ donor will coordinate to the position cis to NHC selectively. Compared to complex (*R*)-**56**, there is an enlargement of 5.2° in the C(1)–Pd(1) –P(1) angle to accommodate the bulkier triphenylphosphine ligand into the coordination sphere of the palladium centre. With these structural features, the Pd–P bond would not be able to rotate freely, as all the possible rotational motions are blocked by the chloro ligand and the projecting Me2. Therefore, among the three P–Ph phenyl rings, the C(17)–C(22) ring experiences the most intramolecular ligand-ligand repulsion. As a result, the bond angle Pd(1)–P(1)–C(17) is enlarged to 116.61(6)°, which is larger than the two less affected Pd(1)–P(1)–C(23) and Pd(1)–P(1)–C(29) angles [113.30(6)° and 109.87(6)°].

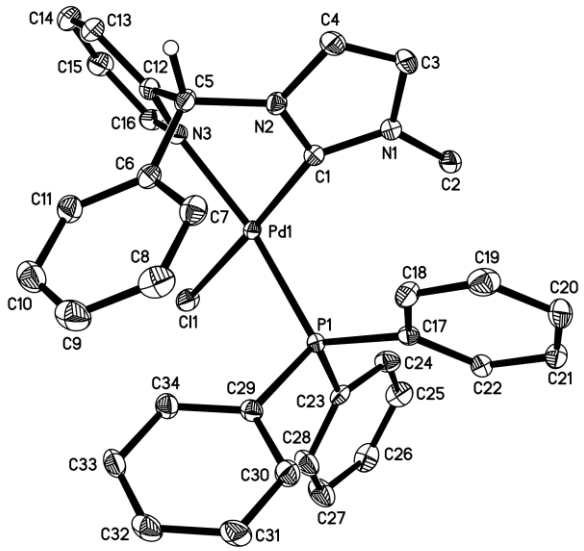

Figure 3.4 Molecular structure of the complex cation in (*R*)-**79** with thermal ellipsoids at 50% probability. Hydrogens except for the H(C5) are omitted for clarity.

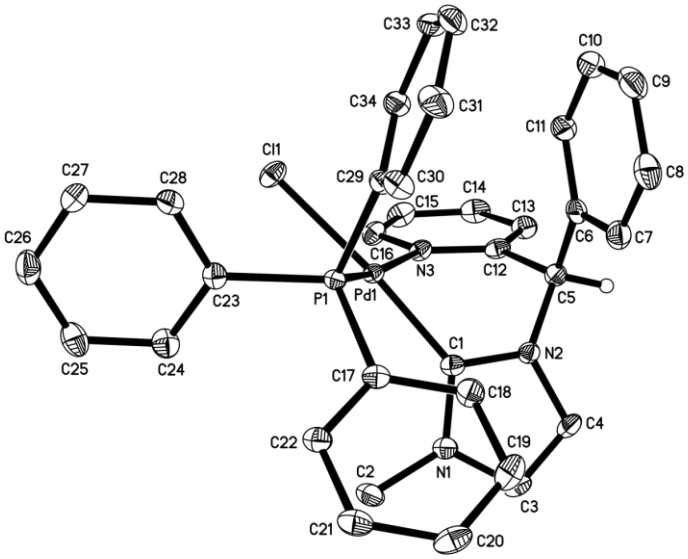

Figure 3.5 Rotated view of the complex cation in (*R*)-**79**

Table 3.4 Selected bond lengths (Å) and angles (°) for complex (*R*)-**79**

Pd(1)–C(1)	1.975(19)	Pd(1)–N(3)	2.115(16)
Pd(1)–Cl(1)	2.331(4)	Pd(1)–P(1)	2.263(5)
N(1)–C(1)	1.347(2)	N(1)–C(2)	1.461(3)
N(1)–C(3)	1.390(3)	N(2)–C(4)	1.388(2)
N(2)–C(5)	1.468(2)	N(2)–C(1)	1.355(2)
C(1)–Pd(1)–N(3)	83.7(7)	C(1)–Pd(1)–P(1)	97.9(6)
N(3)–Pd(1)–P(1)	168.4(5)	C(1)–Pd(1)–Cl(1)	172.3(6)
N(3)–Pd(1)–Cl(1)	92.5(5)	P(1)–Pd(1)–Cl(1)	87.2(18)
C(23)–P(1)–Pd(1)	113.3(6)	C(17)–P(1)–Pd(1)	116.6(6)
C(29)–P(1)–Pd(1)	109.0(6)	-	-

3.2.1.6.3 Molecular Structure of Optically Active Complex (*S*)-79

Crystals suitable for X-ray diffraction studies of complex (*S*)-**79** can be obtained by the slow diffusion of diethyl ether into a MeOH solution of complex (*S*)-**79**. The molecular structure and selected bond lengths and bond angles of complex (*S*)-**79** are displayed in Figure 3.6 and Table 3.5 respectively. The absolute stereochemistry of the α carbon is determined to be *S* and confirmed by the Flack parameter value of 0.013(12). Similar to complex (*R*)-6, the six membered ring is in a boat conformation, with the phenyl group in the axial position and an enlargement of the C(1)–Pd(1)–P(1) angle by 5.1° to accommodate the bulky triphenylphosphine ligand. In complex (*S*)-**79**, the PPh_3 group is located *trans* to the nitrogen donor and the palladium centre has a

distorted square–planar coordination geometry. Analysis of the extent of the tetrahedral distortion on the central Pd atom reveals that it is located in a highly congested environment: the dihedral angle between the {N(3)–Pd(1)–C(1)} and {Cl(1)–Pd(1)–P(1)} planes have a large value of 13.7°. The torsion angle of P(1)–Pd(1)–C(1)–N(1) is 67.9°, such a twisting can be partially attributed to the repulsive interaction between the methyl C2 and the phenyl group (C(17)–C(22)).

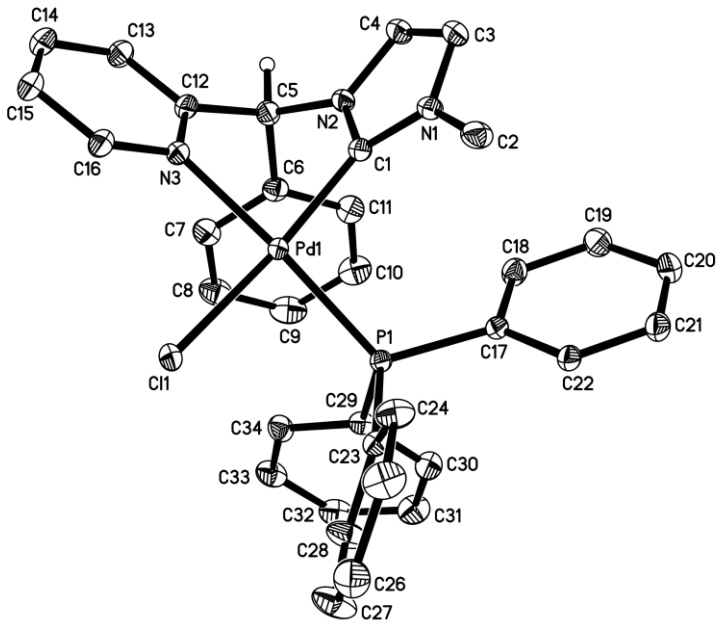

Figure 3.6 Molecular structure of complex cation in (*S*)-**79** with thermal ellipsoids at 50% probability. Hydrogens except for the H(C5) are omitted for clarity.

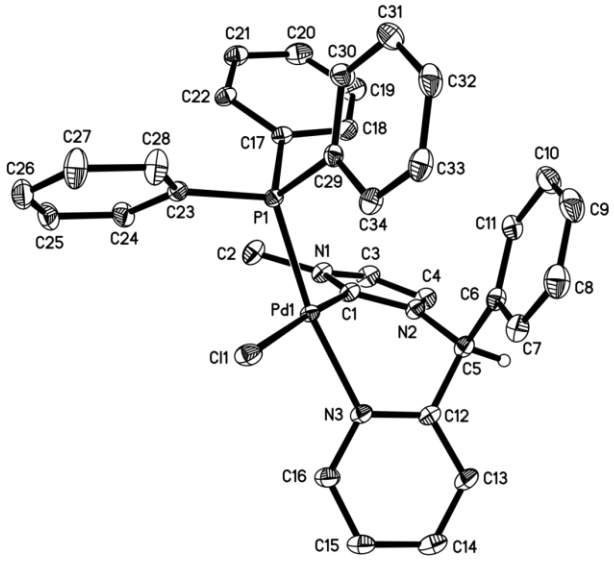

Figure 3.7 Rotated view of the complex cation in (*S*)-**79**

Table 3.5 Selected bond lengths (Å) and angles (°) for complex (*S*)-**79**

Pd(1)–C(1)	1.977(14)	Pd(1)–N(3)	2.115(12)
Pd(1)–Cl(1)	2.329(3)	Pd(1)–P(1)	2.264(4)
N(1)–C(1)	1.346(2)	N(2)–C(1)	1.355(2)
N(1)–C(2)	1.458(2)	N(2)–C(5)	1.472(2)
N(1)–C(3)	1.396(2)	N(2)–C(4)	1.384(2)
C(1)–Pd(1)–N(3)	83.7(5)	C(1)–Pd(1)–P(1)	97.9(4)
N(3)–Pd(1)–P(1)	168.5(4)	C(1)–Pd(1)–Cl(1)	172.1(5)
N(3)–Pd(1)–Cl(1)	92.4(4)	P(1)–Pd(1) –Cl(1)	87.3(14)
C(17)–P(1)–Pd(1)	116.7(5)	C(29)–P(1)–Pd(1)	109.8(5)
C(23)–P(1)–Pd(1)	113.2(5)	-	-

3.2.2 Optical Resolution of Racemic Cyclopalladated Complex (±)-57

3.2.2.1 Synthesis of Complex 80

The synthesis of complex **80** can be achieved *via* coordination of the racemic complex **(**±)-**57** with sodium (S_C)-phenylalanate as shown in Scheme 3.10. Upon coordination with 1 molar equivalent of sodium (S_C)-phenylalanate, the formation of the diastereomeric pair can be confirmed by ^{1}H NMR with the presence of 2 distinct sets of proton peaks for the diastereomeric pair (R_C,S_C)-**80** and (S_C,S_C)-**80**. After screening through several solvents for fractional crystallization, complex (S_C,S_C)-**80** can be selectively crystallized from the slow diffusion of diethyl ether in to an ethanol solution of the diastereomeric mixture. Unlike complex (±)-**56**, fractional crystallization of complex (±)-**57** can be achieved without having to change the counter anion. The diastereomeric purity of the crystals of complex (S_C,S_C)-**80** > 99% *de* is determined by ^{1}H NMR, whereby only 1 set of proton signals were present, with $[\alpha]_{365}$ = +202 (*c* 0.55, MeOH).

After the initial crystallization of diastereomer (S_C,S_C)-**80** from the diastereomeric mixture, further selective crystallization of the pure diastereomer (S_C,S_C)-**80** can no longer be achieved *via* the slow diffusion of diethyl ether into the ethanol solution. Instead, the mixtures of diastereomers were redissolved in acetonitrile and the slow evaporation of the acetonitrile solution resulting in the further fractional crystallization of the pure diastereomer (S_C,S_C)-**80**. However, after repeated efforts at fractional crystallization, the best diastereomeric ratio achieved was only 1:20.

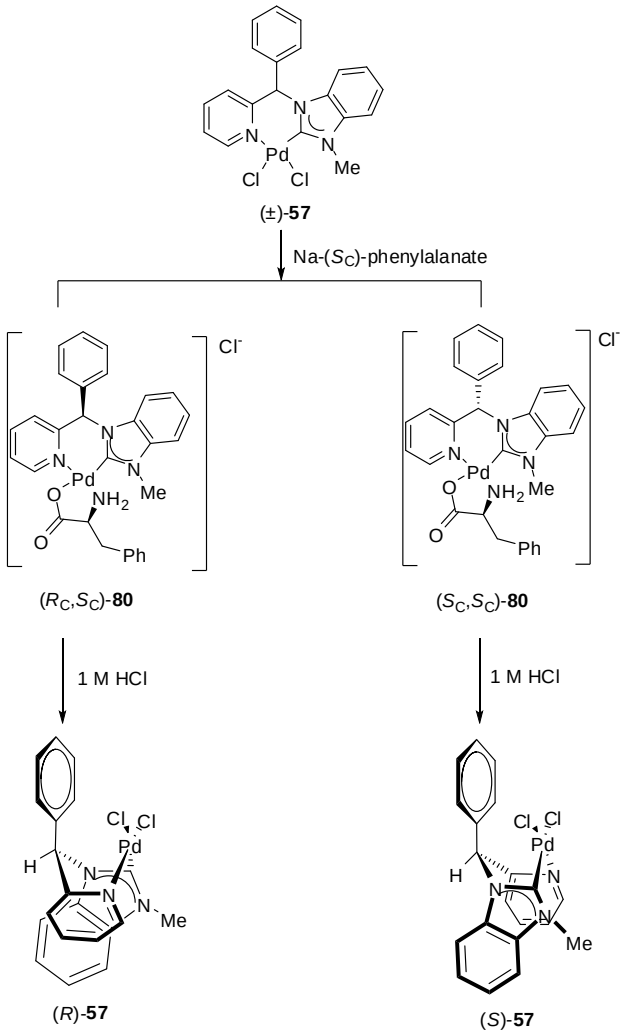

Scheme 3.10

3.2.2.2 Molecular Structure of Diastereomer (S_C,S_C)-80

Slow diffusion of diethyl ether into a MeOH solution of complex (S_C,S_C)-**80** afforded crystals that were suitable for single X-ray diffraction studies. The molecular structure and the selected bond lengths and angles are shown in Figure 3.8 and Table 3.6 respectively. From the molecular structure, *S* absolute configuration of the α carbon stereocenter can be confirmed independently using (S_C)-phenylalanate as a reference point, as well as based on

the anomalous X-ray scattering method with the Flack parameter of 0.001(16). Similar to complex (R_C,S_C)-**79**, complex (S_C,S_C)-**80** also adopts the *trans*-(*N*,*N*) arrangement. The boat configuration of the six membered ring is maintained upon coordination with the amino acid salt with the phenyl group occupying the axial position. The tetrahedral distortion of the palladium coordination environment is minimal, with an angle of 6.2° between the {Pd(1)–C(1)–N(3)} and {Pd(1)–N(4)–O(1)} planes. The bond lengths and bond angles for complex (S_C,S_C)-**80** is comparable to that of complex (R_C,S_C)-**79.** Consistent with complex (R_C,S_C)-**79**, the two nitrogen atoms in complex (S_C,S_C)-**80** are also *trans* related.

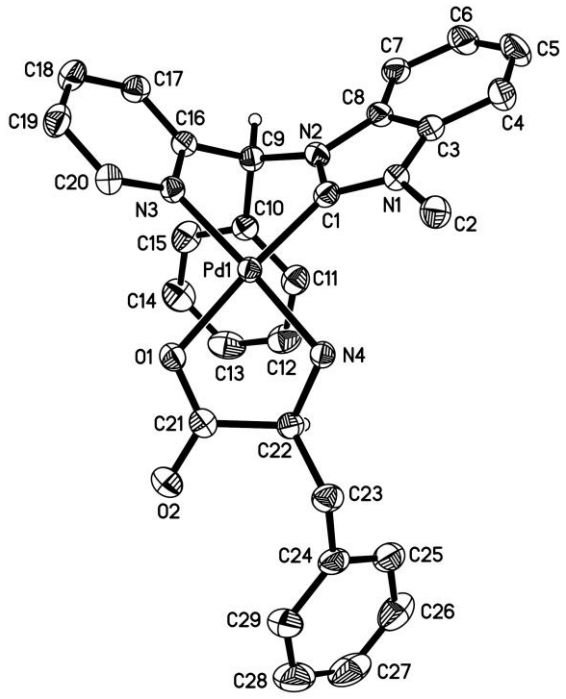

Figure 3.8 Molecular structure of diastereomer (S_C,S_C)-**80** with thermal ellipsoids at 50% probability. Hydrogens except for the H(C9) are omitted for clarity.

Table 3.6 Selected bond lengths (Å) and angles (°) for complex (S_C,S_C)-**80**

Pd(1)–C(1)	1.950(2)	Pd(1)–N(3)	2.030(16)
Pd(1)–N(4)	2.013(15)	Pd(1)–O(1)	2.047(14)
C(1)–Pd(1)–N(4)	96.73(7)	C(1)–Pd(1)–N(3)	86.75(7)
N(4)–Pd(1)–N(3)	176.34(7)	C(1)–Pd(1)–O(1)	172.62(6)
N(4)–Pd(1)–O(1)	80.77(6)	N(3)–Pd(1)–O(1)	95.91(6)
N(2)–C(1)–Pd(1)	119.08(14)	N(1)–C(1)–Pd(1)	133.26(15)
C(16)–N(3)–Pd(1)	122.70(12)	C(20)–N(3)–Pd(1)	118.22(14)

3.2.2.3 Synthesis of Optically Active Complex (*S*)-57

As illustrated in Scheme 3.10, optically active complex (*S*)-**57** can be achieved *via* 1M HCl treatment of the respective optically active diastereomer (S_C,S_C)-**80**. Optically active complex (*S*)-**57** can be isolated in 60% yield in the form of a yellow powder with $[\alpha]_{436}$ = -27.8, (*c* 0.50, DMSO). However, attempts to obtain single crystals suitable for X-ray crystallography proved to be unsuccessful due to the insufficient solubility of complex (*S*)-**57** in a variety of solvents. As demonstrated in Scheme 3.9, upon coordination with 1 molar equivalent of triphenylphosphine, the solubility of the palladacycle can be drastically improved. Therefore, complex (*S*)-**57** was treated with 1 molar equivalent of triphenylphosphine.

3.2.2.4 Synthesis of Optically Active Complex (*S*)-81

The chloride *trans* to $N_{pyridine}$ can be selectively replaced by treatment with 1 molar equivalent of triphenylphosphine as shown in Scheme 3.11. No other regio isomer can be detected by ^{31}P NMR.

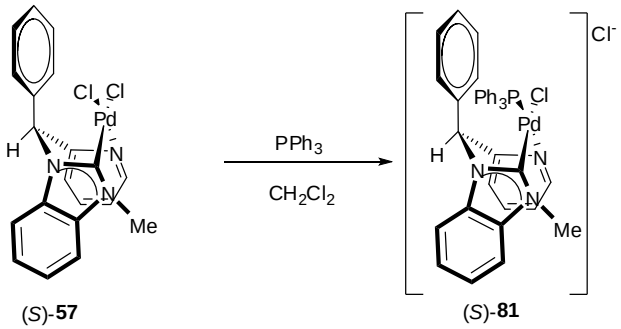

(*S*)-**57** (*S*)-**81**

Scheme 3.11

The progress of the reaction is monitored by ^{31}P NMR in $CDCl_3$. The presence of the new peak at δ = 28.99 ppm and the absence of the starting material peak indicated the completion of the reaction. Complex (*S*)-**81** was isolated in the form of an off white powder in 90 % yield with $[\alpha]_{436}$ = -36.8 (*c* 0.57, MeOH).

3.2.2.5 Molecular Structure of Optically Active Complex (*S*)-81

Single crystal suitable for X-ray crystallography can be obtained *via* the slow diffusion of diethyl ether into a MeOH solution of complex (*S*)-**81**. The molecular structure of complex (*S*)-**81** is displayed in Figure 3.9. Selected bond lengths and bond angles are displayed in Table 3.7. The X ray diffraction study

showed that the six membered ring is in a boat conformation with the phenyl ring occupying the axial position. The absolute stereochemistry of the *α* carbon sterogenic centre is revealed by X-ray crystallography to be *S* and confirmed *via* anomalous X-ray scattering method with the Flack parameter of -0.007(9). Similar to its imidazolium analogue, there is a 4.8° enlargement in the C(1)–Pd(1)–P(1) angle to accommodate the bulkier triphenylphosphine ligand. From the X-ray crystallography, the triphenylphosphine ligand coordinates selectively to the position *trans* to $N_{pyridine}$. The palladium centre is in a square planar geometry with a tetrahedral distortion angle of 6.37° between the {N(3)–Pd(1)–C(1)} and {Cl(1)–Pd(1)–P(1)} planes.

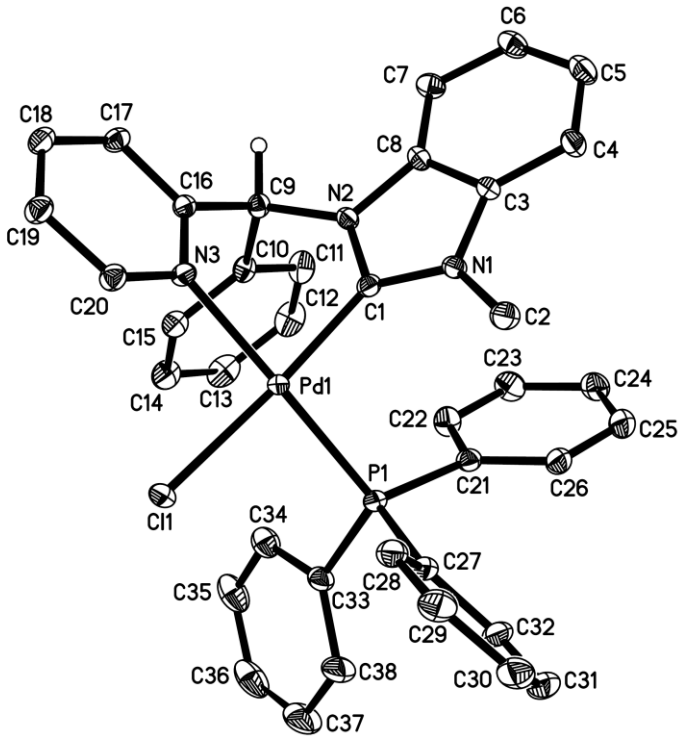

Figure 3.9 Molecular structure of the complex cation in (*S*)-**81** with thermal ellipsoids at 50% probability. Hydrogens are omitted for clarity.

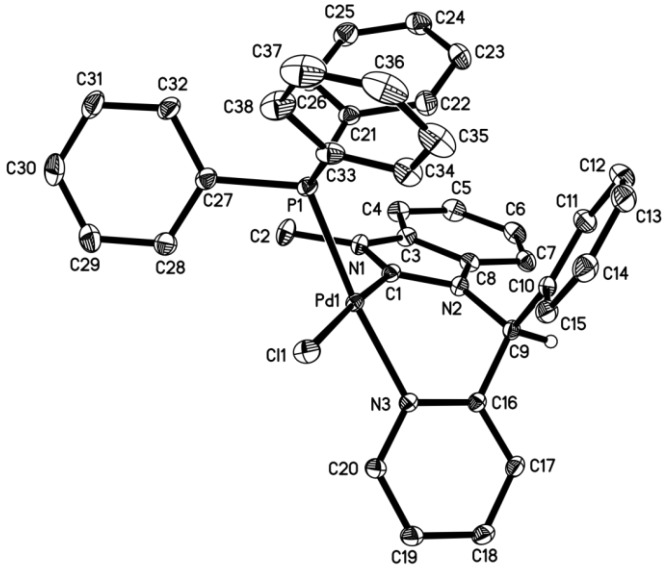

Figure 3.10 Rotated view of complex cation in (*S*)-**81**

Table 3.7 Selected bond lengths (Å) and angles (°) for complex (*S*)-**81**

Pd(1)–C(1)	1.972(1)	Pd(1)–N(3)	2.094(1)
Pd(1)–Cl(1)	2.327(4)	Pd(1)–P(1)	2.274(4)
N(1)–C(1)	1.341(2)	N(2)–C(8)	1.401(2)
N(1)–C(2)	1.456(2)	N(2)–C(9)	1.471(2)
N(1)–C(3)	1.390(2)	N(2)–C(1)	1.354(2)
C(1)–Pd(1)–N(3)	84.12(5)	C(1)–Pd(1)–P(1)	95.78(4)
N(3)–Pd(1)–P(1)	173.55(3)	Cl(1)–Pd(1)–P(1)	88.55(14)
C(1)–Pd(1)–Cl(1)	175.26(4)	N(3)–Pd(1)–Cl(1)	91.80(3)
C(21)–P(1)–Pd(1)	112.2(5)	C(33)–P(1)–Pd(1)	111.9(5)
C(27)–P(1)–Pd(1)	114.3(5)	-	-

3.2.3 Optical Resolution of Racemic Cyclopalladated Complex (±)-58

3.2.3.1 Synthesis of Complex 82

The synthesis of complex **82** can be achieved *via* coordination of the racemic complex **(**±)-**58** with chiral sodium (S_C)-prolinate as shown in Scheme 3.12 instead of sodium (S_C)-phenylalanate in the cases of complex **(**±)-**56** and complex **(**±)-**57**. Upon coordination with 1 molar equivalent of sodium (S_C)-prolinate, the formation of a pair of diastereomers can be confirmed by ^{1}H NMR with the presence of 2 distinct sets of proton peaks for the diastereomeric pair (R_C,S_C)-**82** and (S_C,S_C)-**82**. After screening through different solvent systems for fractional crystallization, (S_C,S_C)-**82** was selectively crystallized from the slow diffusion of diethyl ether into a MeOH solution of the diastereomeric mixture. Similar to complex (±)-**57**, fractional crystallization of complex (±)-**58** can be achieved without having to change the counter anion. The diastereomeric purity of the crystals of complex (S_C,S_C)-**82** > 99% *de* is determined by ^{1}H NMR, whereby only 1 set of proton signals were present, with $[\alpha]_{436}$= -167 (*c* 0.50, MeOH).

After several failed attempts to selectively crystallize out the remaining diastereomer (S_C,S_C)-**82** from the diastereomer (R_C,R_C)-**82** enriched mother liquor in the same solvent system, a different solvent system was attempted for fractional crystallization. The solvent system was changed to an ethanol solution with hexane being slowly added to it. The best diastereomeric ratio obtained is 1:15 as indicated by ^{1}H NMR.

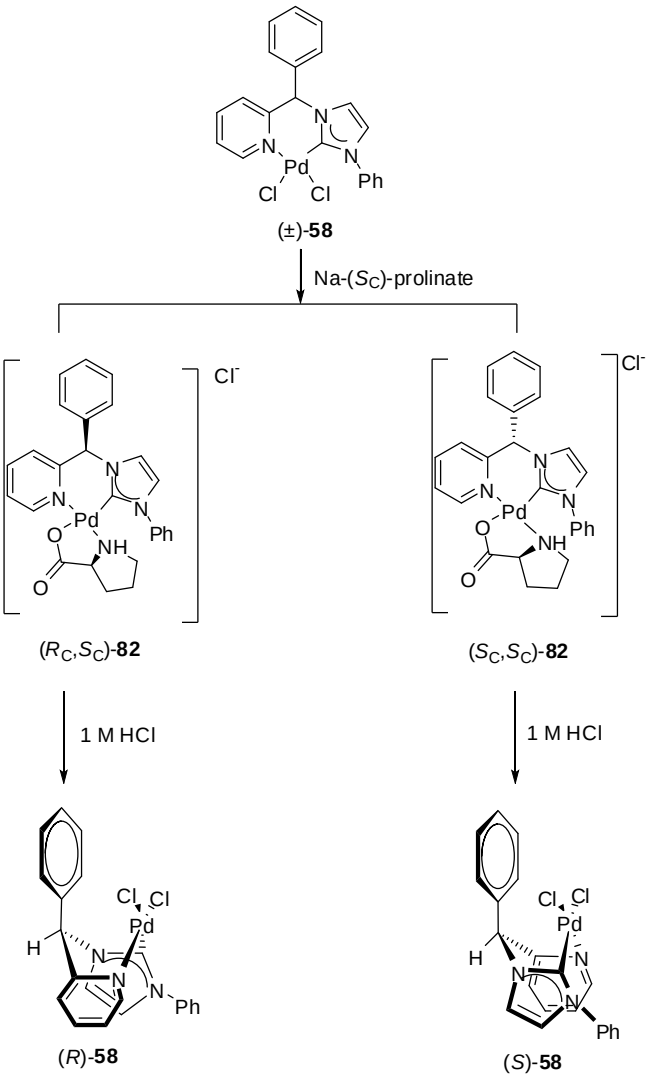

Scheme 3.12

3.2.3.2 Molecular Structure of Diastereomer (S_C,S_C)-82

Slow diffusion of diethyl ether into a methanol solution of diastereomer (S_C,S_C)-**82** afforded crystals that were suitable for single crystal X-ray diffraction studies. The molecular structure and the selected bond lengths and angles are shown in Figure 3.11 and Table 3.8 respectively. From the molecular structure, *S* absolute configuration of the *α* carbon stereocenter can

be confirmed by using (S_C)-prolinate as a reference point, as well as based on the anomalous X-ray scattering method with the Flack parameter of -0.028(17). Similar to complex (S_C,S_C)-**80**, complex (S_C,S_C)-**82** also adopts the *trans*-(*N*,*N*) arrangement. The boat configuration of the six membered ring is maintained upon coordination with the amino acid salt with the phenyl group occupying the axial position. The tetrahedral distortion of the palladium coordination environment is minimal, with an angle of 6.2° between the {Pd(1)–C(1)–N(3)} and {Pd(1)–N(4)–O(1)} planes. The bond lengths and bond angles for complex (S_C,S_C)-**82** is comparable to that of complex (S_C,S_C)-**80.**

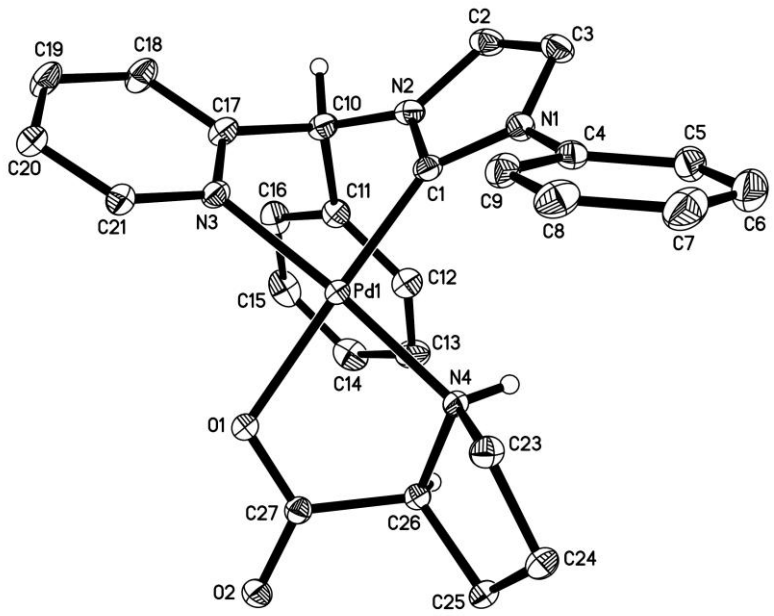

Figure 3.11 Molecular structure of diastereomer (S_C,S_C)-**82** with thermal ellipsoids at 50% probability. Hydrogens except for the H(C10) are omitted for clarity.

Table 3.8 Selected bond lengths (Å) and angles (°) for Complex (S_C,S_C)-**82**

Pd(1)–C(1)	1.952(2)	Pd(1)–N(3)	2.022(18)
Pd(1)–N(4)	2.036(17)	Pd(1)–O(1)	2.053(15)
C(1)–Pd(1)–N(4)	97.87(8)	C(1)–Pd(1)–N(3)	85.97(8)
N(4)–Pd(1)–N(3)	172.97(7)	C(1)–Pd(1)–O(1)	171.17(8)
N(4)–Pd(1)–O(1)	81.37(6)	N(3)–Pd(1)–O(1)	93.93(7)
N(2)–C(1)–Pd(1)	118.24(16)	N(1)–C(1)–Pd(1)	136.04(16)
C(17)–N(3)–Pd(1)	121.21(16)	C(21)–N(3)–Pd(1)	119.30(14)

3.2.3.3 Synthesis of Optically Active Complex (*S*)-58

As illustrated in Scheme 3.12, optically active palladacycle (*S*)-**58** can be achieved *via* treatment of the respective optically active diastereomer (S_C,S_C)-**82** with 1M HCl. Optically active complex (*S*)-**58** can be isolated in 60% yield in the form of a yellow powder with $[\alpha]_{436}$ = -27.8, (*c* 0.20, DMSO).

3.2.3.4 Molecular Structure of Optically Active Complex (*S*)-58

X-ray grade single crystals of palladacycle (*S*)-**58** can be obtained from the slow diffusion of diethyl ether into a solution of MeOH and DMSO. Similar to palladacycles (*R*)-**56** and (*S*)-**56**, the solubility of palladacycle (*S*)-**58** is also quite limited in a range of solvents. Therefore, the addition of a small quantity of DMSO is required to afford a clear solution of complex (*S*)-**58** for crystallization. The absolute configuration at the stereocenter is shown to be *S*

and is supported by the Flack parameter of -0.005(14). Like its racemic complex (±)-**58**, the six membered cyclic ring in palladacycle (*S*)-**58** is in a boat conformation with *α* phenyl ring in the axial position. The strong *trans* inducing effect of the carbene is evident in the elongation of 0.074 Å in the Pd(1)–Cl(2) compared to the Pd(1)–Cl(1) bond. A small tetrahedron distortion angle of 5.54° is observed about the palladium centre which is in a square planar geometry.

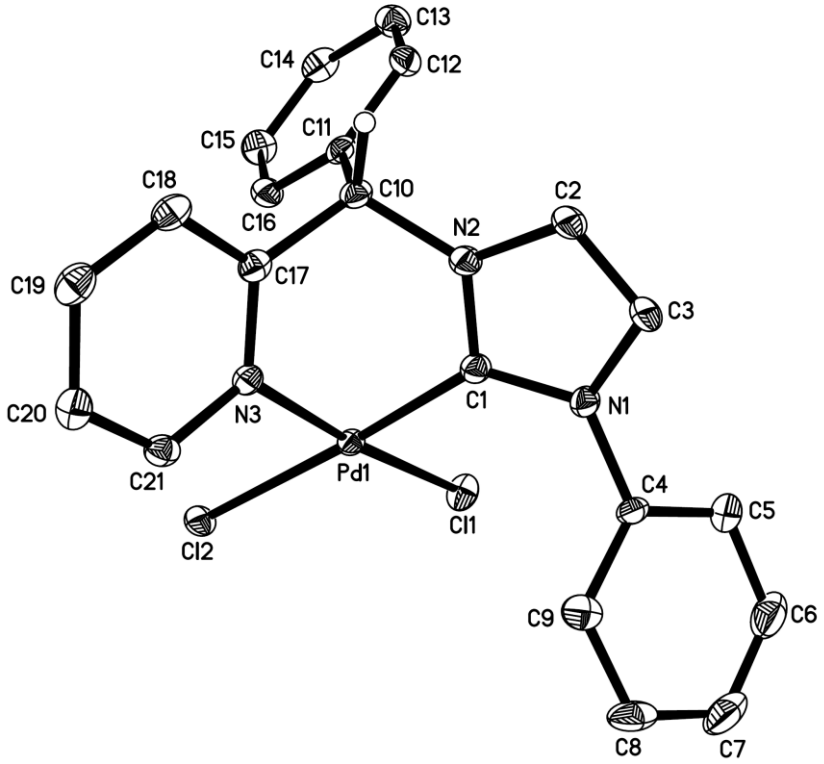

Figure 3.12 Molecular structure of complex (*S*)-**58** with thermal ellipsoids at 50% probability. Hydrogens except for the H(C10) are omitted for clarity.

Table 3.9 Selected bond lengths (Å) and angles (°) for complex (*S*)-**58**

Pd(1)–C(1)	1.948(3)	Pd(1)–N(3)	2.047(3)
Pd(1)–Cl(2)	2.376(7)	Pd(1)–Cl(1)	2.301(8)
N(1)–C(1)	1.356(3)	N(2)–C(1)	1.348(4)
N(1)–C(3)	1.394(4)	N(2)–C(2)	1.394(3)
N(1)–C(4)	1.436(3)	N(2)–C(10)	1.480(3)
C(1)–Pd(1)–N(3)	84.8(11)	C(1)–Pd(1)–Cl(2)	176.2(9)
N(3)–Pd(1)–Cl(2)	91.5(8)	C(1)–Pd(1)–Cl(1)	91.6(9)
N(3)–Pd(1)–Cl(1)	175.3(8)	Cl(2)–Pd(1)–Cl(1)	92.0(3)
N(2)–C(1)–Pd(1)	121.5(19)	N(1)–C(1)–Pd(1)	133.5(2)
C(21)–N(3)–Pd(1)	119.5(2)	C(17)–N(1)–Pd(1)	121.5(2)

3.2.3.5 Synthesis of Racemic Complex (±)-84

During the attempt to synthesized the optically active complex (*S*)-**83** as illustrated in Scheme 3.13, an off white powder in 90 % yield with $[\alpha]_{436}$ = -233 (*c* 0.20, MeOH) was isolated. From ^{31}P NMR, only a single new peak is observed at 1 hour at δ = 26.94 ppm. Therefore, congruent to its imidazolium and benzimidazolium analogues, only 1 regio isomer is observed. The ^{31}P chemical shift of the isolated product was quite similar to palladacycle (*S*)-**79** and palladacycle (*S*)-**81**. Hence, the triphenylphosphine is believed to be coordinated *trans* to the $N_{pyridine}$. However, upon X-ray crystallographic analysis, complex (±)-**84** was generated instead of the expected palladacycle (*S*)-**83** and racemization of the complex (±)-**84** product was observed.

The product was initially isolated as an off white solid after 1 hour and displayed optical activity with $[\alpha]_{436}$ = -233 (*c* 0.20, MeOH). However racemization of the product occurred after 24 hours in solution during the crystallization process and the crystals of racemic complex (±)-**84** was isolated. The product that was stored in the form of the original off white solid was analyzed for its optical activity after 1 week of storage and displayed optical activity. Therefore, racemization of the product only occurred in solution state.

3.2.3.6 Molecular Structure of Racemic Complex (±)-84

X-ray grade single crystal of complex (±)-**84** can be obtained *via* slow diffusion of diethyl ether into a MeOH solution of complex (±)-**84**. The X-ray diffraction study revealed that upon coordination with 1 molar equivalent triphenylphosphine, a bond cleavage occurred between the $N_{pyridine}$ atom and the palladium centre as seen in Figure 3.13 and Scheme 3.14. Instead of the expected complex (*S*)-**83**, a racemic complex (±)-**84** is generated. Selected bond lengths and bond angles of complex (±)-**84** are tabulated in Table 3.10. Prior to the introduction of triphenylphosphine, the respective amino acid adduct complex (S_C,S_C)-**82** was treated with 1M HCl (aq) solution for an hour to remove the chiral amino acid auxiliary. However, after the acid treatment, chiral complex (S)-**58** was successfully achieved without any $N_{pyridine}$–Pd bond cleavage. Hence the possibility of the $N_{pyridine}$–Pd cleavage due to acidic treatment was excluded. The unexpected bond cleavage may be due the bulkiness of the phenyl substituent on the N of the imidazolium since the $N_{pyridine}$–Pd bond cleavage was not observed in complexes (*S*)-**79** and (*S*)-**81**

which have less bulky methyl group as the substituent on the wingtip N. Due to this bulky group, the palladium centre might not be able to accommodate the bulky triphenylphosphine group whilst maintaining the bidentate chelating ligand in its coordination sphere. Therefore, the weaker $N_{pyridine}$–Pd bond cleaved in order to create enough space for the incoming triphenylphosphine group. The triphenylphosphine is believed to coordinate to the Pd centre *via* an associative mechanism as proposed by Lin *et al.* as shown in Scheme 3.14.[88] The hemilability of pyridine functionalized NHC complex **85** has been observed. The triphenylphosphine is introduced in an associative mechanism into complex **85**, upon coordination of the triphenylphosphine, an $N_{pyridine}$–Pd cleavage was also observed for their NHC palladium system.

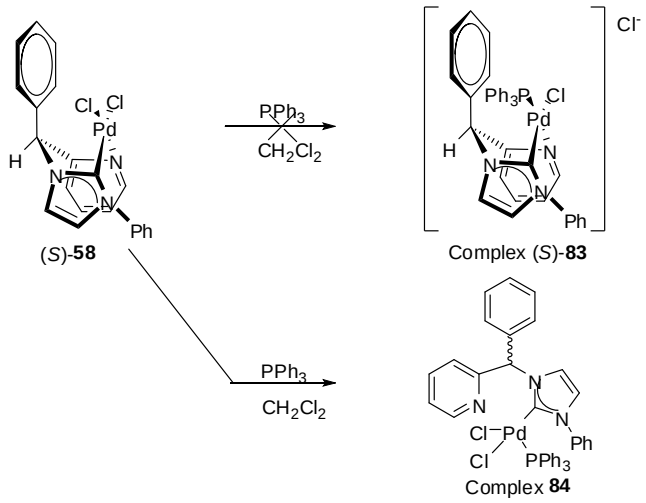

Scheme 3.13

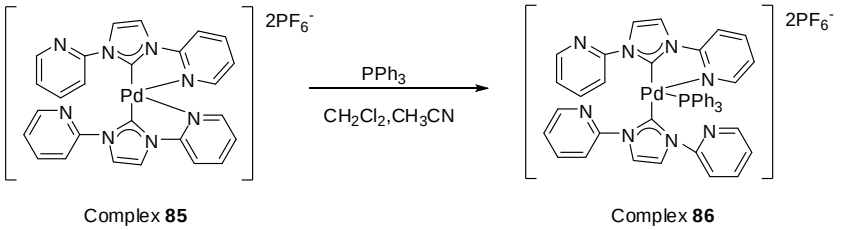

Scheme 3.14

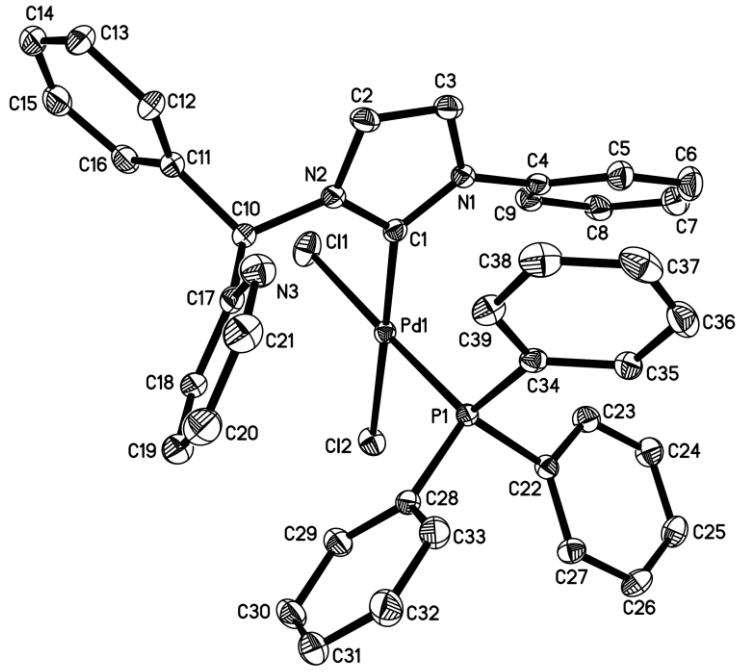

Figure 3.13 Molecular structure of complex (±)-**84** with thermal ellipsoids at 50% probability. Hydrogens are omitted for clarity.

Table 3.10 Selected bond lengths (Å) and angles (°) for complex (±)-**84**

Pd(1)–C(1)	1.979(18)	Pd(1)–P(1)	2.263(5)
Pd(1)–Cl(1)	2.373(5)	Pd(1)–Cl(2)	2.354(5)
N(1)–C(1)	1.351(2)	N(2)–C(1)	1.347(2)
N(1)–C(4)	1.434(2)	N(2)–C(2)	1.388(2)
N(1)–C(3)	1.395(2)	N(2)–C(10)	1.479(2)
C(1)–Pd(1)–Cl(1)	85.5(5)	C(1)–Pd(1)–P(1)	92.7(5)
P(1)–Pd(1)–Cl(2)	89.1(17)	Cl(1)–Pd(1)–Cl(2)	92.4(19)
Pd(1)–P(1)–C(34)	117.16(6)	Pd(1)–P(1)–C(28)	114.49(6)
Pd(1)–P(1)–C(22)	111.15(6)	-	-

3.2.3.7 Synthesis of Arsine Coordinated Complex (±)-87

In order to test out the hemilability in the presence of a weaker coordinating ligand as compared to phosphine, the softer triphenylarsine ligand was added to complex (±)-**58**. Upon addition of triphenylarsine to a CH_2Cl_2 suspension of complex (±)-**58**, the reaction mixture became clear within 10 mins. From previous empirical observations, the clearing of the reaction mixture usually indicated the successful completion of the ligand exchange. As shown in Scheme 3.15, complex (±)-**87** has the possibility of adopting either structure.

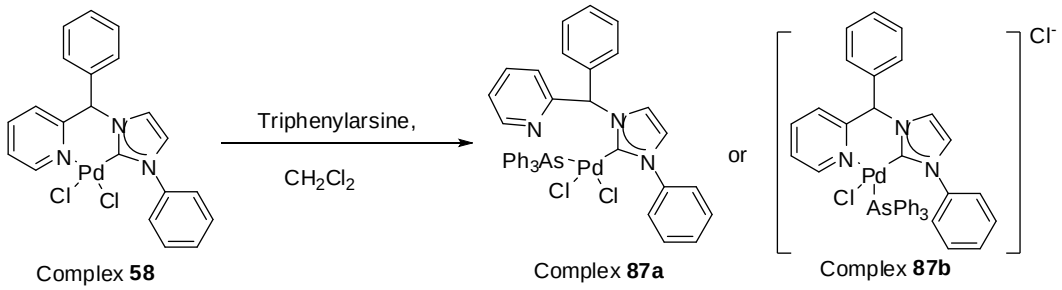

Scheme 3.15

3.2.3.8 Molecular Structure of Arsine Coordinated Complex (±)-87a

X-ray grade crystals of complex (±)-**87** can be afforded from the slow diffusion of diethyl ether into a methanol solution of complex (±)-**87**. The identity of complex (±)-**87a** and (±)-**87b** cannot be conclusively established by the ^{1}H NMR, therefore, the presence of the $N_{pyridine}$–Pd cleavage was confirmed by X-ray crystallography. From the X-ray crystallography study of complex (±)-**87**, complex (±)-**87a** was synthesized. A $N_{pyridine}$–Pd cleavage is observed

even when the coordinating ligand is switched to a weaker arsine ligand as compared to phosphine. The molecular structure of complex (±)-**87a** is depicted in Figure 3.14, selected bond lengths and bond angles are tabulated in Table 3.11.

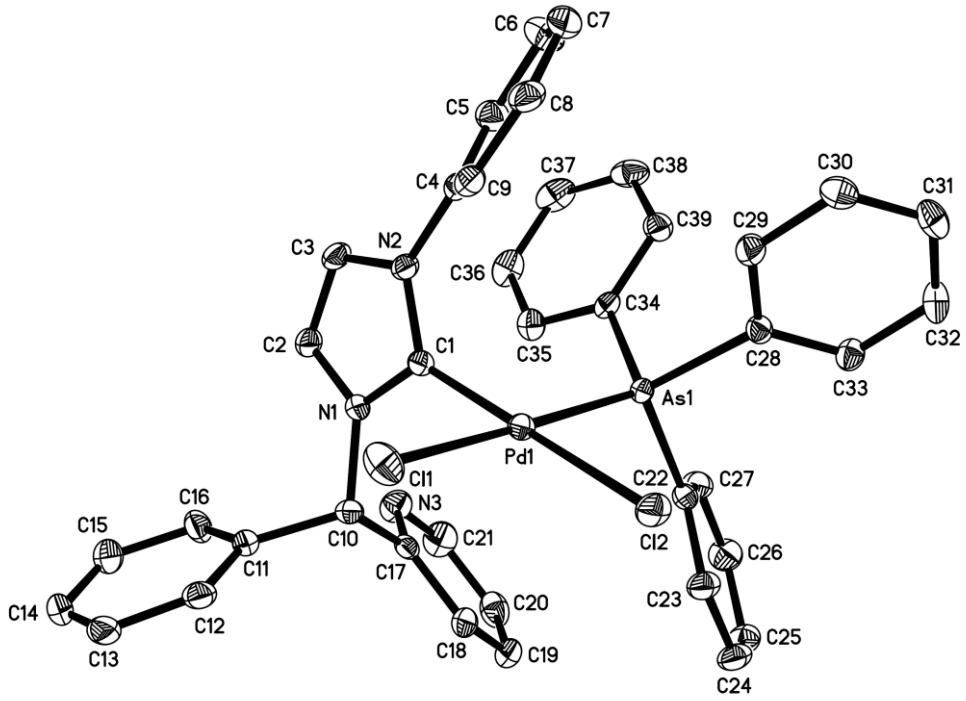

Figure 3.14 Molecular structure of complex (±)-**87a** with thermal ellipsoids at 50% probability. Hydrogens are omitted for clarity.

Table 3.11 Selected bond lengths (Å) and angles (°) for complex (±)-**87a**

Pd(1)–C(1)	1.968(2)	Pd(1)–As(1)	2.359(3)
Pd(1)–Cl(1)	2.358(6)	Pd(1)–Cl(2)	2.357(6)
N(1)–C(1)	1.353(3)	N(2)–C(1)	1.357(3)
N(1)–C(2)	1.381(3)	N(2)–C(3)	1.389(3)
N(1)–C(10)	1.482(3)	N(2)–C(4)	1.436(3)
C(1)–Pd(1)–Cl(1)	86.5(6)	C(1)–Pd(1)–As(1)	91.8(6)
As(1)–Pd(1)–Cl(2)	87.9(17)	Cl(1)–Pd(1)–Cl(2)	93.9(2)

3.3 Conclusion

In this chapter, the synthesis of chiral NHC palladium complexes (*R*)-**56**, (*S*)-81, (*S*)-**58** was achieved *via* the optical resolution of their respective amino acid diastereomers. Although the synthesis of chiral palladacycles *via* optical resolution in the presence of chiral amino acids as auxiliaries is one of the most common methods employed, this is however the first successful application on NHC palladacycle (*S*)-**56** and (*R*)-**56**. This methodology was successful applied in synthesis of chiral complexes (*S*)-**81** and (*S*)-**58**. The hemilability of the pyridine functionalized NHC palladacycle (±)-**58** was demonstrated. The $N_{pyridine}$–Pd bond of complex (±)-**58** can be selectively replaced by either a phosphine or by an arsine ligand.

3.4 Experimental

Reactions involving air-sensitive compounds were performed under a positive pressure of purified argon using standard Schlenk techniques. All the commercially available chemicals and solvents were used without prior drying or purification. Proton nuclear magnetic resonance (^{1}H NMR) and carbon nuclear magnetic resonance (^{13}C NMR) spectroscopy were performed on a Bruker Avance 300, 400 and 500 NMR spectrometers. The number of protons (n) for a given resonance is indicated by nH. Coupling constants are reported as a J value in Hz. Proton nuclear magnetic resonance spectra ^{1}H NMR are reported as δ in units of parts per million (ppm) downfield from $SiMe_4$ (δ 0.0). Carbon nuclear magnetic resonance spectra ^{13}C NMR are reported as δ in units of parts per million (ppm) relative to the signal of chloroform-*d* (δ 77.20, triplet). All chemical shifts reported are referenced to the chemical shifts of their respective residual solvent resonances. Unless stated otherwise, all NMR experiments are carried out at 300K. Mass spectra were recorded on a Thermo Finnigan MAT 95 XP Mass Spectrometer with EI mode and Waters Q-Tof Premimer Mass Spectrometer with ESI mode. Melting points were determined on SRS-Optimelt MPA-100 apparatus and were uncorrected. Optical rotations were measured on the specified solution in 0.1-dm cell at 25 °C with a Perkin-Elmer model 341 polarimeter. The Elemental Analysis Laboratory of the Division of Chemistry and Biological Chemistry at the Nanyang Technological University of Singapore performed elemental analyses.

3.4.1 Optical resolution of Racemic Complex (-)-56 and (+)-56

To a suspension of the racemic complex (±)-**56** (2.45g, 5.7 mmol) in 20 mL of MeOH, $AgNO_3$ (1.94 g, 11.4 mmol) was added. The reaction mixture was allowed to stir in the dark at room temperature for 3 h and was filtered through celite. The filtrate was treated with sodium (S_C)-phenylalanate (1.07 g, 5.7 mmol) in 100 mL of MeOH. The reaction mixture was stirred for 2 h and was concentrated to approximately 50 mL and was left to stand overnight. From the diastereomeric mixture, only complex (R_C,S_C)-**78** crystallized out as off-white crystals the next day and was isolated and washed with MeOH. The mother liquor was enriched in (S_C,S_C)-**78** > 99% *de*.

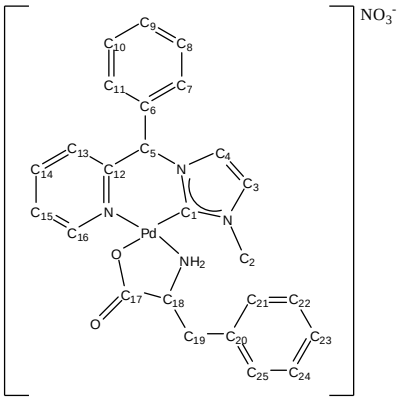

Diastereomer (R_C,S_C)-**78** 1.2g, 35 %, $[\alpha]_{436}$ +83.3 (*c* 0.5, , DMSO), M.p. = 189.5–190.2°C (dec.). ^{1}H NMR (500 MHz, DMSO-d_6): δ = 2.61–2.65 (m, 1 H, H18), 3.16 (d, 1 H, $J_{H,H}$ = 5.2 Hz, H19), 3.50–3.52 (m, 1 H, H19), 3.82 (s, 3 H, H2), 5.00 (d, 1 H, , $J_{H,H}$ = 9.6 Hz, NH), 5.98–6.01 (m, 1 H, NH), 6.94 (s, 1 H, aromatic), 6.96 (s, 1 H, aromatic), 7.15–7.23 (m, 5 H, aromatic), 7.35–7.38 (m, 2 H, aromatic), 7.47–7.50 (m, 2 H, aromatic), 7.59 (d, 1 H, $J_{H,H}$ = 1.8 Hz, aromatic), 7.76–7.79 (m, 1H, aromatic), 7.90 (d, 1 H, $J_{H,H}$ = 1.8 Hz, aromatic), 8.16 (d, 1 H, $J_{H,H}$ = 7.8 Hz, aromatic),

8.33–8.36 (m, 1H, aromatic), 8.71 (d, 1 H, $J_{H,H}$ = 4.7 Hz, H16) ppm. ^{13}C NMR (100 MHz, DMSO-d_6): δ = 37.26 (C2), 49.06 (C19), 62.71 (C5), 66.34 (C18), 123.58 (C3), 124.62 (C4), 126.61(C15), 126.79 (C13), 127.08, 127.65, 128.55, 128.91, 129.29, 129.57, 129.78, 137.35, 139.71, 142.10, 151.70 and 153.07 (aromatic), 154.77 (C16), 179.24 (C17) ppm. Anal Calcd for $C_{25}H_{25}N_5O_5Pd$ (581.09): C, 51.60; H, 4.33; N, 12.03. Found: C, 50.44; H, 4.33; N, 12.05.

The mother liquor is enriched in the other diastereomer (S_C,S_C)-**78**> 99% *de*.

Diastereomer (S_C, S_C)-**78** 1.1g, 34%. $[\alpha]_{436}$ +42.1 (*c* 0.5, CD_3OD). M.p. = 189–190 °C (dec.). ^{1}H NMR (400 MHz, MeOD): δ = 2.56 (s, 1 H, H18), 3.13–3.17 (m, 1 H, H19), 3.27–3.29 (m, 1 H, H19), 3.65 (s, 3 H, H2), 7.07 (s, 2 H, NH_2), 7.09–7.33 (m, 13 H, aromatic), 7.56–7.59 (m, 1 H, aromatic), 7.68 (d, 1 H, $J_{H,H}$ = 7.7 Hz, aromatic), 8.14–8.18 (m, 1 H, aromatic), 8.70 (d, 1 H, $J_{H,H}$ = 5.5 Hz, H16) ppm. ^{13}C NMR (100 MHz, CD_3OD): δ = 37.49 (C2), 40.62 (C19), 63.24 (C5), 68.62 (C18), 124.35 (C3), 125.50 (C4), 127.27 (C15) , 128.13 (C13), 128.21, 128.27, 130.03, 130.42, 130.67, 138.36, 140.43, 142.90 and 154.12 (aromatic), 156.39 (C16), 181.86 (C17) ppm. HRMS (ESI) *m/*z: $[M–NO_3]^+$ calcd for $C_{25}H_{25}N_4O_2{}^{106}Pd$ 519.1012, found 519.1013.

.

3.4.2 Synthesis of Complex (*R*)-56.

To a suspension of complex (R_C,S_C)-**78** (0.50g, 0.86 mmol) in MeOH (50 mL), 1 M HCl (aq) (4.3 mL, 4.3 mmol) was added. The reaction mixture

was stirred vigorously for approximately 1 hour and was concentrated down to give an orange yellow solid. The solid was washed three times with copious amount of methanol to give a pale yellow solid 0.2g, 51 %, $[\alpha]_{436}$ –12.5 (*c* 0.5, DMSO).

Similarly, complex (*S*)-**56** was achieved using the same method from complex (S_C, S_C)-**78** 0.2g, 50 %. $[\alpha]_{436}$ +11.8 (*c* 0.5, DMSO).

3.4.3 Synthesis of Complex (*R*)-79.

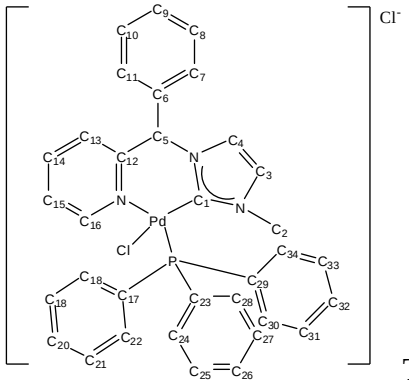

To a suspension of complex (*R*)-**56** (0.1 g, 0.23 mmol) in 10 mL of CH_2Cl_2, triphenylphosphine (0.061 g, 0.23 mmol) was added. The product was purified through precipitation in DCM and diethyl ether to give an off white solid 0.16, 97%, $[\alpha]_{436}$ = -92 (*c* 0.25, MeOH), M.p. = 203.0 – 204.8 °C (dec.). ^{1}H NMR (400 MHz, CD_3OD): δ = 3.05 (s, 3 H, H2), 7.07 (d, 1 H, $J_{H,H}$ = 1.9 Hz, aromatic), 7.11 (t, 2 H, $J_{H,H}$ = 7.0 Hz, aromatic), 7.24–7.31 (m, 7 H, aromatic), 7.39–7.42 (m, 6 H, aromatic), 7.57–7.60 (m, 2 H, aromatic), 7.75–7.79(m, 2 H, aromatic), 7.90 (d, 1 H, $J_{H,H}$ = 2 Hz, aromatic), 7.99 (d, 1 H, $J_{H,H}$ = 7.7 Hz, aromatic), 8.26 (td, 1 H, $J_{H,H}$ = 7.7 Hz, $J_{H,H}$ = 1.5 Hz, aromatic), 9.33–9.35 (m, 1 H, H16) ppm. ^{13}C NMR (100 MHz, CD_3OD): δ

= 38.08 (C2), 69.48 (C5), 124.62 (C3), 125.43 (C4), 126.83, 126.85, 127.69, 127.72, 128.75, 129.68, 129.79, 130.39, 130.57, 132.84, 135.74, 139.90, 142.39 and 154.99 (aromatic), 155.26 (C16), 162.17 (C1) ppm. $^{31}P\{1H\}$ (161 MHz, CD_3OD): δ = 28.31 ppm. HRMS (ESI) *m/*z: $[M\text{-}Cl]^+$ calcd for $C_{34}H_{30}Cl_1N_3PPd$ 652.0901, found 652.0903. Anal Calcd for $C_{34}H_{30}ClN_3PPd$ (653.47): C, 62.49; H, 4.63; N, 6.43. Found: C, 62.34; H, 4.65; N, 6.35.

Similarly, complex (*S*)-**79** was achieved using the same method from complex (*S*)-**56** 0.2g, 98 %. $[\alpha]_{436\ =}$ +95 (*c* 0.2, MeOH).

3.4.4 Optical resolution of Racemic Complex (-)-57 and (+)-57

Sodium (S_C)-phenylalanate (0.98 g, 5.2 mmol) was added to a suspension of the racemic complex (±)-**57** (2.50g, 5.2 mmol) in 100 mL of MeOH. The reaction mixture was stirred for 1 h and was concentrated *in vacuo*. The residue was redissolved in ethanol and diethyl ether was allowed to diffuse into the solution slowly. Diastereomer (S_C,S_C)-**80** which crystallized out as off-white crystals the next day was isolated and washed with ethanol. complex (R_C,S_C)-**80** enriched mother liquor was concentrated to dryness and redissolved in acetonitrile. Slow evaporation of the acetonitrile solution allowed the remaining diastereomer (S_C,S_C)-**80** to crystallize out.

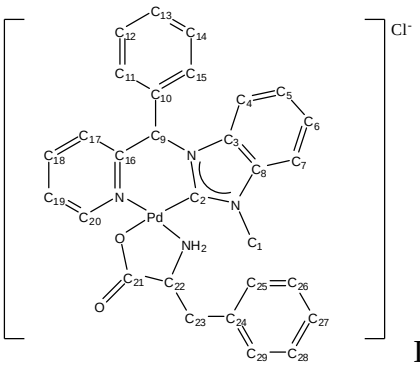

Diastereomer (S_C,S_C)-**80** 0.9 g, 60 %, $[\alpha]_{365}$ = +202 (*c* 0.55, MeOH), M.p. = 215.9–216.5°C (dec.). ^{1}H NMR (400 MHz, DMSO-d_6): δ = 2.82–2.87 (m, 1 H, H22), 3.13 (dd, 1 H, $J_{H,H}$ = 14.0 Hz, $J_{H,H}$ =1.7, H23), 3.22–3.24 (m, 1 H, H23), 3.95 (s, 3 H, H1), 5.73–5.77 (m, 2 H, NH_2), 7.23 (t, 1 H, $J_{H,H}$ = 6.9 Hz, aromatic), 7.29–7.36 (m, 4 H, aromatic), 7.39–7.40 (m, 3 H, aromatic), 7.49–7.52 (m, 4 H, aromatic), 7.73–7.77 (m, 1 H, aromatic), 7.82–7.86 (m, 1 H, aromatic), 8.01 (s, 1 H, aromatic), 8.13–8.17 (m, 1 H, aromatic), 8.32–8.39 (m, 2 H, aromatic), 8.72 (d, 1 H, $J_{H,H}$ = 5.4 Hz, H20) ppm. ^{13}C NMR (100 MHz, DMSO-d_6): δ = 34.00 (C1) 40.13 (C23), 61.46 (C9), 62.48 (C22), 111.12, 111.82, 124.50, 126.08, 126.40, 126.67, 128.43, 128.53, 128.86, 129.26, 132.76, 134.01, 137.78, 137.91, 141.73, 152.22 and 154.85 (aromatic), 164.25 (C20), 177.30 (C21) ppm. HRMS (ESI) *m/*z: $[M\text{-}Cl]^+$ calcd for $C_{29}H_{27}N_4O_2{}^{106}Pd$ 569.1169, found 569.1183. $C_{29}H_{27}ClN_4O_2Pd$ (605.42): calcd. C 57.53, H 4.50, N 9.25; found C 57.69, H 4.10, N 9.31.

3.4.5 Synthesis of Chiral Complex (*S*)-57

To a suspension of complex (S_C,S_C)-**80** (0.50g, 0.83 mmol) in 1 mL of MeOH, 1 M HCl (aq) (8.3 mL, 8.3 mmol) was added. The reaction mixture was stirred vigorously for approximately 1 h and was concentrated down to give a

pale yellow solid. The solid was washed three times with copious amount of MeOH to give a pale yellow solid 0.26g, 66 %, $[\alpha]_{365}$ = +405 (*c* 0.21, DMSO).

3.4.6 Synthesis of Chiral Complex (*S*)-81

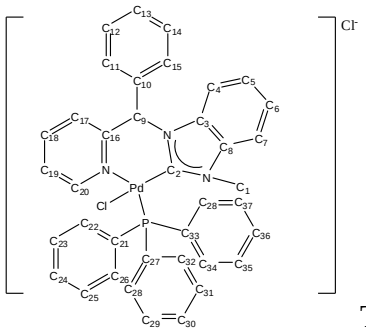

To a suspension of complex (*S*)-**57** (0.1g, 0.21mmol) in 10 ml of CH_2Cl_2, triphenylphosphine (0.055g, 0.21g) was added. The solution was stirred for 1 h. After 1 h, the clear solution was concentrated to dryness. The product was purified through precipitation in CH_2Cl_2 and diethyl ether to give an off white solid 0.15, 97%, $[\alpha]_{436}$ = -37 (*c* 0.57, MeOH), M.p. = 209.0 – 210.9°C (dec.). ^{1}H NMR (400 MHz, CD_3OD): δ = 3.15 (s, 3 H, H1), 6.51 (s, 1 H, aromatic), 6.97 (t, 2 H, $J_{H,H}$ = 7.8 Hz, aromatic), 7.11–7.25 (m, 11 H, aromatic), 7.36–7.42 (m, 6 H, aromatic), 7.51 (t, 2 H, aromatic protons), 7.09–7.33 (m, 11 H, aromatic), 7.56–7.59 (m, 1 H, $J_{H,H}$ = 7.1 Hz, aromatic), 7.65 (t, 2 H, $J_{H,H}$ = 6.0 Hz, aromatic), 7.72 (s, 1 H, aromatic), 8.04 (d, 1 H, $J_{H,H}$ = 7.10 Hz, aromatic), 8.14 (t, 1 H, $J_{H,H}$ = 8.2 Hz, aromatic), 8.18 (d, 1 H, $J_{H,H}$ = 7.8 Hz, aromatic), 9.23–9.24 (m, 1 H, H20) ppm. ^{13}C NMR (100 MHz, CD_3OD): δ = 36.17(C1), 65.95 (C9) ,112.06, 112.79, 126.79, 126.68, 127.01, 127.80, 127.82, 128.73, 129.69, 129.80, 130.47, 130.64, 132.90, 135.14, 135.81, 140. 09, 142.48, 151.25 and 155.02 (aromatic), 155.11 (C20), 174.15 (C2) ppm. ^{31}P{1H} (161 MHz, CD_3OD): δ = 28.99 ppm. HRMS (ESI) *m/*z: $[M\text{-}Cl]^+$ calcd

for $C_{38}H_{32}ClN_3PPd$ 704.1061, found 704.1055. Anal Calcd for $C_{38}H_{32}ClN_3PPd$ (703.53): C, 64.87; H, 4.58; N, 5.97. Found: C, 65.12; H, 4.69; N, 6.23.

3.4.7 Optical resolution of Racemic Complex (-)-58 and (+)-58

Sodium (S_C)-prolinate (0.70 g, 5.1 mmol) was added to a suspension of the racemic complex (±)-**58** (2.50 g, 5.1 mmol) in 100 mL of MeOH. The reaction mixture was stirred for 1 h and was concentrated *in vacuo*. The residue was redissolved in MeOH and diethyl ether was allowed to diffuse into the solution slowly. Diastereomer (S_C,S_C)-**82** which crystallized out as off-white crystals the next day was isolated and washed with CH_2Cl_2. The complex (R_C,S_C)-**82** enriched mother liquor was concentrated to dryness and redissolved in ethanol. Slow diffusion of diethyl ether into the ethanol solution of the complex (R_C,S_C)-**82** enrichedmother liquor is currently in progress to allow the remaining diastereomer (S_C,S_C)-**82** to crystallize out.

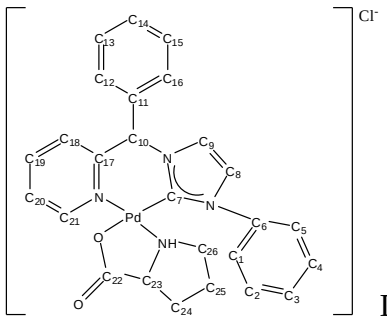

Diastereomer (S_C,S_C)-**82** 1.8g, 62 %, $[\alpha]_{436}$ = -167 (*c* 0.5, MeOH), M.p. = 222.4 –223.5 °C (dec.). ^{1}H NMR (400 MHz, DMSO-d_6): δ = 0.98–1.04 (m, 1 H, H24), 1.15–1.26 (m, 1 H, H24), 1.40–1.52 (m, 1 H, H25), 1.56–1.66 (m, 1 H, H25), 1.86–2.01 (m, 1H, H26), 2.29–2.38 (m, 1 H, H26), 3.22 (dd, 1 H, $J_{H,H}$ = 8.6 Hz, $J_{H,H}$ = 2.9 Hz, H23), 7.23 (d, 2 H, $J_{H,H}$ = 7.0

Hz, aromatic), 7.34 (s, 1 H, H10), 7.43–7.51 (m, 3 H, aromatic), 7.62–7.70 (m, 3 H, aromatic), 7.74–7.79 (m, 2 H, aromatic), 7.86–7.87 (m, 2 H, aromatic), 8.10 (d, 1 H, $J_{H,H}$ = 2.0 Hz, aromatic), 8.13 (d, 1 H, $J_{H,H}$ =7.4 Hz, aromatic), 8.32 (td, 1 H, $J_{H,H}$ = 7.7 Hz, $J_{H,H}$ =1.5 Hz, H19), 8.88 (d, 1 H, $J_{H,H}$ = 4.8 Hz, H21) ppm. ^{13}C NMR (100 MHz, , DMSO-d_6): δ = 23.74 (C24), 29.15 (C25) , 50.92 (C26) 68.19 (C10) , 69.07 (C23), 125.23 (C9), 125.63(C8), 127.27 (C20), 127.37 (C18) , 128.28, 130.13, 130.37, 131.46 and 139.74 (Ph), 140.56 (C19), 142.87 and 154.42 (Ph), 155.95 (C21), 182.17 (C22) ppm. HRMS (ESI) *m/*z: $[M–Cl]^+$ calcd for $C_{26}H_{25}N_4O_2{}^{106}Pd$ 531.1012, found 531.1014. Anal Calcd for $C_{26}H_{25}ClN_4O_2Pd$ (567.38): C, 55.04; H, 4.44; N, 9.87. Found: C, 54.97; H, 4.15; N, 10.15.

3.4.8 Synthesis of Chiral Complex (*S*)-58

To a suspension of complex (S_C,S_C)-**82** (0.50g, 0.88 mmol) in 1 mL of MeOH, 1 M HCl (aq) (8.8 mL, 8.8 mmol) was added. The reaction mixture was stirred vigorously for approximately 1 hour and was concentrated down to give a pale yellow solid. The solid was washed three times with copious amount of MeOH to give a pale yellow solid 0.28g, 65 %, $[\alpha]_{436}$ = -27.8 (*c* 0.20, DMSO).

3.4.9 Synthesis of Complex (±)-84

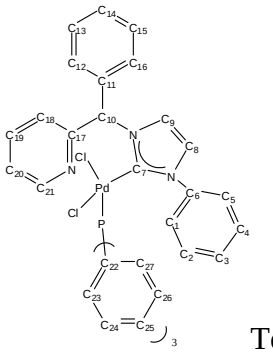

To a suspension of complex (*S*)-**58** (0.1g, 0.20 mmol) in 10 ml of CH_2Cl_2, triphenylphosphine (0.053g, 0.20mmol) was added. The solution was stirred for 1 h. After 1 h, the clear solution was concentrated to dryness. The product was purified through precipitation in DCM and diethyl ether to give an off white solid 0.148g, 98%. ^{1}H NMR (400 MHz, CD_3OD): δ = 6.33 (s, 1 H, H10), 7.03 (t, 2 H, $J_{H,H}$ = 7.8 Hz, aromatic), 7.17–7.27 (m, 13 H, aromatic), 7.32–7.35 (m, 4 H, aromatic), 7.39 (s, 2 H, aromatic), 7.41–7.47 (m, 5 H, aromatic), 7.82 (t, 1 H, $J_{H,H}$ = 6.6 Hz, aromatic), 8.04 (d, 1 H, $J_{H,H}$ 7.6 Hz, aromatic), 8.13 (s, 1 H, aromatic), 8.29 (t, 1 H, $J_{H,H}$ = 7.7 Hz, H19), 9.45–9.46 (m, 1 H, H21). ^{13}C NMR (100 MHz, CD_3OD): δ = 70.17 (C10), 125.12 (C9), 125.29 (C8), 126.25 (C20), 127.08 (C18), 127.96, 128.58, 129.41, 130.34, 130.40, 130.70, 130.96, 132.46, 136.14, 138.93 and 139.36 (Ph), 142.46 (C19), 155.00 (Ph), 155.23 (C21), 161.88. ppm (C7). ^{31}P{1H} (161 MHz, CD_3OD): δ = 26.94 ppm. HRMS (ESI) *m/z*: $[M–Cl]^+$ calcd for $C_{39}H_{32}N_3ClP^{108}Pd$ 716.1016, found 716.1068. Anal Calcd for $C_{39}H_{32}ClN_3PPd$ (715.54): C, 65.46; H, 4.51; N, 5.87. Found: C, 65.34; H, 4.65; N, 5.69.

3.4.9 Synthesis of Complex (±)-87a

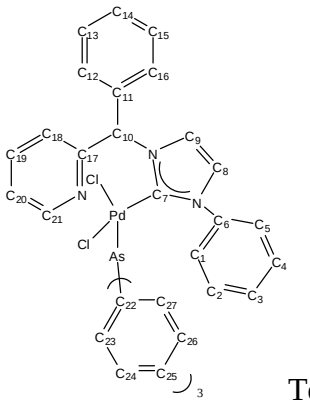

To a suspension of complex (±)-**58** (0.1g, 0.20 mmol) in 10 ml of DCM, triphenylarsine (0.063g, 0.20mmol) was added. The solution was stirred for 1 hr. After 1 hr, the clear solution was concentrated to dryness. The product was purified through precipitation in DCM and diethyl ether to give an off white solid 0.16g, 98%. ^{1}H NMR (400 MHz, CD_3OD): δ = 6.63 (s, 1 H, H10), 6.94–6,97 (m, 2 H, aromatic), 7.19 (t, 2 H, $J_{H,H}$ = 8.0 Hz, aromatic), 7.25–7.37 (m, 14 H, aromatic), 7.40 (s, 1 H, aromatic), 7.49 (t, 3 H, $J_{H,H}$ = 8.0 Hz, aromatic proton), 7.54 (d, 1 H, $J_{H,H}$ = 4.0 Hz, aromatic protons), 7.63–7.67 (m, 1 H, aromatic proton), 7.71–7.75 (m, 2 H, aromatic protons), 7.84–7.87 (m, 1 H, aromatic proton), 8.08 (d, 1 H, $J_{H,H}$ = 8.0 Hz, aromatic proton), 8.16 (d, 1 H, $J_{H,H}$ = 2.0 Hz, aromatic proton), 8.33 (dt, 1 H, $J_{H,H}$ = 7.7 Hz, $J_{H,H}$ = 1.5 Hz, H18), 9.49 (d, 1 H, $J_{H,H}$ = 4.7 Hz, H21) ppm. ^{13}C NMR (100 MHz, CD_3OD): δ = 70.17 (C10), 116.82 (Ph), 124.87 (C9), 124.96 (C8), 126.12 (C20), 126.26 (C18), 127.25, 128.10, 128.56, 129.78, 129.94, 130.13, 130.35, 130.50, 130.95, 131.03, 131.97, 132.46, 134.09, 134.71, 139.01 and 139.62 (Ph), 142.61 (C19), 154.90 (Ph), 155.32 (C21), 164.02 (C7) ppm. HRMS (ESI) *m/z*: $[MH–Cl]^+$ calcd for $C_{39}H_{33}N_3ClAs^{108}Pd$ 761.0618, found 761.0627. Anal Calcd for

$C_{39}H_{32}Cl_2N_3AsPd$ (794.94.): C, 58.92; H, 4.06; N, 5.29. Found: C, 59.13; H, 4.09; N, 5.35.

Chapter 4

Catalysis: Allylic Alkylation

4.1 Introduction

Phosphine ligands have been widely used in catalysis owing to the fact that it is easy to "fine-tune" their stereogenic and electronic properties through small changes in ligand structure. Recently, NHC has emerged as a promising alternative to phosphines. Being a σ donor and a π acceptor like phosphines, its stereogenic and electronic properties too can be modified like phosphines. Therefore, NHC has become an attractive functional analogue to phosphines for the design of organometallic catalysts.

In the past decade, NHC based palladium complexes have demonstrated their catalytic activity especially in the field of cross coupling reactions as highlighted in chapter 1. In particular interest to our discussion is its ability to catalyze allylic substitution reactions. Ever since 2003, whereby Mori *et al.* showed that NHC based palladium complexes were able to catalyze the achiral version of allylic alkylation, there has been a rapid development in allylic alkylation using both chiral and achiral palladium complexes (Scheme 4.1).[89] Excellent reactivity was achieved in the reaction described in Scheme 4.1, with quantitative yield when Cs_2CO_3 was used as the base. However a reaction time of 10 hours was required for complete conversion. In comparison, when NaH was used as the base, the reaction required only 2 hours to complete with 98% yield. In Mori's report, he further demonstrated that retention of

stereochemistry is possible in the presence of a chiral acetate substrate under the conditions as highlighted in Scheme 4.1.

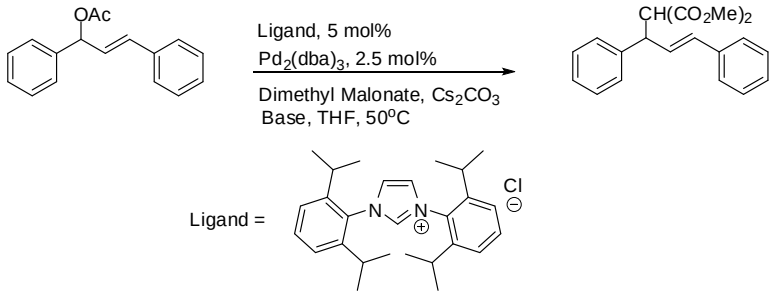

Scheme 4.1

In the same year, Douthwaite *et al.* synthesized a series of chiral chelating imino-NHC palladium complexes that displayed both excellent reactivity and selectivity of up to 92 % ee in the asymmetric version of allylic alkylation (Scheme 4.2).[90]

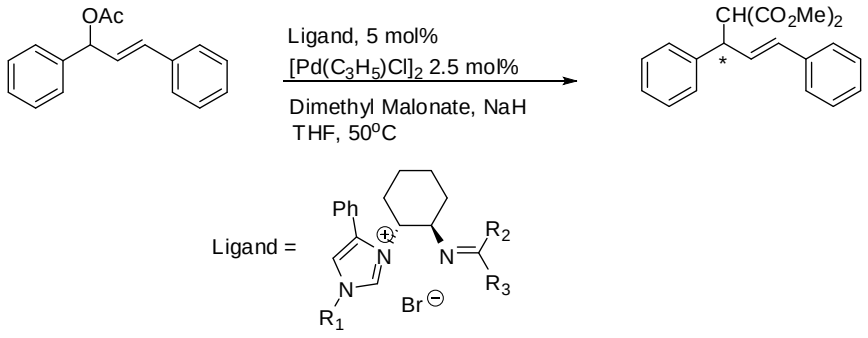

Scheme 4.2

Following the development of asymmetric allylic alkylation mediated by chiral NHC palladium complexes, the reaction has become a popular benchmark reaction to test of the reactivity and selectivity of newly synthesized chiral NHC complexes.

Allylic amination is another variation of the allylic substitution that can be mediated by NHC palladium complexes. However, the reported selectivties have been quite disappointing to date. Ability of the NHC palladium complexes to mediate allylic amination reaction was first tested out by Togni in 2007 using ferrocenyl functionalized chiral NHC palladium complex **88** as seen in Scheme 4.3.[91] However, both the yield and ee value of the reaction were disappointing. The highest obtained yield was 58% and the enantioselectivity value of 5% was almost negligible.

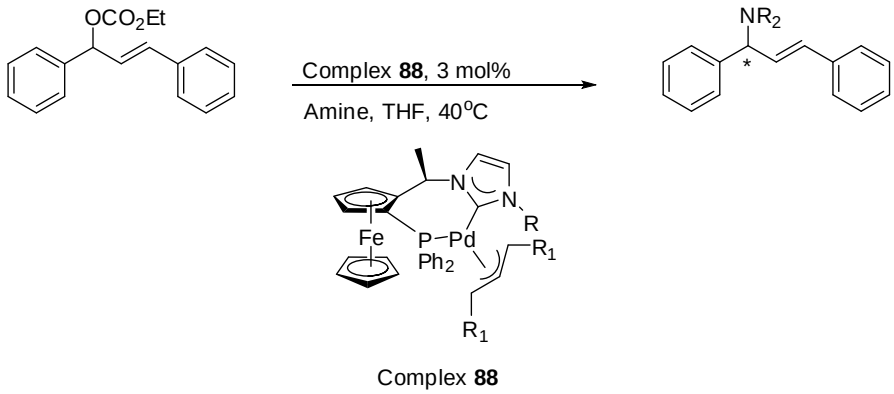

Complex **88**

Scheme 4.3

In the same year, Roland *et al.* reported that the rates of allylic amination can be greatly enhanced by adding triphenylphosphine as an additive.[92](Scheme 4.4) Complete conversion can be achieved after 6 hours at 20°C, compared to Togni's conditions which required 72 hours at 40°C. The yield obtained in the presence of triphenylphosphine is also much higher with >98% when K_2CO_3 as base. However, when KOH is added as the base, the percentage yield of the desired homoallylic amine decreased to 68% with 16% of the ether side product isolated.

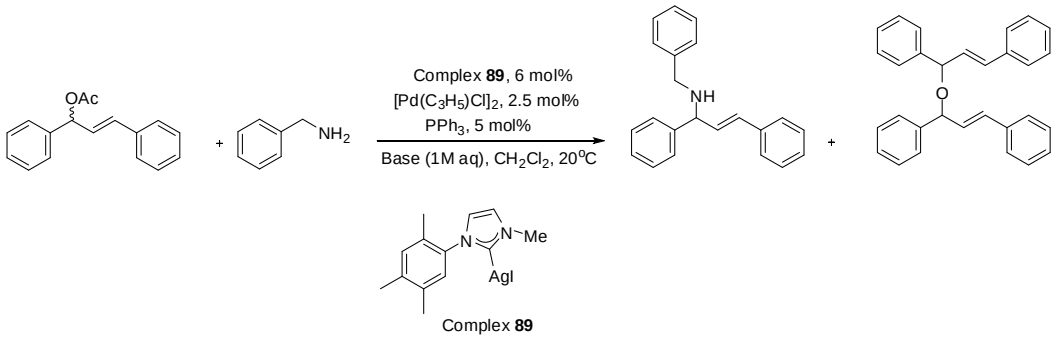

Scheme 4.4

In a subsequent report, Roland further investigated the substrate scope of the mixed NHC phosphine palladium system against the allylic amination reaction.[93] The mixed system is applicable towards both aliphatic and aromatic amines and allylic substrates. When a chiral amine (S)-α-methylbenzylamine is used as the incoming nucleophile, a high yield of 95 % can be achieved, but a 1:1 diastereomeric ratio is obtained (Scheme 4.5). The authors attributed the lack of selectivity to the similar *trans* effect influence of the phosphine and NHC, hence the incoming nucleophile will no longer selectively attack the site *trans* to the NHC.

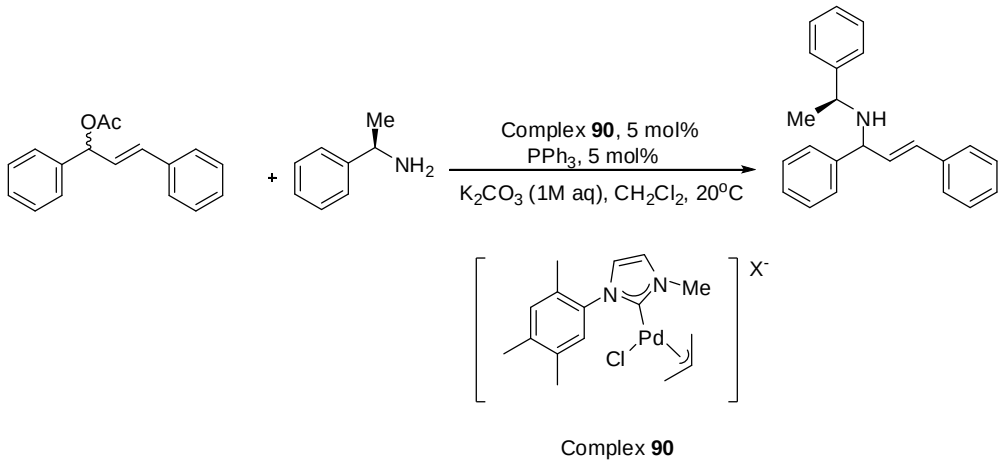

Complex **90**

Scheme 4.5

Chianese *et al.* also tested the reactivity of their novel pyridine functionalized NHC palladium complex **91** against the allylic amination (Scheme 4.5).[94] Three different substituted amines were isolated, with amine **B** as the major product formed in which the authors attributed it to the reversible nature of the amination under their proposed conditions.

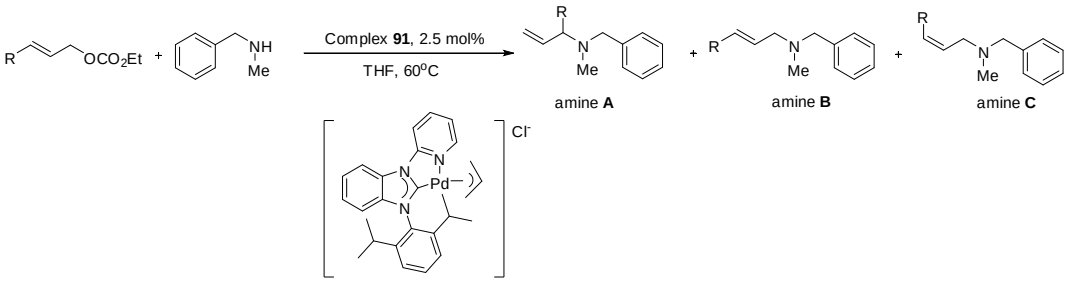

Complex **91**

Scheme 4.6

4.1.1 Asymmetric Allylic Alkylation

For the palladium catalyzed asymmetric allylic alkylation reaction, it has been accepted that Pd (0) is the active catalyst. The substrate will coordinate to the Pd (0) centre via the double bond and upon elimination of the acetyl leaving group, a Pd allyl species will be formed. The selectivity of this reaction is achieved when the incoming nucleophile preferentially attacks either from **a** or **b** (Figure 4.1).

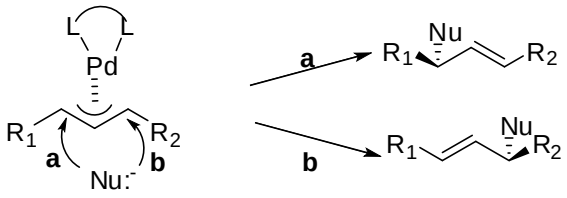

Figure 4.1 Possible sites of nucleophilic attack

The site of attack is believed to be determined by the electronic nature of the chelating ligand on the Pd catalyst.[95] In Douthwaite's paper, they prepared a series of imino chelating NHC palladacycles and tested their reactivity and selectivity in asymmetric allylic alkylation. They observed that by increasing the bulkiness in R_1 and decreasing that of R_3, they can improve the enantioselectivity of the asymmetric allylic alkylation to 92 % which can be explained by their proposed Pd allyl intermediate as seen in Figure 4.2. The incoming nucleophile is expected to attack the position *trans* to the carbene. In the presence of a bulky R_3, the original pathway of the *trans* attack to the NHC by the nucleophile will be hindered by the bulky group and hence the electronic preference provided by the carbene is lost and ultimately selectivity of the reaction will be compromised.[96] Therefore, an ideal N functionalized NHC Pd

catalyst for asymmetric allylic alkylation can by hypothesized to be a have a sterically bulky substituent on the wingtip N group of the carbene and a sterically unconstraint site for easy attack of the nucleophile.

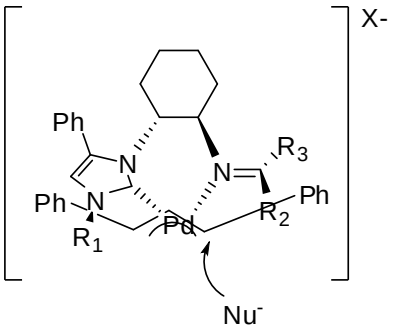

Figure 4.2 Proposed Pd allyl intermediate

4.2 Results and Discussions

4.2.1 Model Study with Racemic Palladacycle (±)-56

Heartened by the positive results above, the newly synthesized chiral and achiral palladacycles were applied to the allylic alkylation reaction to test out their reactivity and selectivity. The catalyst loading was kept constant at 2 mg for all the following allylic alkylation reactions that will be discussed. Four methods, methods A to D were employed in the course of optimisation of the catalytic allylic alkylation reactions. In method A as illustrated in Scheme 4.7, the dichloride complexes that were synthesized in chapters 2-3 were used as catalysts. Different combinations of solvents and bases were used to test out the reactivities of the dichloride complexes. In method B, the dichloride complexes were treated with different silver salts *in situ* for approximately an hour to replace the dichlorides with weakly coordinating ligands prior to the

introduction of the substrates (Scheme 4.8). In method C, the dichloride complexes were treated with $AgPF_6$ to replace the dichlorides with weakly coordinating acetonitrile. The bisacetonitrile complexes which were isolated as crude white precipitate were used as catalysts (Scheme 4.9). Lastly, in method D, the triphenylphosphine coordinated complexes were used as catalysts instead of the dichloride complexes (Scheme 4.10).

An initial model study on the reactivity of the palladacycles were conducted with racemic complex (±)-**56**. The reactivity of racemic complex (±)-**56** was tested against the allylic alkylation reaction as shown in Scheme 4.7. Different solvents, temperatures and bases were tested against the reaction and the results are summarised in Table 4.1.

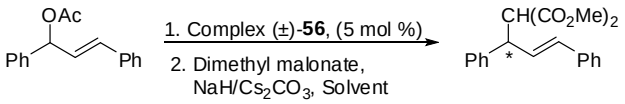

Scheme 4.7 (Method A)

The reaction was tested in CH_2Cl_2 and THF for the initial screening, in the presence of either NaH or Cs_2CO_3. However, after 48 hours at room temperature and at the elevated temperature of 50°C for THF and 35°C for CH_2Cl_2, there was no product formation detected by TLC as shown in table 4.1.

Table 4.1 Achiral Allylic Alkylation (Method A)

Entry	Solvent	Base	Temp. (°C)	Time (h)	Percentage Yield (%)[a]
1	CH_2Cl_2	NaH	22	48	-
2	THF	NaH	22	48	-
3	MeOH/ DMSO	NaH	22	48	-
4	CH_2Cl_2	NaH	35	48	-
5	THF	NaH	50	48	-
6	MeOH/DMSO	NaH	50	48	-
7	CH_2Cl_2	Cs_2CO_3	22	48	-
8	THF	Cs_2CO_3	22	48	-
9	MeOH/ DMSO	Cs_2CO_3	22	48	-
10	CH_2Cl_2	Cs_2CO_3	35	48	-
11	THF	Cs_2CO_3	50	48	-
12	MeOH/DMSO	Cs_2CO_3	50	48	-

(a): Method A as seen in Scheme 4.7

The lack of reactivity of complex (±)-**56** was suspected to be due to the insolubility of the catalyst in the solvent system of either CH_2Cl_2 and THF, therefore the solvent system was switched to a MeOH/DMSO mixture to improve the solubility of the catalyst in the reaction. Even after the switch in solvent mixture, there were no observable improvements in the solubility and

hence, product formation was not observed. No observable differences were found when either Cs_2CO_3 or NaH was used as the base for the reaction.

During the resolution of complex (±)**-56**, upon replacement of the dichloride with nitrate, there was a substantial improvement observed in the solubility of the palladacycle. Moreover, in other catalytic reactions using NHC based palladacycles, it has been observed that by replacing the 2 halides coordinating to the palladium centre with weakly coordinating ligands such as with acetate groups, the reactivity of the palladium catalyst was greatly improved.[97] Therefore, the dichloride in complex (±)**-56** was replaced with weakly coordinating ligands in the presence of different silver salts. The newly formed catalysts were generated *in situ* in the catalysis reactions as shown in Scheme 4.8. The dichloride complex (±)**-56** was stirred with 2.1 molar equivalents of different Ag salts to replace the chlorides with the respective weakly coordinating ligands as tabulated in Table 4.2 for an hour prior to the addition of the catalysis substrates. However, after screening through different silver salts as seen in Table 4.2, the reactivity of the catalysts remained unchanged and no product spots were observed by TLC even at elevated temperature.

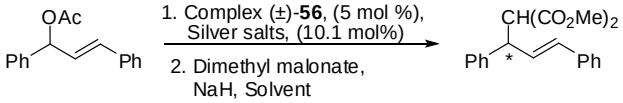

Scheme 4.8 (Method B)

Table 4.2 Achiral Allylic Alkylation (Method B)

Entry	Silver Salt	Solvent	Temp. (°C)	Time (h)	Percentage Yield (%)[b]
1	$AgPF_6$	THF	22	48	-
2	$AgBF_4$	THF	22	48	-
3	$AgNO_3$	THF	22	48	-
4	$AgCH_3COO$	THF	22	48	-
5	$AgCF_3COO$	THF	22	48	-
6	$AgPF_6$	CH_2Cl_2	22	48	-
7	$AgBF_4$	CH_2Cl_2	22	48	-
8	$AgNO_3$	CH_2Cl_2	22	48	-
9	$AgCH_3COO$	CH_2Cl_2	22	48	-
10	$AgCF_3COO$	CH_2Cl_2	22	48	-
11	$AgPF_6$	THF	50	48	-
12	$AgBF_4$	THF	50	48	-
13	$AgNO_3$	THF	50	48	-
14	$AgCH_3COO$	THF	50	48	-
15	$AgCF_3COO$	THF	50	48	-
16	$AgPF_6$	CH_2Cl_2	35	48	-
17	$AgBF_4$	CH_2Cl_2	35	48	-
18	$AgNO_3$	CH_2Cl_2	35	48	-
19	$AgCH_3CHOO$	CH_2Cl_2	35	48	-
20	$AgPF_6$	CH_2Cl_2	35	48	-

(b) Method B as seen in Scheme 4.8

No reaction was detected by TLC when the catalysts as seen in Scheme 4.8 were generated and used *in situ*. Therefore, the catalytic reaction was repeated with the bisacetonitrile coordinated complex (±)-**92** that was synthesized and isolated before addition into the catalysis reaction to examine whether there will be any differences observed in the reactivity of the catalyst (Scheme 4.9). In order to ensure that the dichlorides can be replaced by the bisacetonitrile successfully, complex (±)-**56** was stirred in 4 molar equivalents of $AgPF_6$ and the reaction mixture was allowed to stir at reflux for 6 hours. The results are tabulated in table 4.3. Although product formation can be observed by TLC, the highest isolated yield obtained was only 15% in THF at 50°C after 48 hours. The reaction was repeated in CH_2Cl_2, no product was observable at room temperature. The reaction temperature was raised to 35 °C in CH_2Cl_2 in a bid to accelerate the reaction. However, the starting material remained unreacted after 48 hours at the elevated temperature.

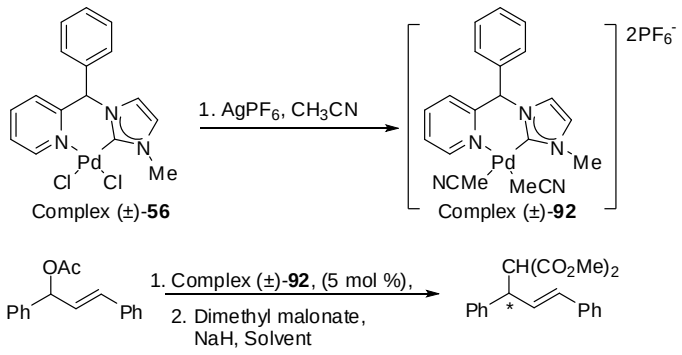

Scheme 4.9 (Method C)

Table 4.3 Achiral Allylic Alkylation (Method C)

Entry	Silver Salt	Solvent	Temp. (°C)	Time (h)	Percentage Yield (%)[c]
1	$AgPF_6$	THF	22	48	-
2	$AgPF_6$	THF	50	48	15
3	$AgPF_6$	CH_2Cl_2	22	48	-
4	$AgPF_6$	CH_2Cl_2	35	48	-

(c) Method C as seen in Scheme 4.9

In chapter 3, triphenylphosphine was added to complex (±)-**56** in order to improve the solubility of the palladacycle. Therefore, the phosphine coordinated complex (±)-**79** may exhibit better selectivity amongst the synthesized palladium complexes. Moreover, as demonstrated by Roland,[93] the addition of triphenylphosphine is crucial in the catalysis. Therefore, the allylic alkylation reaction was repeated using complex (±)-**79** as shown in Scheme 4.10. The 2 allylic alkylation were set up with complex (±)-**79** as the catalyst and NaH as the base, one in THF and the other in CH_2Cl_2. Both reactions were allowed to run for 4 hours at room temperature. After 4 hours, the reaction in CH_2Cl_2 proceeded to completion as indicated by the absence of starting material from TLC monitoring. In the case of the reaction in THF, a very faint starting material spot was still observable by TLC after 4 hours. Both reactions were quenched after 4 hours and their isolated yield after column chromatography purification is shown in Table 4.4. The reactivity of the

catalyst was quite good as the reaction progressed to completion in 4 hours at room temperature in CH_2Cl_2.

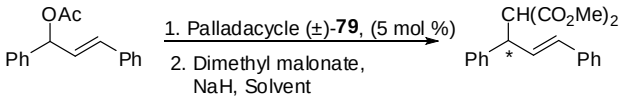

Scheme 4.10 (Method D)

Table 4.4 Achiral Allylic Alkylation (Method D)

Entry	Solvent	Temp. (°C)	Time (h)	Percentage Yield (%)[d]
1	THF	22	4	76
2	CH_2Cl_2	22	4	60

(d) Method D as seen in Scheme 4.10

The model study indicated that the reactivity of the newly synthesized complex (±)-**56** was greatly improved upon coordination with triphenylphosphine to form complex (±)-**79**. The reaction proceeds in either CH_2Cl_2 or THF, with a much faster completion time in the non coordinative CH_2Cl_2. With this rather promising result in the model study, the asymmetric allylic alkylation was tested with the chiral complex (*R*)-**56**, complex (*S*)-**56**, complex (*S*)-**57**, complex (*S*)-**58**, complex (*R*)-**79**, complex (*S*)-**79** and complex (*S*)-**81**

4.2.2 Asymmetric Allylic Alkylation

According to the proposed palladium allyl intermediate by Douthwaite *et al.* (Figure 4.2), complex (*S*)-**58** should be able to offer a better stereo control

over the reaction with its bulkier phenyl group. However, due to its hemilability, the rigidity offered by the chelate ring is lost upon coordination with PPh_3 as seen in Chapter 3. More importantly, the chirality of the palladacycle was also lost upon the cleavage of the $N_{pyridine}$–Pd bond. Hence the conditions established in the optimised method D of the model study with complex (±)-**79** cannot be applied to complex (±)-**84**. Therefore, method D can only be applied to chiral complex (*R*)-**79**, complex (*S*)-**79** and complex (*S*)-**81**.

The asymmetric allylic alkylation reaction was first carried out under the optimised method D that was developed in the model study with the complex (*R*)-**79**, complex (*S*)-**79** and complex (*S*)-**81**. Although the reactions proceeded almost to completion after 4 hours for all the catalysts, the selectivities of all the catalysts were very poor with almost no enantioselectivities in all entries. Since an approximate racemic product mixture is obtained for both complex (*R*)-**79** and complex (*S*)-**79**, a conclusive statement with regards to the difference in selectivity of the enantiomers cannot be drawn. Under similar reaction conditions, the reactivity of complex (*S*)-**81** is by far more superior as compared to the reactivity of both complex (*R*)-**79** and complex (*S*)-**79**, with the reaction proceeding to completion in less than 30 minutes in CH_2Cl_2 with quantitative yield. This can be attributed to the higher σ donor ability of complex (*S*)-**81** as compared to complex (*R*)-**79** and complex (*S*)-**79**, which is evident in the downfield shift in ^{13}C NMR of the carbene carbon from δ = 162.17 ppm in complex (*R*)-**79** and complex (*S*)-**79** to δ = 174.15 ppm in complex(*S*)-**81**. The increased in reactivity of complex (*S*)-**81** can be attributed to the fact the palladium species during the course of the

catalysis is stabilized by benzimidazole which acts as a better donor ligand as compared to imidazole.

The best selectivity was observed with catalyst (*S*)-**81** in THF with ee value of 8.4% where the reaction proceeded at a slower rate. Hence the reaction was repeated in THF but at a lower temperature. The reaction was allowed to stir at -78°C for 24 hours. However, after 24 hours product formation cannot be detected by TLC. The reaction was allowed to slowly warm up to room temperature overnight with isolated yield of 89% and ee value of 9.7%. Hence the reaction temperature was gradually increased by 10°C every 24 hours from -78°C to determine the optimal temperature for the reaction. No product formation was observed from -78°C to -30°C. A faint product spot was only observable after 24 hours of stirring when the reaction temperature was raised to -20°C. The reaction was then allowed to stir at -20°C for another 48 hours in hope that the reaction will proceed to completion. However, after 72 hours at -20°C, the intensity of the product spot observed by TLC remained unchanged. Hence, the reaction temperature was slowly increased by 5°C every 24 hours in search of the optimal temperature for the reaction. Finally the reaction was allowed to stir at 0°C and after 24 hours, a product spot can be observed by TLC, therefore the reaction was left at 0°C to determine the time required for the reaction to proceed to completion at 0°C. However after 3 days at 0°C, several other spots were detected by TLC which was attributed to the decomposition of the starting material.

Table 4.5 Asymmetric Allylic Alkylation Reaction (Method D)

Entry	Catalyst	Solvent	Temp. (°C)	Time (h)	Percentage Yield (%)[d]	ee *R* (%)
1	(*R*)-**79**	THF	22	4	60	1.5
2	(*S*)-**79**	THF	22	4	62	2.6
3	(*S*)-**79**	CH_2Cl_2	22	4	76	2.8
4	(*S*)-**81**	THF	22	4	84	8.4
5	(*S*)-**81**	CH_2Cl_2	22	1	89	3.1
6	(*S*)-**81**	THF	-79 to 22	overnight	60	9.7

(d) Method D as seen in Scheme 4.10

The low ee values can be partly attributed to the small methyl group which cannot effectively exert a significant steric influence at the site of attack of the incoming nucleophiles. Another plausible factor contributing to the lack of selectivity in the catalysts is the introduction of the triphenylphosphine group. As mentioned above, Roland *et al.*[92] ascribed the dismal selectivity for the phosphine-NHC system to the similarity in the *trans* effect caused by the phoshine and NHC that is present in the system. As illustrated in Figure 4.3 with complex (*S*)-**79**, due to in triphenylphosphine, the incoming nucleophile can no longer differentiate site **a** from **b,** since both site appears to have similar *trans* effect. Therefore, the nucleophile can attack the allyl from either site **a** or site **b**, ultimately resulting in the loss of selectivity for the triphenylphosphine coordinated complex (*S*)-**79**.

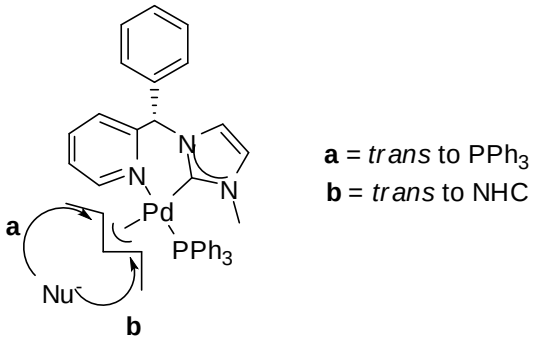

Figure 4.3 Proposed Pd intermediate for complex (*S*)-**79**

Although complex (±)-**79** in method C gave dismal yield in the model study, method C was the only method available presently to test out the selectivity of complex (*S*)-**58** that has the bulkiest Ph group. As seen in Figure 4.4, complex (*S*)-**58** is predicted to be a good catalyst for asymmetric allylic alkylation. According to the Pd allyl intermediate proposed by Douthwaite,[96] the incoming nucleophile can be predicted to exclusively attack site **b** in the case of complex (*S*)-**58** since it has met all the three requirements that Douthwaite had laid down for good selectivity in the asymmetric allylic alkylation reaction. Firstly site **b** is *trans* to the NHC which exerts a greater *trans* effect as compared to site **a** will be preferably attacked by the nucleophile. Secondly, approach of the nucleophile *via* site **b** is unrestricted with only H atoms on the pyridine. Thirdly, the approach of the nucleophile *via* site **a** has been blocked by the bulky Ph group. Therefore complex (*S*)-**58** is predicted to display excellent ee for the asymmetric allylic alkylation reaction.

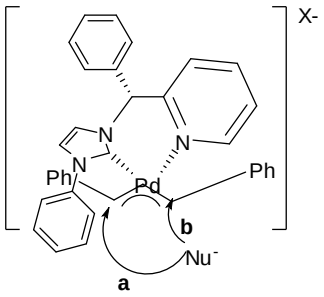

Figure 4.4 Propose Pd intermediate for complex (*S*)-**58**

Hence method C was employed to test out the selectivities of the chiral complex (*R*)-**56**, complex (*S*)-**57** and complex (*S*)-**58**. The results are summarised in Table 4.6. As seen in Scheme 4.11, all the chiral catalysts were converted their bisacetonitrile derivatives prior to their employment as catalysts.

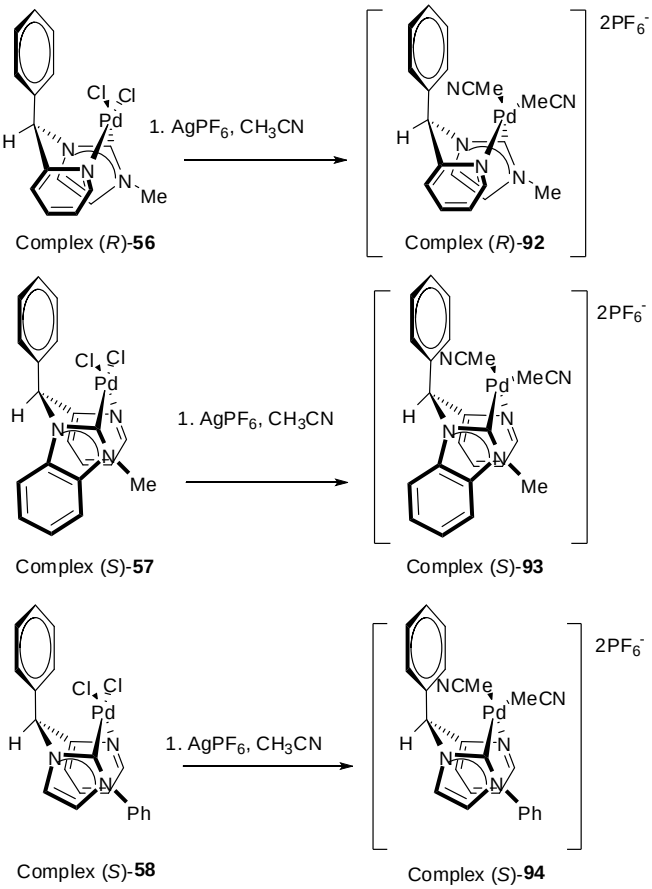

Scheme 4.11

The reaction was firstly tested out on complex (*R*)-**92** in THF. After stirring at room temperature for 48 hours, no product formation was detected by TLC. Therefore the reaction was heated at 50°C. After 48 hours, the reaction was quenched and the isolated yield was 10%. The ee value was an insignificant 10.3%. The reaction was repeated in CH_2Cl_2 in an attempt to improve the reactivity of the catalyst. However the starting material remained unreacted even after stirring for 48 hours at 35°C. As compared to complex (*R*)-**92**, complex (*S*)-**93** displayed better reactivity. The isolated yield with complex (*S*)-**93** as the catalyst after stirring for 48 hours at 50°C is 25% although the ee value remained at an almost insignificant value of 8.3%. In the case of complex (*S*)-**94**, no product formation was detected even after 48 hours at 50°C.

Table 4.6 Asymmetric Allylic Alkylation Reaction (Method C)

Entry	Catalyst	Solvent	Temp. (°C)	Time (h)	Percentage Yield (%)[c]	ee *R* (%)
1	(*R*)-**92**	THF	50	4	10	10.3
2	(*R*)-**92**	CH_2Cl_2	35	4	-	-
3	(*S*)-**93**	THF	50	4	25	8.3
4	(*S*)-**94**	THF	50	4	-	-

(d) Method C as seen in Scheme 4.9

4.3 Conclusion

The novel pyridine functionalized NHC chiral complexes that were described in chapter 3 were tested against the allylic alkylation reaction. Although the lack of reactivity of the dichloro complexes can be solved *via* the introduction of either 1 molar equivalent of triphenylphosphine or by replacing the chloro ligands with weakly coordinating ligands like acetonitrile, both conditions however gave disappointing results. In the case of ligand exchange with triphenylphosphine, although system exhibited excellent reactivities with most of the reactions completing within 4 hours giving high yields, the selectivities observed for this system is almost negligible, with the highest obtained ee value of 10.3%. In an attempt to improve the selectivities of the chiral complexes, the chloro ligands were replaced with weakly coordinating acetonitrile. Upon ligand exchange, the reactivities of the chiral complexes decreased dramatically with the highest achievable yield of 25% at the elevated temperature of 50°C. However, the selectivities of the catalysts did not improve. In this chapter, the reactivities and selectivities of the newly synthesized complexes were tested against the allylic substitution reaction. Reconciliation of the reactivities and the selectivities of the chiral complexes cannot be achieved.

In this thesis, a series of pyridine functionalized NHC based palladacycles have been synthesized. Through a simple and efficient novel methodology that was developed and illustrated in chapter 3, the enantiomerically pure forms of the palladacycles can be easily accessible via optical resolution of their respective amino acid adducts. The newly synthesized

palladacycles displayed moderate to excellent reactivities for the allylic alkylation reaction. However, they were unable to exert a steric environment to cause a significant influence in the selectivity of the allylic alkylation reaction.

4.4 Experimental

All catalysis reactions were performed under a positive pressure of purified argon using standard Schlenk techniques. All the commercially available chemicals were used without prior drying or purification. Solvents were freshly distilled. (±)-trans-1,3-diphenylallyl acetate was purchased from Sigma Aldrich and used without further purification. Proton nuclear magnetic resonance (^{1}H NMR) and carbon nuclear magnetic resonance (^{13}C NMR) spectroscopy were performed on a Bruker Avance 400 NMR spectrometers. The number of protons (n) for a given resonance is indicated by nH. Coupling constants are reported as a J value in Hz. Proton nuclear magnetic resonance spectra ^{1}H NMR are reported as δ in units of parts per million (ppm) downfield from $SiMe_4$ (δ 0.0). Carbon nuclear magnetic resonance spectra ^{13}C NMR are reported as δ in units of parts per million (ppm) relative to the signal of chloroform-*d* (δ 77.20, triplet). All chemical shifts reported are referenced to the chemical shifts of their respective residual solvent resonances. Unless stated otherwise, all NMR experiments are carried out at 300K.

4.4.1 Typical procedure for Asymmetric Allylic Alkylation

Method A : A mixture of dimethyl malonate (3mol), base (3 mol) that was dissolved in 2 ml of solvent was introduced dropwise to a stirring solution of catalyst (2mg, 5 mol%) and (±)-trans-1,3-diphenylallyl acetate (1 mol) in 2ml of solvent. The reaction was allowed to stir at the designated time and temperature. After stirring at the designated time, 3 mL of sat. NH_4Cl(aq) was added to the reaction mixture. The reaction mixture was extracted with diethyl ether (3 X 5 mL) and the combined organic layers were dried over anhydrous $MgSO_4$. The crude product was subjected to a flash column (diethyl ether / petroleum ether =1/4, V/V) to give a colourless oil. ^{1}H NMR (400 MHz, $CDCl_3$): δ = 3.52 (s, 3H, *CH*$_3$), 3.70 (s, 3H, *CH*$_3$), 3.95 (d, 1H, O=C*CH*CC=O), 4.24–4.29 (m, 1 H, Ph*CH*), 6.33 (dd, 1 H, $J_{H,H}$ = 15.4 Hz, $J_{H,H}$ = 8.7 Hz CH*C*=*H*), 6.48 (d, 1 H, $J_{H,H}$ = 15.8 Hz, Ph*C*=*H*), 7.20–7.32 (m, 10 H, aromatic protons) ppm. ^{13}C NMR (100 MHz, $CDCl_3$): δ = 29.89, 49.38, 52.65, 52.75, 52.83, 57.84, 126.58, 127.36, 127.77, 128.06, 128.67, 128.92, 129.30, 132.02, 137.01, 140.35, 167.76, 168.39 ppm.

Method B: Silver salt (10.1 mol %) was added stirring solution of catalyst (2mg, 5mol %) in 2 mL of solvent. The mixture was allowed to stir at room temperature for an hour in the dark. After 1 hour, (±)-trans-1,3-diphenylallyl acetate (1 mol) was added to the stirring solution. To this solution, a mixture of dimethyl malonate (3mol), base (3 mol) that was dissolved in 2 ml of solvent was introduced dropwise. The reaction was allowed to stir at the designated time and temperature. Similar workup and purification as method A.

Method C: Similar to method A. Enantiomeric excess values were determined by HPLC analysis (Chiral OD-H column; 254 nm hexane/isopropanol = 99:1, flow rate 0.5 mL/min; t_R = 25.3 min, 27.2 min)

Method D: $AgPF_6$ (20.1 mol %) was added to a CH_3CN solution of catalyst (2mg, 5 mol %). The reaction mixture was allowed to stir at reflux overnight. The reaction mixture was passed through celite the next day and the filtrate was concentrated and the bisacetonitrile complex was precipitated out as an off white solid in diethyl ether. The solid is collected and dried under vacuum. The solid was used as catalyst without further purification. Similar procedure as method A. Enantiomeric excess values were determined by HPLC analysis (Chiral OD-H column; 254 nm hexane/isopropanol = 99:1, flow rate 0.85 mL/min; t_R = 12.4 min, 13.9 min).

REFERENCES

[1] E. O. Fischer, A. Maasbol, *Angew. Chem., Int. Ed. Engl.* **1964**, *3*, 580

[2] O. S. Mills, A. D. Redhouse, *Angew. Chem. Int., Int. Ed. Engl.* **1965**, *4*, 1082

[3] R. R. Schrock, *J. Am Chem Soc.* **1974**, *96*, 6796

[4] A. J. Arduengo, R. L. Harlow, M. Kline, *J. Am. Chem. Soc.* **1991**, *113*, 361

[5] W. A. Herrmann, *Angew. Chem. Int. Ed.* **2002**, *41*, 1290

[6] W. A. Herrmann, L. J. Goossen, G. R. J. Artus, C. Köcher, *Organometallics* **1997**, *16*, 2472

[7] S. W. Lee, J. F. Hartwig, *J. Org. Chem.* **2001**, *66*, 3402

[8] T. J. Seiders, D. W. Ward, R. H. Grubbs, *Org. Lett.* **2001**, *3*, 3225

[9] (a) R. Altman, S. L. Buchwald, *Org. Lett.* **2006**, *8*, 2779 (b) M. H. Yang, F. Liu, *J. Org. Chem.* **2007**, *72*, 8968 (c) P. Suresh, K. Pitchumani, *J. Org. Chem.* **2008**, *73*, 9121 (d) F. Xue, C. Y. Cai, H. M. Sun, R. J. Qi, *Tetrahedron Lett.* **2008**, *49*, 4386

[10] M. T. Powell, D. R. Hou, M. C. Perry, X. H. Cui, K. Burgess, *J. Am. Chem. Soc.* **2001**, *123*, 8878

[11] A. C. Hillier, W. J. Sommer, B. S. Yong, J. L. Petersen, L. Cavallo, S. P. Nolan, *Organometallics* **2003**, *22*, 4322

[12] A. Poater, B. Cosenza, A. Correa, S. Giudi, F. Ragone, L. Cavallo, *J. Organomet. Chem.* **2005**, *690*, 5407

[13] H. Clavier, S. P. Nolan, *Chem. Comm.* **2010**, *46*, 841

[14] S. Würtz, C. Lohre, R. Frölich, K. Bergander, F. Glorius, *J. Am. Chem. Soc.* **2009**, *131*, 8344

[15] (a) N. Fröhlich, U. Pidun, M. Stahl, G. Frenking, *Organometallics* **1997**, *16*, 442 (b) H. Jacobsen, A. Correa, C. Costabile, L. Cavallo, *J. Organomet. Chem*. **2006**, *691*, 4350 (c) S. Díez-González, S. P. Nolan, *Coord. Chem. Rev.* **2007**, *251*, 874-883. (d) S. Fantasia, J. L. Petersen, H. Jacobsen, L. Cavallo, S. P. Nolan, *Organometallics* **2007**, *26*, 5880 (e) D. M. Karamov, V. M. Lynch, C. W. Bielawski, *Organometallics* **2007**, *26*, 6042(f) F. E. Hahn, M. C. Jahnke, *Angew. Chem. Int. Ed.* 2008, *47*, 3122

[16] (a) W. A. Herrmann, J. Schütz, G. D. Frey, E. Herdtweck, *Organometallics* **2006**, *25*, 2437 (b) S. Leuthäuβer, P. Schwarz, H. Plenio, *Chem. Eur. J.* **2007**, *13*, 7195 (c) D. M. Gusev, *Organometallics* **2009**, *28*, 6458

[17] (a) M. V. Baker, P. J. Barnard, S. K. Brayshaw, J. L. Hickey, B. W. Skelton, A. H. White, *Dal. Trans.* **2005**, 37 (b) D. Tapu, D. A. Dixon, C. Roe, *Chem. Rev.* **2009**, *109*, 3385 (c) H. V. Huynh, Y. Han, R. Jothibasu, J. A. Yang, *Organometallics* **2009**, *28*, 5395

[18] L. J. Liu, F. J. Wang, M. Shi, *Organometallics* **2009**, *28*, 4416

[19] A. R. Chianese, P. T. Bremer, C. Wong, R. J. Reynes, *Organometallics* **2009**, *28*, 5244

[20] (a) N. Marion, P. deFrémont, I. M. Puijik, E. C. Ecarnot, D. Amoroso, A. Bell, S. P. Nolan, *Adv. Synth. Catal.* **2007**, *349*, 2380 (b) H. V. Huynh, Y. X. Chew, *Inorg. Chim. Acta.* **2010**, *363*, 1979

[21] H. M. J. Wang, I. J. B. Lin, *Organometallics* **1998**, *17*, 972

[22] A. Flahaut, J. P. Baltaze, S. Roland, P. Mangeney, *J. Organomet. Chem.* **2006**, *691*, 3498

[23] D. S. McGuinness, K. J. Cavell, *Organometallics* **2000**, *19*, 741

[24] L. G. Bonnet, R. E. Douthwaite, R. Hodgson, J. Houghton, B. M. Kariuki, S. Simonovic, *Dal. Trans.* **2004**, 3528

[25] H. V. Huynh, C. H. Yeo, Y. X. Chew, *Organometallics* **2010**, *29*, 1479

[26] S. T. Liu, C. I. Lee, C. F. Fu, C. H. Chen, Y. H. Liu, C. J. Elsevier, S. M. Peng, J. T. Chen, *Organometallics* **2009**, *28*, 6957

[27] M. V. Baker, D. H. Brown, V. J. Hesler, B. W. Skelton, A. H. White, *Organometallics* **2007**, *26*, 250

[28] M. School, S. Ding, C. W. Lee, R. H. Grubbs, *Org. Lett.* **1999**, *1*, 953

[29] W. A. Herrmann, M. Elison, J. Fischer, C. Köcher, G. R. J. Artus, *Angew. Chem. Int. Ed.* **1995**, *34*, 2371

[30] W. A. Herrman, C. P. Reisinger, M. Spiegler, *J. Organomet. Chem.* **1998**, *557*, 93

[31] S. Caddick, F. G. N. Cloke, G. K. B. Clentsmith, P. B. Hitchcock, D. McKerrecher, L. R. Titcomb, M. R. V. Wiliams, *J. Organomet. Chem.* **2001**, *617-618*, 635

[32] J. Huang, S. P. Nolan, *J. Am. Chem. Soc.* **1999**, *121*, 9889

[33] A. C. Frisch, F. Rataboul, A. Zapf, M. Beller, *J. Organomet. Chem.* **2003**, *687*, 403

[34] J. R. Zhou, G. C. Fu, *J. Am. Chem. Soc.* **2003**, *125*, 12527

[35] N. Hadei, E. A. B. Kantchev, C. J. O'Brien, M. G. Organ, *Org. Lett.* **2005**, *7*, 3805

[36] N. Hadei, E. A. B. Kantchev, C. J. O'Brien, M. G. Organ, *J. Org. Chem.* **2005**, *70*, 8503

[37] M. G. Organ, S. Arola, I. Dubovyk, N. Hadei, E. A. B. Kantchev, C. J. O'Brien, C. Valente, *Chem. Eur. J.* **2006**, *12*, 4749

[38] W. A. Herrmann, V. P. W. Böhm, G. W. K. Gstöttmayr, M. Grosche, C. P. Resinger, T. Weskamp, *J. Organomet. Chem.* **2001**, *617*, 616

[39] G. A. Grasa, S. P. Nolan, *Org. Lett.* **2001**, *3*, 119

[40] J. K. Huang, G. Grasa, S. P. Nolan, *Org. Lett.* **1991**, *1*, 1307

[41] (a) L. J. Goossen, J. Paetzold, O. Briel, A. Rivas-Nass, R. Karch, B. Kayser, *Synlett* **2005**, *2*, 275 (b) N. Marion, O. Navarro, J. G. Mei, E. D. Stevens, N. M. Scott, S. P. Nolan, *J. Am. Chem. Soc.* **2006**, *128*, 4101 (c) N. Marion, E. C. Ecarnot, O. Navarro, D. Amoroso, A. Bell, S. P. Nolan, *J. Org. Chem.* **2006**, *71*, 3816 (d) J. Broggi, H. Clavier, S. P. Nolan *Organometallics* **2008**, *27*, 5525

[42] S. W. Lee, J. F. Hartwig, *J. Org. Chem.* **2001**, *66*, 3402

[43] E. P. Kündig, T. M. Seidel, Y. X. Jia, G. Bernardinelli, *Angew. Chem. Int. Ed.* **2007**, *46*, 8484

[44] T. Zhang, M. Shi, *Chem. Eur. J.* **2008**, *14*, 3759

[45] Q. Xu, R. Zhang, T. Zhang, M. Shi, *J. Org. Chem.* **2010**, *75*, 3935

[46] G. N. Ma, T. Zhang, M. Shi, *Org. Lett.* **2009**, *11*, 875

[47] Z. Liu, M. Shi, *Tetrahedron* **2010**, *66*, 2619

[48] Z. Liu, M. Shi, *Tetrahedron Asymm.* **2009**, *20*, 119

[49] W. F. Wang, T. Zhang, M. Shi, *Organometallics* **2009**, *28*, 2640

[50] Z. Liu, M. Shi, *Organometallics* **2010**, *29*, 2831

[51] Y. A. Wanniarachchi, Y. Kogiso, L. M. Slaughter, *Organometallics 2008*, *27*, 21

[52] K. S. Yoo, J. O'Neill, S. Sakaguchi, R. Giles, J. H. Lee, K. W. Jung, *J. Org. Chem.* **2010**, *75*, 95

[53] R. Jensen, S. M. Sigman, *Org. Lett.* **2003**, *5*, 63

[54] T. Chen, J. J. Jiang, Q. Xu, M. Shi, *Org. Lett.* **2007**, *9*, 865

[55] O. Kühl, *Chem. Soc. Rev.* **2007**, *36*, 592

[56] W. A. Herrmann, L. J. Goossen, M. Spiegler, *Organometallics* **1998**, *17*, 2162

[57] M. T. Powell, D. R. Hou, M. C. Perry, X. H. Cui, K. Burgess, *J. Am. Chem. Soc.* **2001**, *123*, 8878

[58] V. César, S. Bellemin-Laponnaz, L. H. Gade, *Organometallics* **2002**, *21*, 5204

[59] (a) L. H. Gade, S. Bellemin-Laponnaz, *Coord. Chem. Rev.* **2007**, *251*, 718 (b) N. Schneider, M. Kruck, S. Bellemin-Lapponaz, H. Wadepohl, L. H. Gade, *Eur. J. Inorg. Chem.* **2009**, *4*, 493

[60] (a) D. Sellmann, W. Prechtel, F. Knoch, M. Moll, *Organometallics* **1992**, *11*, 291, (b) H. Seo, H. J. Park, B. Y. Kim, J. H. Lee, S. U. Son, Y. K. Chung, *Organometallics* **2003**, *22*, 618 (c) J. A. Cabeza, I. del Río, M. G. Sánchez-Vega, M. Suárez, *Organometallics* **2006**, *25*, 1831

[61] H. V. Huynh, H. Y. Chun, G. K. Tan, *Chem. Commun.* **2006**, *36*, 3833

[62] (a) M. Kuriyama, R. Shimazawa, R. Shirai, *Tetrahedron* **2007**, *63*, 9393 (b) M. Kuriyama, R. Shimazawa, T. Enomoto, R. Shirai, *J. Org. Chem.* **2008**, *73*, 6939 (c) H. V. Huynh, D. Yuan, Y. Dan, *Dal. Trans.* **2009**, 7262

[63] A. Ros, D. Monge, M. Alcarazo, E. Álvarez, J. M. Lassaletta, R. Fernández, *Organometallics* **2006**, *25*, 6039

[64] S. J. Roseblade, A. Ros, D. Monge, M. Alcarazo, E. Álvarez, J. M. Lassaletta, R. Fernández, *Organometallics* **2007**, *26*, 2570

[65](a) M. V. Jiménez, J. J. Pérez-Torrente, M. I. Bartolomé, V. Gierz, F. J. Lahoz, L. A. Oro, *Organometallics* **2008**, *27* , 224 (b) Y. P. Huang, C. C. Tsai, W. C. Shih, Y. C. Chang, S. T. Lin, G. P. A. Yap, I. Chao, T. G. Ong, *Organometallics* **2009**, *28*, 4316 (c) A. J. Lough, R. H. Morris, *Organometallics* **2009**, *28*, 6755 (d) Y. C. Hu, C. C. Tsai, W. C. Shih, G. P. A. Yap, T. G. Ong, *Organometallics* **2010**, *29*, 516

[66] (a) L. G Bonnet, R. E. Douthwaite, R. Hodgson, J. Houghton, B. M. Kariuki, S. Simonovic, *Dal. Trans*. **2004**, 3528 (b) A. Flahaut, J. P. Blataze, S. Roland, P. Mangeney, *J. Organometallic Chem.* **2006**, *691*, 3498

[67] L. G. Bonnet, R. E. Douthwaite, B. M. Kariuki, *Organometallics* **2003**, *22*, 4187

[68](a) A. A. D. Tulloch, A. A. Danopoulos, R. P. Tooze, S. M. Cafferkey, S. Kleinhenz, M. B. Hursthouse, *Chem. Commun.* **2000**, *14*, 1247 (b) A. A. D. Tulloch, A. A. Danopoulos, S. Kleinhenz, M. E. Light, M. B. Hursthouse, G. Eastham, *Organometallics* **2001**, *20*, 2027 (c) A. A. D. Tulloch, S. Winston, A. A. Danopoulos, G. Eastham, M. B. Hursthouse, *Dal. Trans.* **2003**, 699 (d) S. Winston, N. Stylianides, A. A. D. Tulloch, J. A. Wright, A. A. Danopoulos, *Poly.* **2004**, *23*, 2813 (e) C. Y. Wang, Y. H. Liu, S. M. Peng, S. T. Lin, *J. Organometallic Chem.* **2006**, *691*, 4012 (f) Y. Chang, H. J. Xu, J. F. Sun, Y. Z. Li, X. T. Chen, Z. L. Xue, *Dal. Trans.* **2009**, 7132 (g) A. A. Danopoulos, N. Tsoureas, S. A. Macgregor, C. Smith, *Organometallics* **2007**, *26*, 253 (h) A. R. Chianese, P. T. Bremer, C. Wang, R. J. Reynes, *Organometallics* **2009**, *28*, 5244

[69] D. S. McGuinness, V. C. Gibson, D. F. Wass, J. W. Steed, *J. Am. Chem. Soc.* **2003**, *125*, 12716

[70] (a) A. A. Danopoulos, N. Tsoureas, J. A. Wright, M. E. Light, *Organometallics* **2004**, *23*, 166 (b) A. A. Danopoulos, J. A. Wright, W. B. Motherwell, *Chem. Commun.* **2005**, *6*, 784

[71] R. S. Simons, P. Custer, C. A. Tessier, W. J. Youngs, *Organometallics* **2003**, *22*, 1979

[72] C. Y. Wong, L. M. Lai, P. K. Pat, L. H. Chung, *Organometallics* **2010**, *29*, 2533

[73] (a) S. Gründemann, M. Albrecht, J. A. Loch, J. W. Faller, R. H. Crabtree, *Organometallics* **2001**, *20*, 5485 (b) J. A. Loch, M. Albrecht, E. Peris, J. Mata, J. W. Faller, R. H. Crabtree, *Organometallics* **2002**, *21*, 700

[74] F. E. Hahn, M. C. Jahnke, V. Gomez-Benitez, P. Morales-Morales, T. Pape, *Organometallics* **2005**, *24*, 6458

[75] T. Kawano, M. Kurimoto, U. Hanatanaka, I. Ueda, *Chem. Phar. Bull.* **1992**, *40*, 3067

[76] H. M. J. Wang, I. J. B. Lin, *Organometallics* **1998**, *17*, 1972

[77] L. Rout, S. Jammi, T. Punniyamurthy, *Org. Lett.* **2007**, *9*, 3397

[78] R. E. Cowley, R. P. Bontchev, E. N. Duesler, J. M. Smith, *Inorg. Chem.* **2006**, *45*, 9771

[79] (a) Y. Tang, J. Liu, X. Wang, L. Shao, *Tetrahedron* **2010**, *66*, 7970 (b) M. Sie, Y. Hsieh, Y. Tsai, J. Wu, S. Chen, P. V. Kumar, J. Lii, H. M. Lee, *Organometallics* **2010**, *29*, 6473 (c) Y. Kong, L. Wen, H. Song, S. Xu, M. Yang, B. Liu, B. Wang, *Organometallics* **2011**, *30*, 153 (d) J. Zhong, X. P. Gu, L. L. Qiu, G. P. Wu, H. B. Song, J. X. Fang, *J. Organomet. Chem.* **2011**, *696*, 859

[80](a) A. Yoneda, T. Hakushi, *Organometallics* **1994**, *13*, 4912 (b) J. Spencer, F. Maassarani, M. Pfeffer, A. DeCian, J. Fischer, *Tetrahedron Asymm.* **1994**, *5*, 321 (c) J. Spencer, M. Pfeffer, *Tetrahedron Asymm.* **1995**, *6*, 419 (d) W. J. Wu, X. L Cui, C. X. Du, W. L. Wang, R. Y. Guo, R. F. Chen, *Dal. Trans.* **1998**, 3727 (e) V. V. Dunina, E. D. Razmyslova, L. G. Kuz'mina, A. V. Churakov, M. Y. Rubina, Y. K. Grishin, *Tetrahedron Asymm.* **1999**, *10*, 3147 (f) V. V. Dunina, O. N. Gorunova, L. G. Kuz'mina, N. A. Kataeva, Y. K. Grishin, *Tetrahedron Asymm.* **1999**, *10*, 3951 (g) V. V. Dunina, O. N. Gorunova, M. V. Livantsov, Y. K. Grishin, L. G. Kuz'mina, N. A. Kataeva, A. V. Churakov, *Tetrahedron Asymm.* **2000**, *11*, 3967 (h) Y. X. Li, S. Selvaratnam, J. J. Vittal, P. H. Leung, *Inorg. Chem.* **2003**, *42*, 3229 (i) Y. Ding, Y. X. Li, Y. Zhang, S. A. Pullarkat, P. H. Leung, *Eur. J. Inorg. Chem.* **2008**, *11*, 1880 (j) Y. Ding, Y. X. Li, S. A. Pullarkat, S. L. Yap, P. H. Leung, *Eur. J. Inorg. Chem.* **2009**, *2*, 267 (k) Y. Ding, M. Y. Chiang, S. A. Pullarkat, Y. X. Li, P. H. Leung, *Organometallics* **2009**, *28*, 4358

[81] (a) L. G. Bonnet, R. E. Douthwaite, *Organometallics* **2003**, *22*, 4187 (b) L. G. Bonnet, R. E. Douthwaite, R. Hodgson, J. Houghton, B. M. Kariuki, S. Simonovic, *Dal. Trans*. **2004**, *3528*

[82] M. Merzouk, T. Moore, N. A. Williams, *Tetrahedron Lett*. **2007**, *48*, 8914

[83] (a) A. Flahaut, J. P. Blataze, S. Roland, P. Mangeney, *J. Organomet. Chem.* **2006**, *691*, 3498 (b) A. Flahaut, S. Roland, P. Mangeney, *Tetrahedron Asymm.* **2007**, *18*, 229

[84] D. S. Clyne, J. Jin, E. Genest, J. C. Gallucci, T. V. Rajanbabu, *Org. Lett.* **2000**, *2* 1125

[85] (a) T. Chen, J. J. Jiang, Q. Xu, M. Shi, *Org. Lett.* **2007**, *9*, 865 (b) T. Zhang, M. Shi, *Chem. Eur. J.* **2008**, *14*, 3759 (c) G. N. Ma, T. Zhang, M. Shi, *Org. Lett*. **2009**, *11*, 875, (d) Z. Liu, M. Shi, *Tetrahedron Asymm.* **2009**, *20*, 119 (e) W. F. Wang, T. Zhang, M. Shi, *Organometallics* **2009**, *28*, 2640

[86] (a) T. Chen, J. Gao, M. Shi, *Tetrahedron* **2006**, *62*, 6289 (b) T. Zhang, S. J. Liu, M. Shi, M. X. Zhao, *Syn. Stutt.* **2008**, *17*, 2819

[87] I. Abdellah, N. Debono, Y. Canac, C. Duhayon, R. Chauvin, *Dal. Trans.* **2009**, 7196

[88] J. C. C. Chen, I. J. B. Lin, *Organometallics* **2000**, *19*, 5113

[89] Y. Sato, T. Yoshino, M. Mori, *Org. Lett.* **2003**, *5*, 31

[90] L. G. Bonnet, R. E. Douthwaite, *Organometallics* **2003**, *22*, 4187

[91] F. Visentin, A. Togni, *Organometallics* **2007**, *26*, 3746

[92] A. Flahaut, S. Roland, P. Mangeney, *J. Orgnomet. Chem.* **2007**, 692, 5754

[93] S. Roland, W. Cotet, P. Mangeney, *Eur. J. Inorg. Chem.* **2009**, *13*, 1796

[94] A. R. Chianese, P. T. Bremer, C. Wong, R. J. Reynes, *Organometallics* **2009**, *28*, 5244

[95] (a) H. Steinhagen, M. Reggelin, G. Helmchen, *Angew. Chem.,Int. Ed. Engl.* **1997**, *36*, 2108. (b) J. Junker, B. Reif, H. Steinhagen, B. Junker, I. C. Felli, M. Reggelin, C. Griesinger, *Chem. Eur. J.* **2000**, *6*, 3281. (c) M. Widhalm, U. Nettekoven, H. Kalchhauser, K. Mereiter, M. J. Calhorda, V. Felix, *Organometallics* **2002**, *21*, 315.

[96] R. E. Douthwaite, *Coord. Chem. Rev.* **2007**, *251*, 702

[97] T. Zhang, M. Shi, *Chem. Eur. J.* **2008**, *14*, 3759

APPENDICES

Table A1 Crystallographic Data for compound **63**

Empirical formula	C16 H16 F6 N3 P
Formula weight	395.29
Temperature	173(2) K
Wavelength	0.71073 Å
Crystal system	Triclinic
Space group	P-1
Unit cell dimensions	
a = 8.5898(3) Å	α= 65.087(2)°.
b = 10.2948(4) Å	β= 85.056(2)°.
c = 11.0236(4) Å	γ = 80.326(2)°.
Volume	871.41(6) $Å^3$
Z	2
Density (calculated)	1.507 Mg/m^3
Absorption coefficient	0.223 mm^{-1}
F(000)	404
Crystal size	0.25 x 0.20 x 0.10 mm^3
Theta range for data collection	2.04 to 30.60°.
Index ranges	-12<=h<=12, -14<=k<=14, -15<=l<=15
Reflections collected	17133
Independent reflections	5248 [R(int) = 0.0263]
Completeness to theta = 30.60°	97.8 %
Absorption correction	Semi-empirical from equivalents
Max. and min. transmission	0.9780 and 0.9463
Refinement method	Full-matrix least-squares on F^2
Data / restraints / parameters	5248 / 0 / 235
Goodness-of-fit on F^2	1.108
Final R indices [I>2sigma(I)]	R1 = 0.0528, wR2 = 0.1364
R indices (all data)	R1 = 0.0780, wR2 = 0.1625
Largest diff. peak and hole	0.428 and -0.404 $e.Å^{-3}$

Table A2 Crystallographic Data for Complex (±)-**56**

Empirical formula	C16 H15 Cl2 N3 Pd
Formula weight	426.61
Temperature	223(2) K
Wavelength	0.71073 Å
Crystal system	Orthorhombic
Space group	Pbca
Unit cell dimensions	
a = 12.1801(5) Å	α= 90°.
b = 15.4613(7) Å	β= 90°.
c = 17.8198(7) Å	γ = 90°.
Volume	3355.8(2) $Å^3$
Z	8
Density (calculated)	1.689 Mg/m^3
Absorption coefficient	1.423 mm^{-1}
F(000)	1696
Crystal size	0.30 x 0.27 x 0.13 mm^3
Theta range for data collection	2.29 to 30.51°.
Index ranges	-17<=h<=15, -22<=k<=22, -25<=l<=25
Reflections collected	29824
Independent reflections	5089 [R(int) = 0.0372]
Completeness to theta = 30.51°	99.5 %
Absorption correction	Semi-empirical from equivalents
Max. and min. transmission	0.8366 and 0.6749
Refinement method	Full-matrix least-squares on F^2
Data / restraints / parameters	5089 / 200 / 255
Goodness-of-fit on F^2	1.042
Final R indices [I>2sigma(I)]	R1 = 0.0272, wR2 = 0.0672
R indices (all data)	R1 = 0.0393, wR2 = 0.0821
Largest diff. peak and hole	0.851 and -0.644 $e.Å^{-3}$

Table A3 Crystallographic Data for Complex (±)-**57**

Empirical formula	C22 H23 Cl2 N3 O Pd S
Formula weight	554.79
Temperature	173(2) K
Wavelength	0.71073 Å
Crystal system	Monoclinic
Space group	P2(1)/c
Unit cell dimensions	
a = 10.5157(5) Å	α= 90°.
b = 20.5533(8) Å	β= 110.514(2)°.
c = 11.2020(5) Å	γ = 90°.
Volume	2267.58(17) $Å^3$
Z	4
Density (calculated)	1.625 Mg/m^3
Absorption coefficient	1.165 mm^{-1}
F(000)	1120
Crystal size	0.36 x 0.30 x 0.14 mm^3
Theta range for data collection	2.77 to 30.62°.
Index ranges	-15<=h<=14, -29<=k<=29, -13<=l<=16
Reflections collected	42700
Independent reflections	6954 [R(int) = 0.0449]
Completeness to theta = 30.62°	99.6 %
Absorption correction	Semi-empirical from equivalents
Max. and min. transmission	0.8538 and 0.6790
Refinement method	Full-matrix least-squares on F^2
Data / restraints / parameters	6954 / 0 / 274
Goodness-of-fit on F^2	1.095
Final R indices [I>2sigma(I)]	R1 = 0.0380, wR2 = 0.0911
R indices (all data)	R1 = 0.0581, wR2 = 0.1036
Largest diff. peak and hole	1.424 and -0.868 $e.Å^{-3}$

Table A4 Crystallographic Data for Complex (±)-**58**

Empirical formula	C22.50 H20 Cl2 N3 O0.50 Pd
Formula weight	517.71
Temperature	173(2) K
Wavelength	0.71073 Å
Crystal system	Monoclinic
Space group	C2/c
Unit cell dimensions	
a = 30.197(3) Å	α= 90°.
b = 8.6378(8) Å	β= 106.645(5)°.
c = 16.6051(15) Å	γ = 90°.
Volume	4149.7(6) $Å^3$
Z	8
Density (calculated)	1.657 Mg/m^3
Absorption coefficient	1.169 mm^{-1}
F(000)	2080
Crystal size	0.20 x 0.18 x 0.02 mm^3
Theta range for data collection	2.54 to 28.47°.
Index ranges	-39<=h<=40, -11<=k<=11, -22<=l<=17
Reflections collected	28575
Independent reflections	5218 [R(int) = 0.0335]
Completeness to theta = 28.47°	99.3 %
Absorption correction	Semi-empirical from equivalents
Max. and min. transmission	0.9770 and 0.7999
Refinement method	Full-matrix least-squares on F^2
Data / restraints / parameters	5218 / 30 / 264
Goodness-of-fit on F^2	1.144
Final R indices [I>2sigma(I)]	R1 = 0.0327, wR2 = 0.0939
R indices (all data)	R1 = 0.0398, wR2 = 0.0977
Largest diff. peak and hole	1.150 and -0.703 $e.Å^{-3}$

Table A5 Crystallographic Data for Complex (±)-**59**

Empirical formula	C19 H21 Cl2 N3 Pd
Formula weight	468.69
Temperature	173(2) K
Wavelength	0.71073 Å
Crystal system	Triclinic
Space group	P1
Unit cell dimensions	
a = 10.1479(4) Å	α= 92.174(2)°.
b = 10.3057(4) Å	β= 116.919(2)°.
c = 10.4185(4) Å	γ = 91.415(2)°.
Volume	969.75(7) $Å^3$
Z	2
Density (calculated)	1.605 Mg/m^3
Absorption coefficient	1.239 mm^{-1}
F(000)	472
Crystal size	0.40 x 0.10 x 0.06 mm^3
Theta range for data collection	1.98 to 28.00°.
Index ranges	-13<=h<=13, -13<=k<=13, -13<=l<=13
Reflections collected	23082
Independent reflections	8655 [R(int) = 0.0332]
Completeness to theta = 28.00°	98.6 %
Absorption correction	Semi-empirical from equivalents
Max. and min. transmission	0.9294 and 0.6371
Refinement method	Full-matrix least-squares on F^2
Data / restraints / parameters	8655 / 3 / 457
Goodness-of-fit on F^2	1.258
Final R indices [I>2sigma(I)]	R1 = 0.0390, wR2 = 0.1069
R indices (all data)	R1 = 0.0433, wR2 = 0.1135
Absolute structure parameter	0.02(4)
Largest diff. peak and hole	1.491 and -2.064 $e.Å^{-3}$

Table A6 Crystallographic Data for Diastereomer (R_C,S_C)-**78**

Empirical formula	C25 H25 N5 O5 Pd
Formula weight	581.90
Temperature	173(2) K
Wavelength	0.71073 Å
Crystal system	Monoclinic
Space group	P2(1)
Unit cell dimensions	
a = 9.3999(4) Å	α= 90°.
b = 10.6789(4) Å	β= 100.453(3)°.
c = 11.9827(5) Å	γ = 90°.
Volume	1182.87(8) Å^3
Z	2
Density (calculated)	1.634 Mg/m^3
Absorption coefficient	0.832 mm^{-1}
F(000)	592
Crystal size	0.30 x 0.20 x 0.02 mm^3
Theta range for data collection	1.73 to 31.07°.
Index ranges	-13<=h<=13, -15<=k<=15, -17<=l<=17
Reflections collected	22621
Independent reflections	7300 [R(int) = 0.0251]
Completeness to theta = 31.07°	99.9 %
Absorption correction	Semi-empirical from equivalents
Max. and min. transmission	0.9835 and 0.7883
Refinement method	Full-matrix least-squares on F^2
Data / restraints / parameters	7300 / 1 / 326
Goodness-of-fit on F^2	1.123
Final R indices [I>2sigma(I)]	R1 = 0.0234, wR2 = 0.0583
R indices (all data)	R1 = 0.0265, wR2 = 0.0711
Absolute structure parameter	0.003(18)
Largest diff. peak and hole	0.508 and -0.617 e.Å^{-3}

Table A7 Crystallographic Data for Complex (*R*)-**56**

Empirical formula	C16 H15 Cl2 N3 Pd
Formula weight	426.61
Temperature	173(2) K
Wavelength	0.71073 Å
Crystal system	Orthorhombic
Space group	P2(1)2(1)2(1)
Unit cell dimensions	
a = 9.7816(3) Å	α= 90°.
b = 12.7776(3) Å	β= 90°.
c = 13.0825(4) Å	γ = 90°.
Volume	1635.12(8) Å^3
Z	4
Density (calculated)	1.733 Mg/m^3
Absorption coefficient	1.460 mm^{-1}
F(000)	848
Crystal size	0.18 x 0.12 x 0.06 mm^3
Theta range for data collection	2.23 to 37.07°.
Index ranges	-16<=h<=16, -21<=k<=21, -22<=l<=19
Reflections collected	31688
Independent reflections	8345 [R(int) = 0.0304]
Completeness to theta = 37.07°	99.8 %
Absorption correction	Semi-empirical from equivalents
Max. and min. transmission	0.9175 and 0.7791
Refinement method	Full-matrix least-squares on F^2
Data / restraints / parameters	8345 / 0 / 200
Goodness-of-fit on F^2	1.179
Final R indices [I>2sigma(I)]	R1 = 0.0233, wR2 = 0.0538
R indices (all data)	R1 = 0.0290, wR2 = 0.0741
Absolute structure parameter	-0.01(2)
Largest diff. peak and hole	0.742 and -0.797 e.Å^{-3}

Table A8 Crystallographic Data for Complex (*S*)-**56**

Empirical formula	C16 H15 Cl2 N3 Pd
Formula weight	426.61
Temperature	173(2) K
Wavelength	0.71073 Å
Crystal system	Orthorhombic
Space group	P2(1)2(1)2(1)
Unit cell dimensions	
a = 9.7843(5) Å	α= 90°.
b = 12.7883(6) Å	β= 90°.
c = 13.0945(6) Å	γ = 90°.
Volume	1638.44(14) $Å^3$
Z	4
Density (calculated)	1.729 Mg/m^3
Absorption coefficient	1.457 mm^{-1}
F(000)	848
Crystal size	0.12 x 0.12 x 0.06 mm^3
Theta range for data collection	2.23 to 31.84°.
Index ranges	-14<=h<=14, -18<=k<=18, -19<=l<=19
Reflections collected	26899
Independent reflections	5590 [R(int) = 0.0327]
Completeness to theta = 31.84°	99.6 %
Absorption correction	Semi-empirical from equivalents
Max. and min. transmission	0.9177 and 0.8446
Refinement method	Full-matrix least-squares on F^2
Data / restraints / parameters	5590 / 0 / 200
Goodness-of-fit on F^2	1.138
Final R indices [I>2sigma(I)]	R1 = 0.0205, wR2 = 0.0442
R indices (all data)	R1 = 0.0234, wR2 = 0.0497
Absolute structure parameter	-0.008(19)
Largest diff. peak and hole	0.480 and -0.376 $e.Å^{-3}$

Table A9 Crystallographic Data for Complex (*R*)-**79**

Empirical formula	C35 H34 Cl2 N3 O P Pd
Formula weight	720.92
Temperature	103(2) K
Wavelength	0.71073 Å
Crystal system	Orthorhombic
Space group	P2(1)2(1)2(1)
Unit cell dimensions	
a = 9.4437(3) Å	α= 90°.
b = 10.5477(3) Å	β= 90°.
c = 32.1650(10) Å	γ = 90°.
Volume	3203.93(17) $Å^3$
Z	4
Density (calculated)	1.495 Mg/m^3
Absorption coefficient	0.829 mm^{-1}
F(000)	1472
Crystal size	0.40 x 0.36 x 0.30 mm^3
Theta range for data collection	2.90 to 29.00°.
Index ranges	-12<=h<=12, -11<=k<=14, -43<=l<=43
Reflections collected	28967
Independent reflections	8465 [R(int) = 0.0260]
Completeness to theta = 29.00°	99.7 %
Absorption correction	Semi-empirical from equivalents
Max. and min. transmission	0.7890 and 0.7327
Refinement method	Full-matrix least-squares on F^2
Data / restraints / parameters	8465 / 0 / 391
Goodness-of-fit on F^2	1.096
Final R indices [I>2sigma(I)]	R1 = 0.0227, wR2 = 0.0546
R indices (all data)	R1 = 0.0236, wR2 = 0.0550
Absolute structure parameter	0.007(13)
Largest diff. peak and hole	0.360 and -0.720 $e.Å^{-3}$

Table A10 Crystallographic Data for Complex (*S*)-**79**

Empirical formula	C35 H34 Cl2 N3 O P Pd
Formula weight	720.92
Temperature	103(2) K
Wavelength	0.71073 Å
Crystal system	Orthorhombic
Space group	P2(1)2(1)2(1)
Unit cell dimensions	
a = 9.4479(2) Å	α= 90°.
b = 10.5523(3) Å	β= 90°.
c = 32.1532(8) Å	γ = 90°.
Volume	3205.58(14) Å^3
Z	4
Density (calculated)	1.494 Mg/m^3
Absorption coefficient	0.829 mm^{-1}
F(000)	1472
Crystal size	0.26 x 0.24 x 0.08 mm^3
Theta range for data collection	3.19 to 38.64°.
Index ranges	-15<=h<=16, -18<=k<=18, -56<=l<=56
Reflections collected	60547
Independent reflections	18026 [R(int) = 0.0353]
Completeness to theta = 38.64°	99.6 %
Absorption correction	Semi-empirical from equivalents
Max. and min. transmission	0.9367 and 0.8134
Refinement method	Full-matrix least-squares on F^2
Data / restraints / parameters	18026 / 0 / 391
Goodness-of-fit on F^2	1.087
Final R indices [I>2sigma(I)]	R1 = 0.0328, wR2 = 0.0721
R indices (all data)	R1 = 0.0369, wR2 = 0.0736
Absolute structure parameter	0.013(12)
Largest diff. peak and hole	2.378 and -0.718 e.Å^{-3}

Table A11 Crystallographic Data for Complex (S_C,S_C)-**80**

Empirical formula	C29 H27 Cl N4 O2 Pd
Formula weight	605.40
Temperature	173(2) K
Wavelength	0.71073 Å
Crystal system	Orthorhombic
Space group	P2(1)2(1)2(1)
Unit cell dimensions	
a = 9.6502(10) Å	α= 90°.
b = 14.3632(15) Å	β= 90°.
c = 18.9695(19) Å	γ = 90°.
Volume	2629.3(5) Å^3
Z	4
Density (calculated)	1.529 Mg/m^3
Absorption coefficient	0.842 mm^{-1}
F(000)	1232
Crystal size	0.30 x 0.08 x 0.06 mm^3
Theta range for data collection	2.76 to 33.37°.
Index ranges	-14<=h<=14, -22<=k<=21, -29<=l<=29
Reflections collected	55040
Independent reflections	10025 [R(int) = 0.0536]
Completeness to theta = 33.37°	99.2 %
Absorption correction	Semi-empirical from equivalents
Max. and min. transmission	0.9512 and 0.7864
Refinement method	Full-matrix least-squares on F^2
Data / restraints / parameters	10025 / 0 / 335
Goodness-of-fit on F^2	1.003
Final R indices [I>2sigma(I)]	R1 = 0.0326, wR2 = 0.0578
R indices (all data)	R1 = 0.0466, wR2 = 0.0624
Absolute structure parameter	0.001(16)
Largest diff. peak and hole	0.357 and -0.652 e.Å^{-3}

Table A12 Crystallographic Data for Complex (*S*)-**81**

Empirical formula	C40 H40 Cl2 N3 O2 P Pd
Formula weight	803.02
Temperature	103(2) K
Wavelength	0.71073 Å
Crystal system	Monoclinic
Space group	P2(1)
Unit cell dimensions	
a = 9.8910(9) Å	α= 90°.
b = 14.2476(13) Å	β= 97.322(4)°.
c = 13.0277(11) Å	γ = 90°.
Volume	1820.9(3) Å^3
Z	2
Density (calculated)	1.465 Mg/m^3
Absorption coefficient	0.740 mm^{-1}
F(000)	824
Crystal size	0.38 x 0.14 x 0.08 mm^3
Theta range for data collection	2.52 to 32.99°.
Index ranges	-14<=h<=15, -21<=k<=21, -19<=l<=19
Reflections collected	36120
Independent reflections	13425 [R(int) = 0.0282]
Completeness to theta = 32.99°	98.8 %
Absorption correction	Semi-empirical from equivalents
Max. and min. transmission	0.9432 and 0.7663
Refinement method	Full-matrix least-squares on F^2
Data / restraints / parameters	13425 / 1 / 447
Goodness-of-fit on F^2	1.033
Final R indices [I>2sigma(I)]	R1 = 0.0215, wR2 = 0.0544
R indices (all data)	R1 = 0.0227, wR2 = 0.0555
Absolute structure parameter	-0.007(9)
Largest diff. peak and hole	0.779 and -0.949 e.Å^{-3}

Table A13 Crystallographic Data for Complex (S_C,S_C)-**82**

Empirical formula	C26 H27 Cl N4 O3 Pd
Formula weight	585.37
Temperature	103(2) K
Wavelength	0.71073 Å
Crystal system	Orthorhombic
Space group	P2(1)2(1)2(1)
Unit cell dimensions	
a = 9.2939(7) Å	α= 90°.
b = 11.0308(9) Å	β= 90°.
c = 23.327(2) Å	γ = 90°.
Volume	2391.4(3) Å^3
Z	4
Density (calculated)	1.626 Mg/m^3
Absorption coefficient	0.925 mm^{-1}
F(000)	1192
Crystal size	0.40 x 0.34 x 0.08 mm^3
Theta range for data collection	1.75 to 38.92°.
Index ranges	-8<=h<=16, -19<=k<=19, -40<=l<=30
Reflections collected	36892
Independent reflections	13037 [R(int) = 0.0360]
Completeness to theta = 38.92°	98.5 %
Absorption correction	Semi-empirical from equivalents
Max. and min. transmission	0.9297 and 0.7086
Refinement method	Full-matrix least-squares on F^2
Data / restraints / parameters	13037 / 3 / 325
Goodness-of-fit on F^2	1.110
Final R indices [I>2sigma(I)]	R1 = 0.0348, wR2 = 0.0793
R indices (all data)	R1 = 0.0446, wR2 = 0.0970
Absolute structure parameter	-0.028(17)
Largest diff. peak and hole	1.664 and -1.068 e.Å^{-3}

Table A14 Crystallographic Data for Complex (*S*)-**58**

Empirical formula	C21 H17 Cl2 N3 Pd
Formula weight	488.68
Temperature	103(2) K
Wavelength	0.71073 Å
Crystal system	Triclinic
Space group	P1
Unit cell dimensions	
a = 10.2032(10) Å	α= 116.711(2)°.
b = 10.2739(5) Å	β= 96.515(3)°.
c = 10.4485(5) Å	γ = 92.994(3)°.
Volume	965.48(12) $Å^3$
Z	2
Density (calculated)	1.681 Mg/m^3
Absorption coefficient	1.248 mm^{-1}
F(000)	488
Crystal size	0.40 x 0.36 x 0.04 mm^3
Theta range for data collection	2.21 to 31.10°.
Index ranges	-12<=h<=14, -14<=k<=14, -15<=l<=15
Reflections collected	23445
Independent reflections	9976 [R(int) = 0.0263]
Completeness to theta = 31.10°	98.5 %
Absorption correction	Semi-empirical from equivalents
Max. and min. transmission	0.9518 and 0.6351
Refinement method	Full-matrix least-squares on F^2
Data / restraints / parameters	9976 / 3 / 487
Goodness-of-fit on F^2	1.160
Final R indices [I>2sigma(I)]	R1 = 0.0209, wR2 = 0.0512
R indices (all data)	R1 = 0.0226, wR2 = 0.0678
Absolute structure parameter	-0.005(14)
Largest diff. peak and hole	0.597 and -0.772 $e.Å^{-3}$

Table A15 Crystallographic Data for Complex (±)-**84**

Empirical formula	C43 H42 Cl2 N3 O P Pd
Formula weight	825.07
Temperature	103(2) K
Wavelength	0.71073 Å
Crystal system	Monoclinic
Space group	C2/c
Unit cell dimensions	
a = 23.1070(4) Å	α= 90°.
b = 12.7839(2) Å	β= 92.4730(10)°.
c = 24.3470(4) Å	γ = 90°.
Volume	7185.3(2) $Å^3$
Z	8
Density (calculated)	1.525 Mg/m^3
Absorption coefficient	0.750 mm^{-1}
F(000)	3392
Crystal size	0.40 x 0.30 x 0.26 mm^3
Theta range for data collection	2.02 to 30.00°.
Index ranges	-32<=h<=23, -17<=k<=16, -34<=l<=34
Reflections collected	46867
Independent reflections	10483 [R(int) = 0.0346]
Completeness to theta = 30.00°	99.9 %
Absorption correction	Semi-empirical from equivalents
Max. and min. transmission	0.8288 and 0.7535
Refinement method	Full-matrix least-squares on F^2
Data / restraints / parameters	10483 / 0 / 415
Goodness-of-fit on F^2	1.083
Final R indices [I>2sigma(I)]	R1 = 0.0307, wR2 = 0.0868
R indices (all data)	R1 = 0.0376, wR2 = 0.0914
Largest diff. peak and hole	0.521 and -0.612 e.$Å^{-3}$

Table A16 Crystallographic Data for Complex (±)-**87a**

Empirical formula	C40.50 H38 As Cl2 N3 O1.50 Pd
Formula weight	842.96
Temperature	103(2) K
Wavelength	0.71073 Å
Crystal system	Monoclinic
Space group	C2/c
Unit cell dimensions	
a = 23.2347(7) Å	α= 90°.
b = 12.8104(4) Å	β= 93.059(2)°.
c = 24.4166(8) Å	γ = 90°.
Volume	7257.1(4) Å^3
Z	8
Density (calculated)	1.543 Mg/m^3
Absorption coefficient	1.602 mm^{-1}
F(000)	3416
Crystal size	0.40 x 0.20 x 0.18 mm^3
Theta range for data collection	1.67 to 31.52°.
Index ranges	-33<=h<=31, -16<=k<=18, -35<=l<=29
Reflections collected	52202
Independent reflections	11737 [R(int) = 0.0381]
Completeness to theta = 31.52°	97.0 %
Absorption correction	Semi-empirical from equivalents
Max. and min. transmission	0.7614 and 0.5666
Refinement method	Full-matrix least-squares on F^2
Data / restraints / parameters	11737 / 75 / 470
Goodness-of-fit on F^2	1.134
Final R indices [I>2sigma(I)]	R1 = 0.0324, wR2 = 0.0805
R indices (all data)	R1 = 0.0479, wR2 = 0.0988
Largest diff. peak and hole	1.065 and -0.774 e.Å^{-3}